Using the double-ring infiltrometer to evaluate key unsaturated and saturated hydrological properties

Master's thesis report

10/06/2021 Pavel Petkov Water and environment

AALBORG UNIVERSITY

STUDENT REPORT

Title:

Using the double-ring infiltrometer to evaluate key unsaturated and saturated hydrological properties

Institution:

Department of the Built Environment
Aalborg University

Thomas Mans Vej 23
9220 Aalborg Øst
www.build.aau.dk

Project Period:

October 2020 – June 2021

Author:

Pavel Petkov

Supervisors:

Per Møldrup
Charles Pesch

Key words:

Double ring infiltrometer, retention, conductivity, Campbell model, pedotransfer functions, Philip sorptivity, moisture sensors, inverse modelling, HYDRUS-1D

Page Numbers:

60
excluding appendices

Date of Completion:

June 10, 2021

Foreword

This master thesis has been prepared in the period of October 2020 - June 2021 and amounts to a 60 ECTS workload. The thesis is presented as a completion of the master's program in Water and Environment at Aalborg university. The work has been inspired in a very large degree by the 1st semester of this study, specifically the Environmental Soil Science and Experimental Hydrology courses which have been what I consider the best learning experiences in my education career. The specific idea behind this thesis came from a conversation with professor Per Møldrup who was kind enough to accept my request to "do something with soil for my thesis" and from whom I have learned much.

Thanks for the sand Per, I'll try to hold onto as much as I can!

Special thanks go to Charles Pesch who has been a tremendous help not only with performing the experiments but also making sense of the data. Thanks for carrying water with me and standing on the ring Charles!

The concept drawings throughout this project are done by my close friend and gifted tattoo artist Tsvete Toncheva. Thanks for bringing my explanations of what I am working on to life!

Thanks to Jacob Jensen and Ole Johansen from WatsonC for their time and for introducing us to the Gistrup site.

And finally, thanks to Nanna Vestergaard, a fellow student and friend who has kept me brave.

Sources are referred to using the 7th edition APA style with full list of the references found at the end. Figures, tables and equations are numbered and referred to throughout the text and appendices are found at the very end of the report.

Table of Contents

1 Introduction

1.1 Motivation and objectives

A farmer whose business is to grow crops and produce food, a geotechnical engineer who works with structural foundations, an environmental scientist studying groundwater pollution and a municipal worker managing the water resources of a city are all united in their fields by two things – soil and water. More specifically how does water behave in the soil – how much water can be found in the soil, how freely is it accessed and how does it move.

The answer to these questions depends on the specific soil and conditions. Soil specifics include texture, compaction, organic matter content and more but generally relate to how much void space there is in the soil and how are these pores distributed in size which directly determines how much water the soil can hold. The conditions are the specific water content of the soil at a given time which can range anywhere from fully saturated where all the pores filled with water to sun dried where water is only held in on surface of the particulates and the pores are empty. The movement of water in a fully saturated soil is relatively straight forward – water follows an elevation gradient and always moves from high to low potential. Water flow in an unsaturated soil is pulled downwards by gravity but also in any direction in which water content is relatively lower due to suction and capillary forces generated by the air-filled pores. Another distinction is that the flow is also governed by the degree of saturation – the more water in the system the faster it can move downwards due to gravity and the less water in the system the faster it can move laterally due to suction. All this paints a complicated picture built on the interplay of soil, water, suction and gravity. The relationship between how much water there is in the soil and how difficult it is to get it out, also known as water potential, can be conveniently expressed by the soil-water retention curve. Additionally, how fast water travels through a given soil at a given water potential is expressed by the hydraulic conductivity curve. As water potential and water content are linked the hydraulic conductivity curve can also be expressed as the relationship between water content and the ability of the soil to conduct that water.

It is paramount for the farmer to know how much water there is in the soil at a given time but more importantly how difficult it is for the plant roots to suck it out. In other words, is it available to the plant? The geotechnical engineer needs to know the stability of the soil on which he plans to build a structure and how that changes with the water content. The environmental scientist wants to track pollution how fast it can spread for which he needs to track water as the vehicle of pollution. The municipal worker wants to know the relationship between groundwater extraction and recharge which is governed by how fast water moves through the unsaturated upper layer of the soil to the saturated aquifer. Infiltration is therefore crucial in all these regards.

Recently (Rahmati et al., 2018) introduced the Soil Water Infiltration Global (SWIG) database which is an impressive collection of 5023 infiltration experiments across multiple countries. The authors' purpose was to agglomerate scattered data from multiple publications and provide the basis for further research towards answering the above questions. This review article acknowledged the importance of the relationship between water content, water potential and hydraulic conductivity which governs infiltration and the authors provided additional meta information, however some key parameters which characterize the twin curves of retention and conductivity are missing. Additionally, Scandinavia and Denmark specifically is completely absent from the database. Given the importance of knowledge of the twin curves and soil-water infiltration the aim of this paper can be summarized as follows:

To present a quick, cheap, and simple method to estimate both soil-water retention and hydraulic conductivity curves which in combination with infiltration data can contribute to a local or global database. The method is a combination of field infiltration experiments and basic laboratory soil measurements and relies heavily on empirical relationships to obtain the twin curves.

The concept is illustrated in Figure 1.

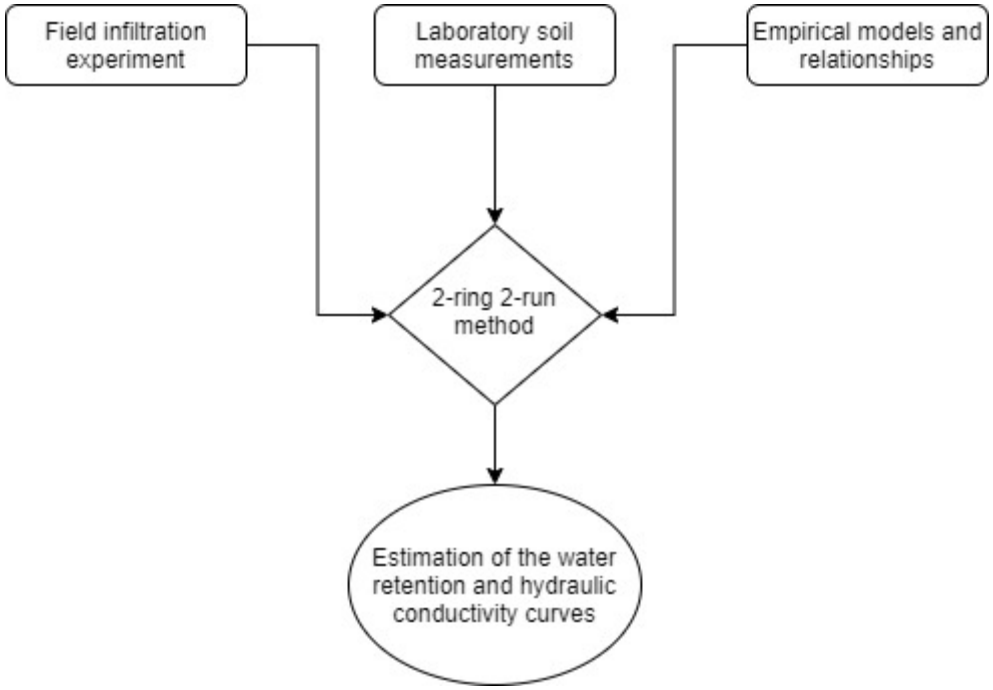

Figure 1 Concept of the new Two-ring Two-run method for estimating the twin curves.

1.2 Report structure

This report can be divided into three sections:

I. Chapter 2 reviews in-situ methods for measuring conductivity and retention with a focus on field methods. The main body of theory used in this project is also introduced in this chapter.

II. Chapter 3 introduces the new Two-ring Two-run method in detailed step-by-step manner.
Chapter 4 shows the application of the new method at six different soil sites including urban, cultivated and forest.
Chapter 5 briefly evaluates one of the key assumptions of the method.

III. Chapter 6 builds upon the method with the use of soil moisture sensors and hydrodynamic modelling (HYDRUS-1D) and can be considered a validation of the method.

Finally, chapter 7 offers reflection on the new method, its potential and possible shortcomings.

2 Review of in-situ infiltration methods for measuring retention and conductivity

This chapter reviews some of the field in-situ methods for obtaining unsaturated and saturated hydraulic parameters, namely the soil water content and hydraulic conductivity as functions of soil-water potential. The focus is on methods which include infiltration as part of their approach.

Five methods for determining the hydraulic conductivity are described – pressure infiltrometer, tension infiltrometer, well permeameter, pit infiltration and ring infiltrometers. Within these three dimensions of boundary conditions are identified – constant and falling head with positive or negative pressure heads where the flow can either be confined (1D) or unconfined (3D). Two approaches are also briefly discussed – the BEST method and numerical inversion are as way of estimating both retention and hydraulic parameters from infiltration experiments.

2.1 Boundary conditions and models

Before reviewing the field methods boundary conditions are briefly examined as a way of understanding how even through the goal of the methods is often times the same the conditions under which it is arrived at differs.

Constant head or falling head boundary conditions refer to the state of the water column over the soil – under constant head it remains static and under falling head it decreases over. The difference between the two conditions is most expressed in the use of equipment and method of inferring the hydraulic conductivity (K). The constant head experiment requires an additional device such as Mariotte bottle to maintain the water level during infiltration whereas the falling head experiment does not require such addons. On the other hand, the calculating method for K in the falling head experiment has to take an additional account of the changing head which is usually solved by taking an incremental timestep approach. In (Gill et al., 2019) the authors compared the two methods via numerical modelling and suggested that the constant head estimated higher hydraulic conductivity values compared to falling head.

Positive or negative pressure head boundary conditions refer to the pressure that the water column over the soil experiences. Naturally in ponded infiltration due to the atmospheric pressure this is positive, however certain devices can introduce negative pressure or suction to the water column. This means that the soil has to “suck” the water out as it is infiltrated into it. Capillary theory dictates that the larger the pore diameter the less suction that pore is capable of, therefore negative pressure head can be used to investigate the effects of macroporosity by excluding the contribution of the largest pores. This is of interest especially in dual-permeability soils but can also apply to regular soils as shown in (Watson & Luxmoore, 1986) where 73% of the flow was conducted through pores with a diameter larger than 0.1 cm.

The infiltration method can attempt to confine the flow into the soil to promote 1D downward infiltration usually done by inserting a structure that limits lateral flow, or leave it unconfined and three-dimensional. Under 3D flow the effects of capillarity are more expressed which requires additional regard when calculating the hydraulic conductivity. In (Smettem et al., 1994) the authors accounted for this and proposed a relationship between 1D confined and 3D unconfined flow. The main advantage of the unconfined boundary condition is that it introduces the least disturbance to the soil, which may affect measurements.

Figure 2 shows how the methods discussed fall within these boundary condition categories.

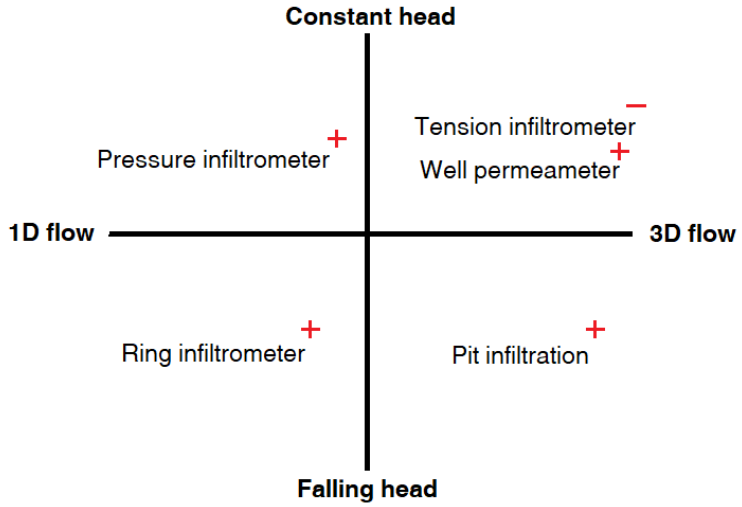

Figure 2 In-situ infiltration methods for hydraulic conductivity, categorized by their boundary conditions. The + and - sign represents the positive and negative pressure head boundary condition.

As mentioned in Chapter 1 soil moisture and water potential are interconnected with infiltration of water in the following subchapter the theory and models for retention, conductivity and infiltration used in this project are presented before the continuing with the different infiltration methods and their yield.

2.1.1 Retention

The soil-water retention curve (SWRC) expresses the relationship between water content and soil-water potential (Loll & Moldrup, 2000). At any point on the curve it is shown how much water there is in the soil system and how much suction would have to be applied to overcome the forces keeping it in the pores. Otherwise said how much water is present within a specific soil system at a given soil-water potential. Direct measurement of retention makes use of various devices such as a pressure plate which involves taking undisturbed soil samples under laboratory conditions and measuring the water content a given potentials (Dane & Clarke Topp, 2002). This requires time for equilibration between sample and unit and, of course, the apparatus itself. This approach was used in (Hansen, 1976) where he generated an impressive library of measured SWRCs across Danish soils over 5 years which can be assumed was neither cheap nor quick. Therefore, often an estimation of the SWRC is prudent. Different models and empirical equations exist for this purpose which estimate the curve – these equations normally include several equation-specific parameters which give the curve its scale and shape.

In (Campbell, 1974) one such model was introduced represented by the empirical function:

$$\theta(\psi) = \theta s \left(\frac{\psi e}{\psi}\right)^{1/b} \qquad \text{Equation 1}$$

Where θ(ψ) [L^3 water/L^3 soil] is the volumetric water content at pressure potential ψ [L], ψe [L] is the air entry potential or the suction at which air first enters a saturated soil, θs [L^3 water/L^3 soil] is the volumetric water content at soil saturation and b an empirical constant originally described by Campbell as the negative slope of the straight line fit in a log(ψ)=pF versus log(θ) plot. θs is an easily obtained parameter often assumed equal to the soil total porosity (Loll & Moldrup, 2000). The unsaturated parameters ψe and the Campbell b which make up the shape and scale of the SWRC are more challenging to obtain and literature values are commonly used for different soil classes. Figure 3 shows the SWRC for different soil types generated by Equation 1 using literature values from (Clapp & Hornberger, 1978) for the parameters θs, ψe and b.

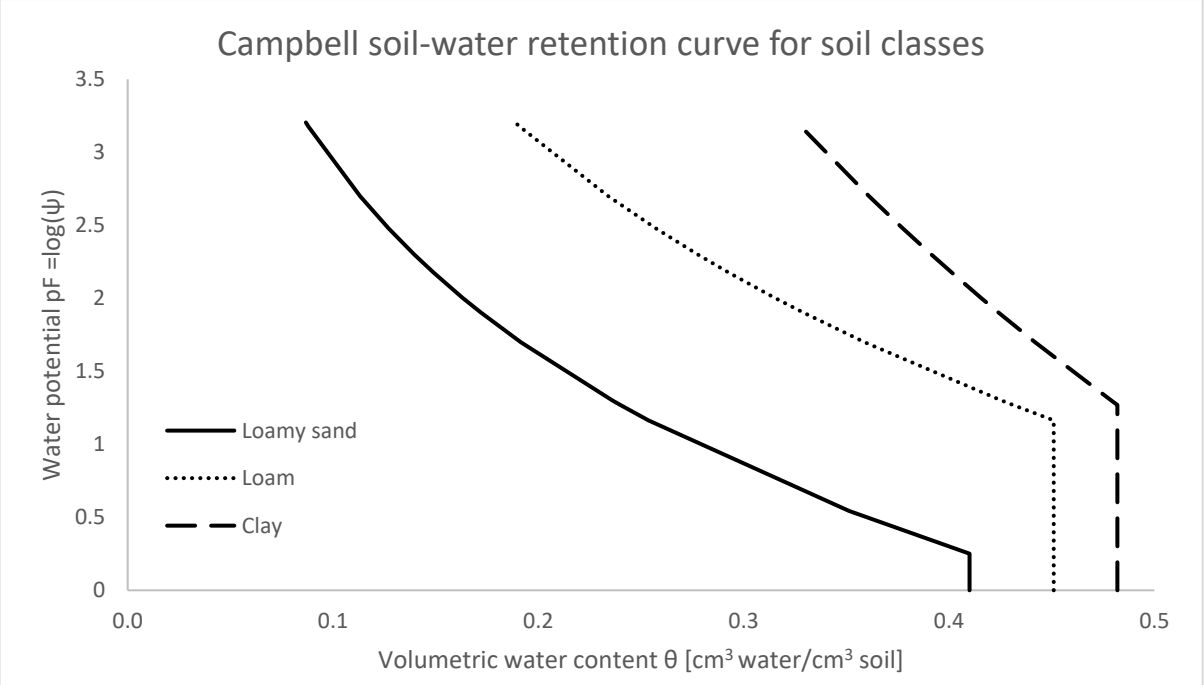

Figure 3 Campbell model for the soil-water retention curve for 3 soil types – loamy sand, loam and clay. Curves generated using Equation 1 with soil data from (Clapp & Hornberger, 1978) - *θs [cm³/cm³] = 0.410 , 0.451 , 0.482 ; ψe [cm] = 1.78 , 14.6 , 18.7 ; b = 4.38 , 5.39 , 11.4 ; for loamy sand, loam and clay, respectively.*

Clayey soils compared to sandy soils have a higher number of pores as indicated by the higher total porosity or saturated water content. Due to the difference in pore size water is retained by clay much more than by sand and it takes more energy to release it from the pore space. Therefore, at the same water potential of pF 2 for example loamy sand has a much lower water content than clay.

A quick note on the use of ψ and ψe – the values of these parameters are negative as they represent suction forces, even though for ease of presentation in this project they are written as positive.

Another retention model was introduced in (van Genuchten, 1980):

$$\theta = \theta r + \frac{\theta s - \theta r}{[1 + (\alpha * \psi)^n]^m} \qquad \text{Equation 2}$$

Where θr is the residual water content [L^3 water/L^3 soil] or the water content under a very dry condition; α, n and m are empirical constants where n is related to the width of the pore-size distribution, m is assumed equal to 1-1/n and α [1/L] is often related to the inverse of air entry potential (α =1/ψe). The main difference between the van Genuchten (vG) and Campbell models is that vG has four parameters instead of Campbell's two and therefore it is easier to produce a more detailed curve shape given the additional data is available. It is perhaps the most widely used for retention and is found in many publications and software.

One approach for building the SWRC is to use several direct measurements and fit the models around those, thereby estimating the whole retention curve out of a few discrete points. Another approach utilizes so-called pedo-transfer functions (PTFs), the term coined in (Bouma, 1989), which are equations and relationships between difficult and laborious parameters and more easily obtainable data (Pachepsky & van Genuchten, 2011). The Rosetta software (Schaap et al., 2001) is an example of this concept which estimates the vG parameters from soil texture (sand, silt and clay contents) with the possibility of augmenting the estimation with additional data.

2.1.2 Conductivity

As mentioned in Chapter 1 the hydraulic conductivity of a soil is its ability to conduct water and is not a constant, per se, but rather a function of how much water there is in the soil. At saturation all the pores are full and contributing to the flow and the conductivity is at its maximum known as the saturated hydraulic conductivity (Ks). As water content drops the more pores empty and are excluded from the flow, thereby reducing it and the conductivity. Given the relationship between water content and water-potential the two are used interchangeably when it comes to hydraulic conductivity which is to say that K can be expressed as a function of either θ or ψ.

One of the most widespread and simplest models that expresses this relationship was introduced by (Gardner, 1958):

$$K(\psi) = Ks \times \exp(a\psi) \qquad \text{Equation 3}$$

Where Ks [L/T] is the saturated hydraulic conductivity, ψ [L] is the soil-water potential and a [1/L] is a parameter that relates to soil texture and structure and is the inverse of the macroscopic capillary length of the soil λ = 1/a [L]. This parameter, *not to be confused with vG α*, can be obtained through fitting the equation to measurements of K at different water potentials much like the Campbell b and is the slope of the ln(K/Ks) versus ψ plot. Values of it can also be looked up in tables as found in (Angulo-Jaramillo, Bagarello, Iovino, Lassabatere, et al., 2016).

In (Campbell, 1974) the author also introduced a model that describes the relationship between unsaturated hydraulic conductivity and water content represented by the empirical function:

$$K(\theta) = Ks\left(\frac{\theta}{\theta s}\right)^{2b+3} \qquad \text{Equation 4}$$

Where K(θ) is the hydraulic conductivity at the given water content θ and Ks is the saturated hydraulic conductivity or the hydraulic conductivity at saturated water content θs. b is the same empirical constant from Equation 1. The model assumes that 1) water flow in soil is controlled by the smaller of two pores in a sequence 2) pores in direct sequence contribute to the flow and 3) pores fit randomly together in the soil.

Figure 4 shows a plot of Equation 4 for different soil types using literature data from (Clapp & Hornberger, 1978).

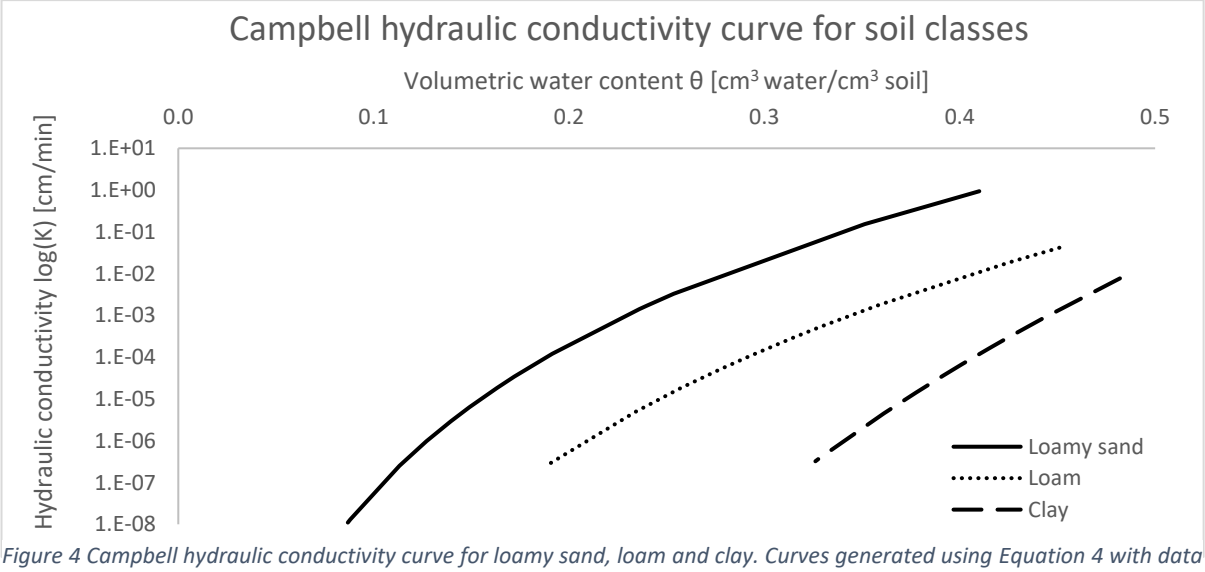

Figure 4 Campbell hydraulic conductivity curve for loamy sand, loam and clay. Curves generated using Equation 4 with data from (Clapp & Hornberger, 1978) - *θs [cm³/cm³] = 0.410 , 0.451 , 0.482 ; b = 4.38 , 5.39 , 11.4 ; for loamy sand, loam and clay, respectively.*

Figure 4 illustrates the uniting principle that as water content drops across the different soils so does the hydraulic conductivity. The key difference between the soils is the specific hydraulic conductivity - at the same water content of 0.4 [cm^3/cm^3] sandy and clayey soils show hydraulic conductivities that differ several orders of magnitude.

The main difference between the two models is that the Gardner model is an easily applicable one-parameter equation for estimating the unsaturated hydraulic conductivity and unlike the Campbell model it is not built on an underlying connection between water content and matric potential. Other models exist such as the ones presented in (van Genuchten, 1980) and (Brooks & Corey, 1964) and the use of such a model for inferring the K from Ks is almost always needed as few methods for direct field measurement of unsaturated K exist.

2.1.3 Infiltration

Henri Darcy was one of the first scientists to conduct experiments on flow through porous mediums and coined the term hydraulic conductivity (Darcy, 1856). The equation known as Darcy's law describes water flux through soil and is mathematically expressed as:

$$v = -Ks\frac{dH}{dx} \quad \text{Equation 5}$$

Where v [L/T] is the Darcy flux/velocity, Ks [L/T] is the saturated hydraulic conductivity and $\frac{dH}{dx}$ is the hydraulic gradient [-]. In Darcy's original experiment consisting of infiltration through sand beds this gradient was the difference in total hydraulic head H [L] (pressure and elevation) between the inlet and outlet of the sand bed divided by its length x [L]. Darcy's law was formerly developed to express flow under saturated conditions and was extended in (Buckingham, 1907) to incorporate unsaturated flow:

$$v = -K(\theta)\frac{dH}{dx} = -K(\psi)\frac{d(\psi - G)}{dx} = -K(\psi)(\frac{d\psi}{dx} - 1) \quad \text{Equation 6}$$

Where K(θ) and K(ψ) [L/T] are the hydraulic conductivities as a function of water content θ [L^3/L^3] or soil-water potential ψ [L], G [L] is the gravitational head and x [L] is calculated positive with depth. This version replaces the saturated with the unsaturated hydraulic conductivity and hydraulic head H is exploded into the sum of suction and gravity. If the infiltration experiment is carried out long enough so that the soil becomes saturated the suction term $\frac{d\psi}{dx}$ is assumed to be negligible and Equation 6 is transformed into:

$$v = -Ks(-1) = Ks \quad \text{Equation 7}$$

Another method for expressing infiltration was introduced in (Philip, 1957) which proposes that the sum of infiltrated water into soil at any given time is:

$$I = S\sqrt{t} + At \quad \text{Equation 8}$$

Where I is accumulated infiltration [L] , S is the sorptivity [L/√T] and A [L/T] is a constant. The first term of the equation represents flow due to the suction forces and capillarity and thus sorptivity relates to the soil suction potential. As such it is not really a constant but depends on the soil content at the start of the experiment. The second term represents gravitational flow and thus the A parameter [L/T] known as transmissivity relates to the soil's ability to transport water and has the same dimensions as

the hydraulic conductivity. For a long timeframe it can be assumed that A = Ks. For shorter times (Angulo-Jaramillo, Bagarello, Iovino, Lassabatere, et al., 2016) lists studies where ranges from A = 0.5 to 0.3Ks have been suggested.

Figure 5 shows the results of Equation 8 applied to data from (Clapp & Hornberger, 1978) for three distinct soil classes – sand, loam and clay.

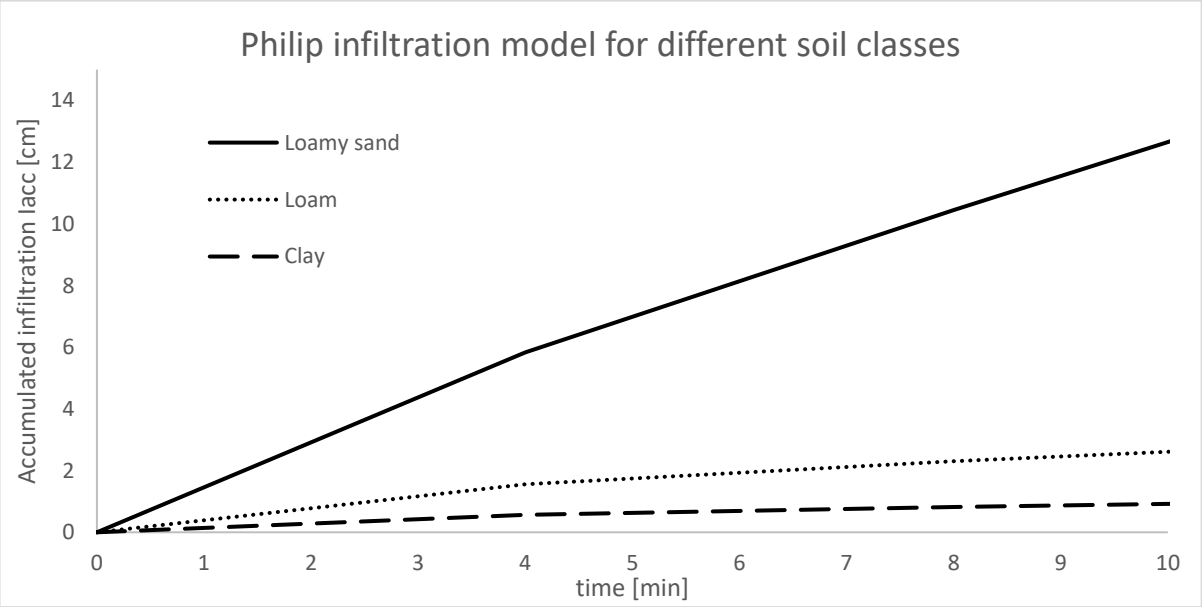

Figure 5 Accumulated infiltration versus time for three soil types – loamy sand, loam and clay. Curves generated using Equation 4 and assuming A=Ks. Hydraulic parameters data from (Clapp & Hornberger, 1978)*. S [cm/√min] = 1.04 , 0.693 , 0.269 ; Ks [cm/min] = 0.938 , 0.0432 , 0.0077 for loamy sand, loam and clay, respectively.*

The difference between the sandy soil and the others is profound due to the second term of the equation and Ks which changes three orders of magnitude from the sandy to the clay soil.

In the SWIG database introduced in (Rahmati et al., 2018) the authors fit measured cumulative infiltration to an equation similar to Equation 8 but with an extra term:

$$I(1D) = S\sqrt{t} + 0.33Ks \times t + At^{3/2} \quad \text{Equation 9}$$

$$I(3D) = S\sqrt{t} + 0.47Ks \times t + At \quad \text{Equation 10}$$

What is important here is that the authors assumed that A in the two-term Philip equation is equal to 0.33Ks and for 3D infiltration the second term weighs more. Following this example going forward the A parameter is assumed equal to 0.33 in unsaturated conditions and approaching 1 in near-saturated conditions as expressed by Equation 7. Furthermore, its weight is also determined by the boundary conditions of the infiltration experiment having more weight under 3D flow.

With boundary conditions and theory of retention, conductivity and infiltration covered the different methods of measuring and estimating the hydraulic parameters related to these processes are presented in the next section.

2.2 Infiltration methods

2.2.1 Pressure infiltrometer

This method involves inserting a single ring into unsaturated soil and mounting a Mariotte-bottle-reservoir on top of it which maintains a ponded water level, thereby facilitating a 1D constant head flow. The pressure head is adjusted by a standpipe, which equilibrates the pressure inside the reservoir and at its level to that of the atmosphere as shown in Figure 6.

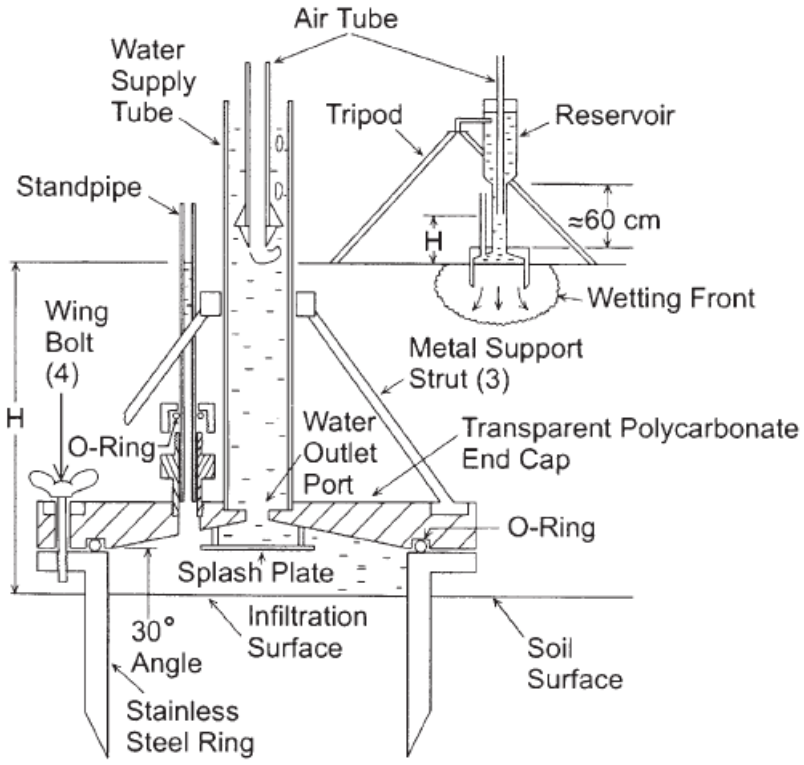

Figure 6 Pressure infiltrometer concept and device. Figure from (Dane and Clarke Topp, 2002).

Performing a single infiltration run yields Ks whereas repeating the experiment with a different elevation of the air tube and therefore different pressure head is required to obtain the Gardner alpha parameter and the Philip sorptivity (Dane & Clarke Topp, 2002).

2.2.2 Well permeameter

The well permeameter (WP) also known as a Guelph permeameter is essentially a field-adapted Mariotte bottle which allows the maintenance of a constant depth of water in an excavated borehole (Reynolds & Elrick, 1986). As seen in Figure 7 the water in the borehole infiltrates downwards and through the sides (3D) and is recharged by the permeameter. This recharge rate is noted on the device itself and the experiment is carried out until steady state is achieved. At this point Ks can be measured knowing the geometry of the borehole and device as described in detail in (Reynolds & Elrick, 1986).

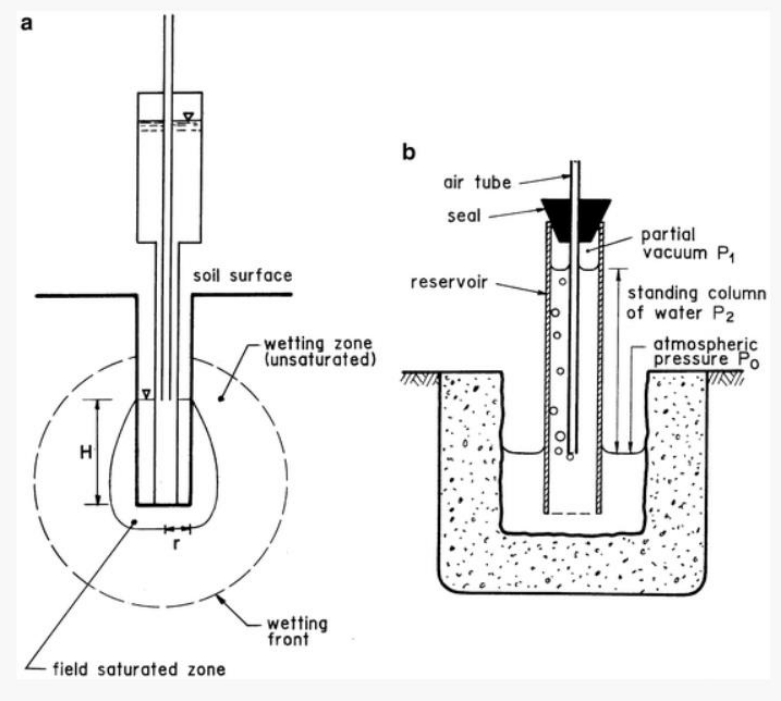

Figure 7 Guelph permeameter concept. (a) shows the outward flow from the borehole into the soil and (b) the operating principles and details. Figure from (Angulo-Jaramillo, Bagarello, Iovino, Lassabatere, et al., 2016).

The well permeameter and pressure infiltrometer are very similar in their use of Mariotte-bottle-reservoir to maintain constant head infiltration. The well permeameter also determines the same array of parameters as the pressure infiltrometer using similar techniques. The main difference is in the calculation of Ks and that the Guelph allows for easier measurements at different soil layers at the cost of a smaller scale measurement.

2.2.3 Pit infiltration

Perhaps the simplest infiltration technique of all pit infiltration essentially involves digging a hole and performing a falling head experiment where the water level is noted at a given interval until steady state is reached as shown in Figure 8. It is very similar to the well permeameter, however under falling head conditions. The main difference is that this procedure requires minimal equipment such as hand drill and it only yields Ks.

Pit infiltration is mainly used for quick evaluations of field infiltration (Mueller et al., 2014) and is widely employed in the area of stormwater infiltration (Minnesota Pollution Control Agency, 2015) where Ks is often less of a desirable value than the infiltration rate.

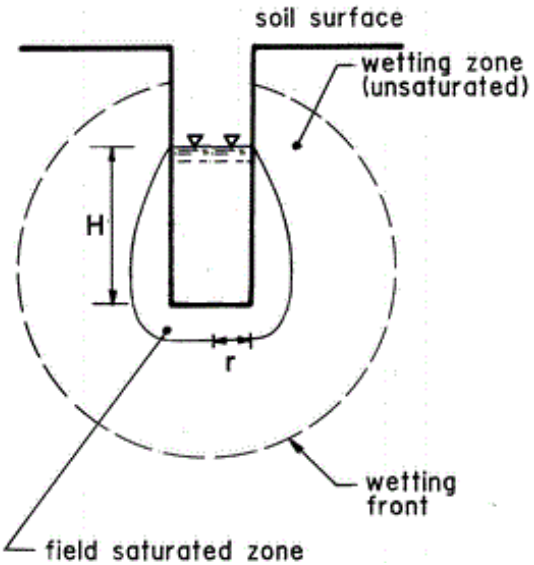

Figure 8 Pit infiltration concept. Figure inspired from (Angulo-Jaramillo, Bagarello, Iovino, Lassabatere, et al., 2016)

2.2.4 Tension infiltrometer

A tension infiltrometer (TI) also known as a disc permeameter/infiltrometer introduced in (Perroux & White, 1988) is a device which allows measurement of infiltration where the water column subject to a negative pressure. The intent is to minimize the influence of preferential flow caused by soil macropores. A porous plate is placed on the ground and a reservoir and bubble tower are mounted on top, as shown in Figure 9. The suction is controlled by the air tube where lowering the tube increases the suction needed to pull water out of the reservoir and thereby excluding pores with a large diameter. Unlike the other methods which directly measure Ks and infer the unsaturated K this device does the opposite (Eijkelkamp, 2021).

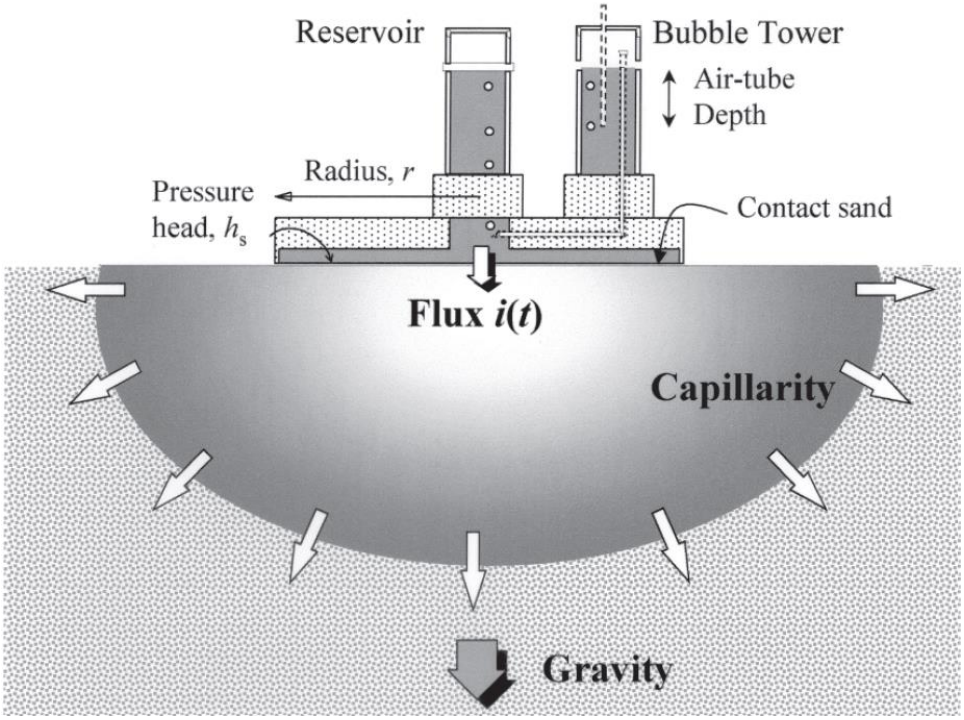

Figure 9 Tension infiltrometer concept and device. Figure from (Dane and Clarke Topp, 2002).

The TI is considered a gentler measurement tool and is likely to cause less soil disturbance than the pressure infiltrometer's inserted ring or the borehole auguring required for the Guelph permeameter. This increases the likelihood of undisturbed and conductivity measurements closer to the natural state of soils especially in heavily aggregated soils. The flow from a tension infiltrometer is not confined in any way as seen in Figure 9 and therefore the influence of sorption and suction compared to gravity are greater when compared to confining methods (Dane & Clarke Topp, 2002).

2.2.5 Single and double ring infiltrometers

Ring infiltrometers are essentially cylindrical metal structures with thin walls that are inserted into the soil for the purpose of ponding water which infiltrates into the soil. The experiment is naturally conducted under falling head conditions where water is simply poured into the ring and the water level inside the ring is noted over time but it can also be adapted to a constant head version utilizing a Mariotte bottle.

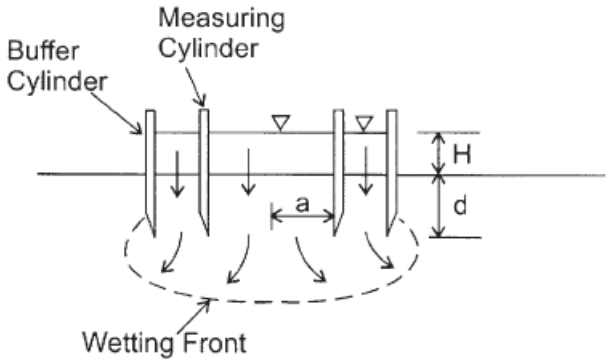

Figure 10 Concept of double-ring infiltration. Figure from (Dane & Clarke Topp, 2002).

The working principle in the single- double-ring infiltrometers is the same, however the intention of the additional ring is to increase the probability of vertical flow 1D flow in the inner ring (Dane & Clarke Topp, 2002). Following pit infiltration this method requires the least equipment and is widely used due to its versatility and simplicity. Even within simplicity there is room for complexity as the demonstrated in (Lai & Ren, 2007) and (Lai et al., 2010) where the authors investigated the effect of ring diameters on Ks and recommended rings with an inner diameter of 90+ cm for reliable measurements. In (Fan et al., 2012) and (Lai et al., 2012) it was shown that the depth of insertion also matters and should be at least 10 cm. Adding to the versatility of the method in (Bodhinayake et al., 2004) it was concluded that there was no effect of terrain slope on the Ks measurements at least up to a 20% slope.

2.2.6 Summary of methods

Below is a summary of the presented methods with their boundary conditions, what each method yields in its conventional version and the scale of the measurement.

Table 1 Summary of infiltration methods

Method	Boundary condition	Output	Scale
Pressure infiltrometer	Constant head / 1D / Positive pressure	Ks / Gardner a / Philip S	10-20 cm Ø (commercially available)
Well permeameter	Constant head / 3D / Positive pressure	Ks / Gardner a / Philip S	6 cm Ø standard borehole
Pit infiltration	Falling head / 3D / Positive pressure	Ks	Varies
Tension infiltrometer	Constant head / 3D / Negative pressure	Near-saturation K / Gardner a / Philip S	20 cm Ø (commercially available)
Ring infiltrometer	Falling head / 1D / Positive pressure	Ks	15-30-60 cm Ø (commercially available)

Ks varies not only between methods but within a single method which is used at a different scale also known as special variability as suggested in the ring infiltrometer section and many studies have shown this (Jang et al., 2011; Schulze-Makuch et al., 1999; Usowicz & Lipiec, 2021). This phenomenon should be considered when comparing Ks between methods especially ones that differ considerably in scale.

2.3 Numerical inversion for estimation of hydraulic parameters

Nearly all simulations of water movement through unsaturated soils map the flow by solving the Richards equation (Hopmans, 2011):

$$\frac{d\theta}{dt} = \frac{d}{dx}\left[K(h)\left(\frac{dh}{dx} + 1\right)\right] - S \qquad \text{Equation 11}$$

Where S [$L^3/L^3/T$] is the sink term representing plant root water uptake. Computer simulation programs such as HYDRUS-1D solve this equation numerically and are a very convenient way of estimating water flow through soil given parameters describing the soil are known. However, the software can also be used "in reverse" to estimate the parameters based on experimental data known as inverse modelling. In essence inverse modelling involves 1) performing water flow experiment and measuring data such as cumulative flux at the lower boundary or water contents/pressure heads at given depths, 2) numerically solving Richard's equation for water flow and 3) an objective function compares modelled and observed data and recalibrates the hydraulic parameters until the difference is minimal (Angulo-Jaramillo, Bagarello, Iovino, & Lassabatere, 2016). This process is illustrated in Figure 11. Note that since HYDRUS only uses the vG parameters as input for retention the use of other models such as Campbell is not possible.

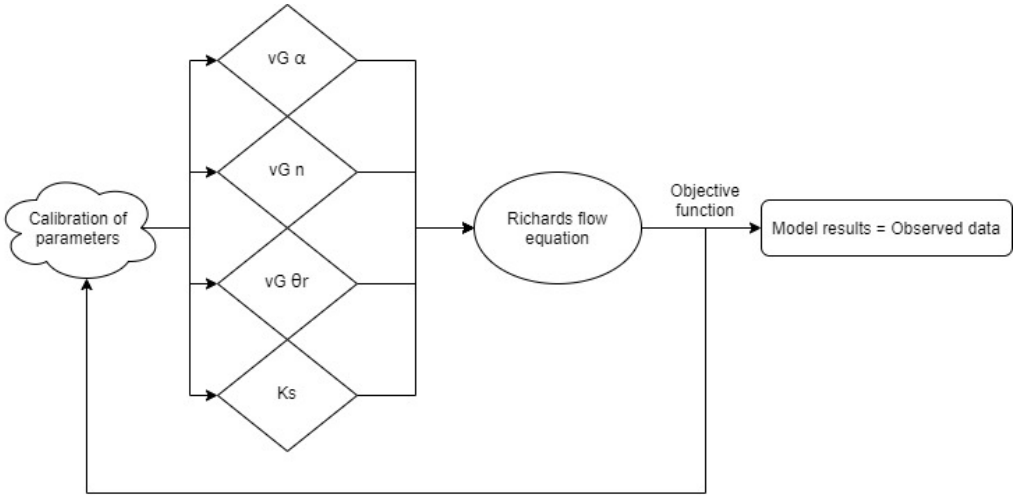

Figure 11 Concept of inverse modelling for estimating the van Genuchten retention parameters (Equation 2) and hydraulic conductivity using HYDRUS 1D.

Originally in (J. Šimůnek & van Genuchten, 1996) and (Jiří Šimůnek et al., 1998) the authors used a tension infiltrometer for this purpose and in (Jiří Šimůnek & Van Genuchten, 1997) it was suggested that a sound strategy for the inverse method consists of cumulative infiltration from a number of infiltration experiments combined with pressure head and water content measurements at different. Since then in (Ket et al., 2018) soil moisture and matric potential probes were used to estimate retention and conductivity in five fields using the HYDRUS-1D software. Furthermore, by combining a soil moisture and matric potential sensors it is possible to generate enough points of water content at given potentials to construct the soil-water retention curve in-sutu with minimum experimentation. This was as shown in (Iiyama, 2016), (Nolz & Kammerer, 2017), (Bordoni et al., 2017), (Degré et al., 2017) and (Zeitoun et al., 2021) where the differences between laboratory and in-situ measurements of the SWRCs were considered acceptable. As the development of these technologies advances and they become more commercially available and robust there is little doubt that the future of soil-water retention will include more in-situ sensor-based methods in combination with hydrodynamic modelling.

2.4 Beerkan Estimation of Soil Transfer parameters

In (Lassabatère et al., 2006) the authors introduced the so-called Beerkan Estimation of Soil Transfer parameters (BEST) method which estimates the shape and scale parameters of the vG retention model and the parameters of the (Brooks & Corey, 1964) conductivity model from 1) soil bulk density and particle size distribution and 2) cumulative infiltration and initial and final water contents. The method combines field and laboratory experiments and makes use of PTFs to estimate the twin curves, as illustrated in Figure 12.

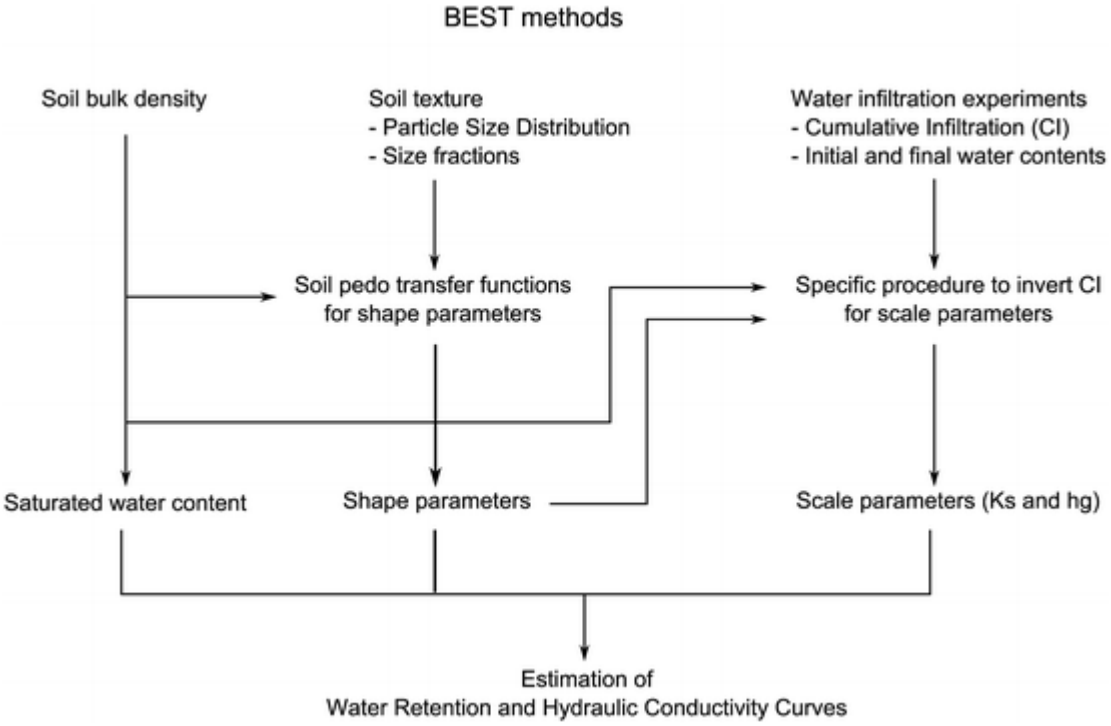

Figure 12 Beerkan Estimation of Soil Transfer properties flowchart, figure from (Angulo-Jaramillo, Bagarello, Iovino, & Lassabatere, 2016).

The method is relatively cheap as the equipment it requires is found in most laboratories and has been shown to be of acceptable precision. However, it is anything but simple utilizing a myriad of steps and equations to estimate the twin curves. In (Gonzalez-Sosa et al., 2010) the authors used the method to study hydraulic properties of pastured and cultivated soils in France using both single-ring and pressure infiltrometers. In (Mubarak et al., 2009) the method was used to investigate how the hydraulic properties of a maize cropping field change under different irrigation treatments. In (Xu et al., 2012) the authors compared the Wu method (presented in (Wu et al., 1999) as a way of estimating Ks based on an infiltration run in combination with initial and final soil moisture measurements) to the BEST method and found that the latter performed poorly for sandy soils where it sometimes produced null or extremely low Ks and alpha values. This was also observed in (Lassabatere et al., 2010) where it was attributed it to lack of sufficient convex in the beginning of the cumulative infiltration curve. In (Alagna et al., 2016) parameters estimated by the BEST method were compared with laboratory soil-water retention measurements and field saturated hydraulic conductivity measurements by both pressure and tension infiltrometers. The authors concluded that at least for loamy soils the method obtained reasonably good predictions of retention and near perfect estimation of hydraulic conductivity. The method is still being improved and broadened as shown in (Fernández-Gálvez et al., 2019) but its characteristics remain the same – estimating both retention and conductivity of soils by relying on simple field and laboratory measurements which has been a large inspiration for this project.

3 Development of the new Two-ring Two-run infiltration method

3.1 Concept and theory

As discussed in Chapter 2 the double-ring infiltrometer (DRI) is a tool traditionally used to obtain the saturated hydraulic conductivity. In this project an expansion of its use is investigated:

Can the early stages of a double-ring infiltration experiment be used to obtain the unsaturated soil parameters of the (Campbell, 1974) model?

Chapter 2 introduced the two governing forces behind infiltration– gravity and capillarity. As water first comes into contact with unsaturated soil it is sucked in as a result of the pressure gradient at the interface between free standing water and air-filled pore space. At the beginning this gradient is at its maximum and decreases as more of the pore space is filled with water. The infiltration rate is highest at the beginning of infiltration when capillarity and gravity are both driving the water downwards and decreases over time until it reaches a steady state rate. In this steady state capillarity is negligible as the soil is saturated and the infiltration rate is determined by how fast the water can move through the soil due to the gravity gradient which is expressed by the hydraulic conductivity. Figure 13 illustrates these two different soil conditions.

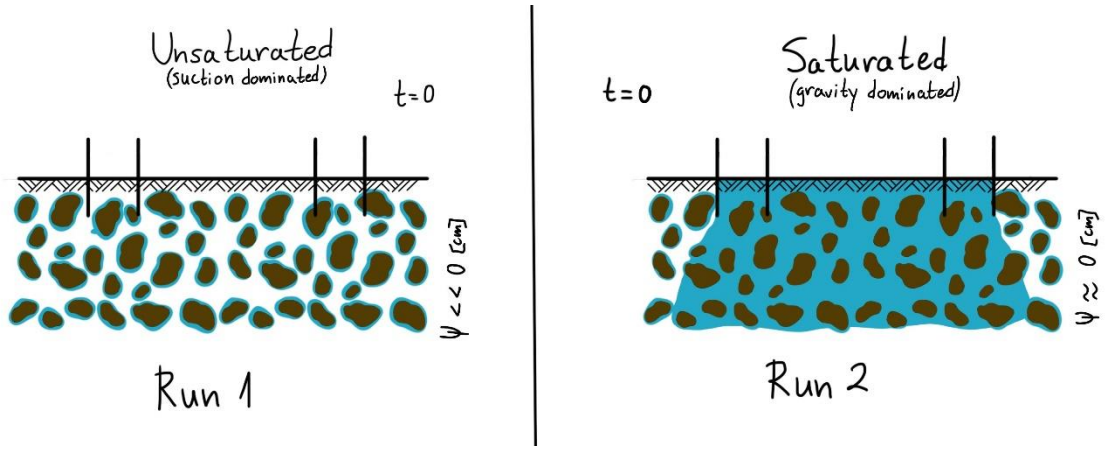

Figure 13 Assumed initial conditions for the two runs. At t = 0 flow in Run 1 the pressure gradient is high as water content in soil is low and suction dominates. At t = 0 in Run 2 the pressure gradient is close to zero as soil water content is saturated and suction is minimal – water drains due to gravity.

If an infiltration experiment is carried out under these two initial conditions and the accumulated infiltration versus time is plotted the two plots would have the following characteristics as illustrated in Figure 14:

- A curved line for the unsaturated Run 1 with a convex in the beginning as suction dominates and becoming linear as the infiltration run progresses and the suction gradient decreases.
- A straight line for the saturated Run 2 indicating steady state and a gravity driven flow where the gradient is constant.

Figure 14 Assumed progress of accumulated infiltration versus time for a double ring infiltrometer experiment under unsaturated and saturated initial conditions. The differences in water infiltration can be seen – for the same duration in the same soil Run 1 is expected to produce a curved line, infiltrating more water than Run 2, which is characterized by its linearity.

The two-run infiltration plot assumes that in the same soil in a timeframe of 50 minutes more water infiltrates under unsaturated conditions than under saturated. If Run 1's convex is barely noticeable or is missing altogether the soil is likely too wet at the start of the experiment. If Run 2's plot is not linear the soil is not saturated - capillarity is still in action and gravity is not dominant yet and the experiment should be carried out for a longer period.

3.2 Main assumptions of the method

This section describes the two governing assumptions on which the Two-ring Two-run method is built - 1) how the Philip two-term model can be used to obtain the Philip sorptivity from infiltration data and 2) how the sorptivity can be used to estimate the Campbell b in the Campbell retention model.

3.2.1 Assumption I – Splitting the Philip infiltration model

Given the initial conditions shown in Figure 13 are present then the Philip model as described in Chapter 2

$$I = S\sqrt{t} + At \qquad \text{Equation 8}$$

can be split and its two terms used separately to plot accumulated infiltration for the two runs. Run 1 is expressed by the first term where suction and sorptivity dominate and the gravity is neglected. Run 2 is expressed by the second term where soil is saturated and suction is be neglected. Figure 15 illustrates this and expands upon Figure 13 showing how infiltration would progress 10 minutes into the experiment under the assumed initial conditions.

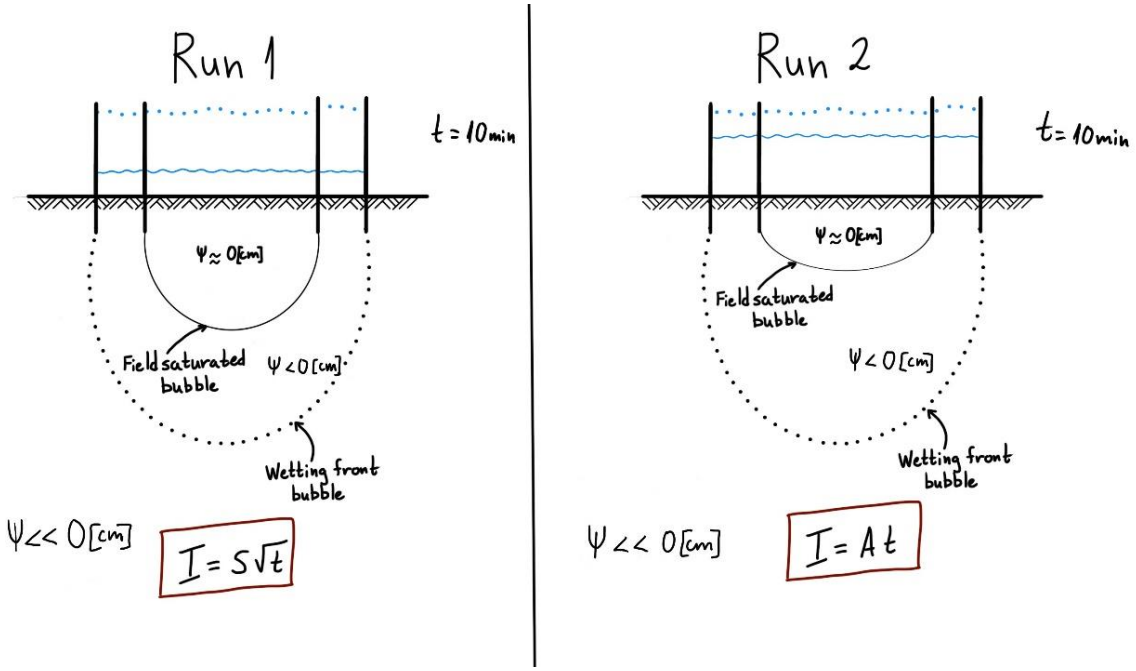

Figure 15 Assumed progression of infiltration under initial conditions in Figure 13. At t= 10 min Run 1, dominated by suction, has infiltrated more water than Run 2, dominated by gravity.

The key assumption here is that **the two runs influence each other minimally** and therefore the Philip model can be split in two. In reality this depends entirely on the specific soil, initial conditions and the way the infiltration experiment is carried out. If the soil is not dry enough i.e at least at field capacity then gravity may already interfere with suction even in the earliest moments of Run 1. If the soil is a very coarse and measurements are not taken frequently enough during the initial stages of Run 1 one might "miss the window" where suction dominates, thus not producing sufficient convex in the accumulate infiltration curve. On the other hand, if the experiment is not carried long enough for the soil to become saturated Run 2 can be influenced by capillarity, however that is a more "traditional problem" and is easily overcome by patience and water management.

3.2.2 Assumption II - Link between the Campbell and Philip models

There are several ways of obtaining the parameters in the Campbell retention model as discussed in Chapter 2. The quickest is to use soil libraries to look these parameters up such as the US one presented in (Clapp & Hornberger, 1978) which lists ψe and b values from 1446 soils, divided into 11 texture categories from sand to clay as shown in Table 2:

Table 2 Soil hydraulic parameters in the American soil library (Clapp & Hornberger, 1978)

Texture	N	mean clay fraction	b	ψe [cm]	Θs [cm^3/cm^3]	Ks [cm/min]	S [cm/√min]
sand	13	0.030	**4.05(1.78)**	**3.5**	0.395(0.056)	1.056	**1.520**
loamy sand	30	0.060	**4.38(1.47)**	**1.78**	0.410(0.068)	0.938	**1.040**
sandy loam	204	0.090	**4.9(1.75)**	**7.18**	0.435(0.086)	0.208	**1.030**
silt loam	384	0.140	**5.3(1.96)**	**56.6**	0.485(0.059)	0.0432	**1.260**
loam	125	0.190	**5.39(1.87)**	**14.6**	0.451(0.078)	0.0417	**0.693**
sandy clay loam	80	0.280	**7.12(2.43)**	**8.63**	0.420(0.059)	0.0378	**0.488**
silty clay loam	147	0.340	**7.75(2.77)**	**14.6**	0.477(0.057)	0.0102	**0.310**
clay loam	262	0.340	**8.52(3.44)**	**36.1**	0.476(0.053)	0.0147	**0.537**
sandy clay	19	0.430	**10.4(1.64)**	**6.16**	0.426(0.057)	0.013	**0.223**
silty clay	441	0.490	**10.4(4.45)**	**17.4**	0.492(0.064)	0.0062	**0.242**
clay	140	0.630	**11.4(3.7)**	**18.6**	0.482(0.050)	0.0077	**0.268**

Another example is the Danish soil library provided in (Hansen, 1976) which although lacking the convenience factor of a ready-made table with parameter values can be used to compare soils with similar physical parameters such as texture, bulk density and organic matter content. Assuming equal similarity in the SWRCs of the two soils, thereby very conveniently relying on the ready-made SWRCs from the library.

Another approach is that of the PTF which attempts to establish an empirical relationship between the sought-after parameters in the Campbell model and an easily measured one. A fitting example is the relationship between the Campbell b and sorptivity and air entry and sorptivity from Table 2:

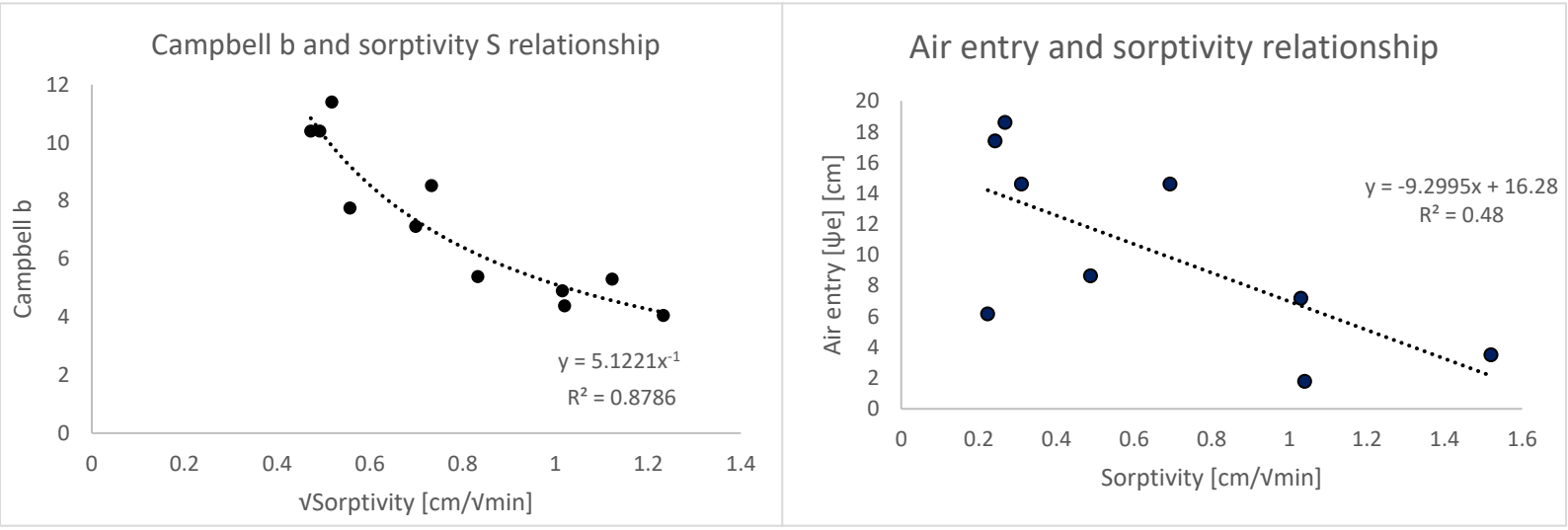

Figure 16 Empirical relationship between a) Campbell b and sorptivity and b) air entry potential ψe and sorptivity, based on Table 2 (Clapp and Hornberger, 1978). Values for silt loam and clay loam are omitted in b), as they are considered outliers.

The relationship between the Philip sorptivity and Campbell b is the second assumption of the method. Mathematically it can be displayed:

$$b = \frac{5.12}{\sqrt{S}} \qquad \text{Equation 12}$$

Regarding air entry the link is not as strong as the one between b and S, however in absence of more options to estimate ψe it may be used.

As for this assumption two things should be considered. Firstly, the relationship is built on the average b from Table 2, however as the standard deviation indicates there can be a high variance even within each soil class leading to some degree of uncertainty. Secondly, it is based on a US soil library and in this project the method is used on Danish soils perhaps introducing further uncertainty.

3.2.3 Method flowchart

The basic Two-ring Two-run method can be briefly described as follows:

1. Two or more DRI runs are performed – sorptivity is estimated from Run 1 using the single-term Philip model and saturated hydraulic conductivity from Run 2.
2. Campbell b and ψe are obtained from the sorptivity via the relationships in Figure 16.
3. Intact soils samples are used to obtain saturated water content from total porosity.

As a summation Figure 17 shows the end goals of this project – the twin Campbell curves, relevant parameters and the experiments or methods used to obtain them.

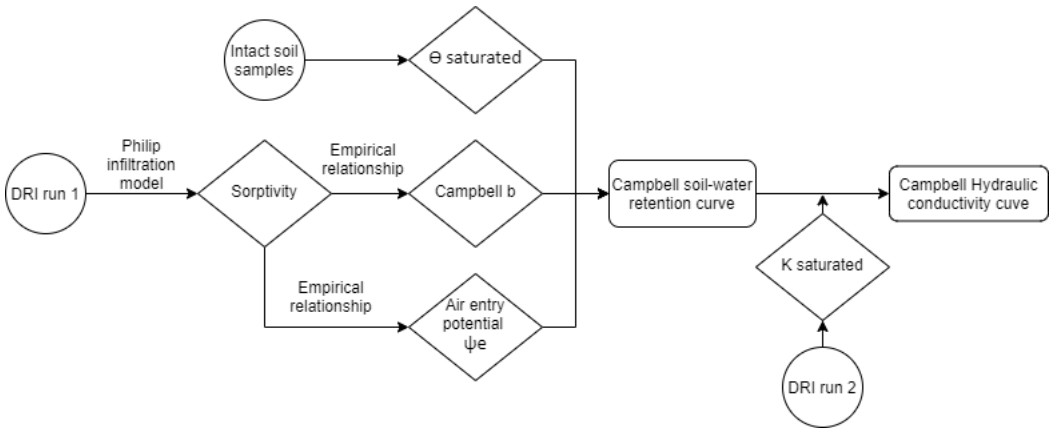

Figure 17 Flowchart illustrating the process of generating the twin Campbell curves (rectangles), the required parameters (diamonds) and the experiments used to obtain them (circles).

The rest of this chapter details the step-by-step procedure of this method of building the twin Campbell curves with a focus on getting a better estimation of ψe by taking a few additional steps.

3.3 Initial test

3.3.1 Location and soil description

In this chapter the step-by-step process of building the twin curves will be described using the experimental site at Thomas Mans Vej 23, Aalborg (TMV). The location is shown in Figure 18 - a grassy turf near Aalborg university's Department of Civil Engineering. The location was chosen due to proximity to the university laboratories and as a representative of urban soil. The infiltration experiment was performed in early October and the soil can is assumed to be at field capacity or drier as there had been no precipitation for over a week.

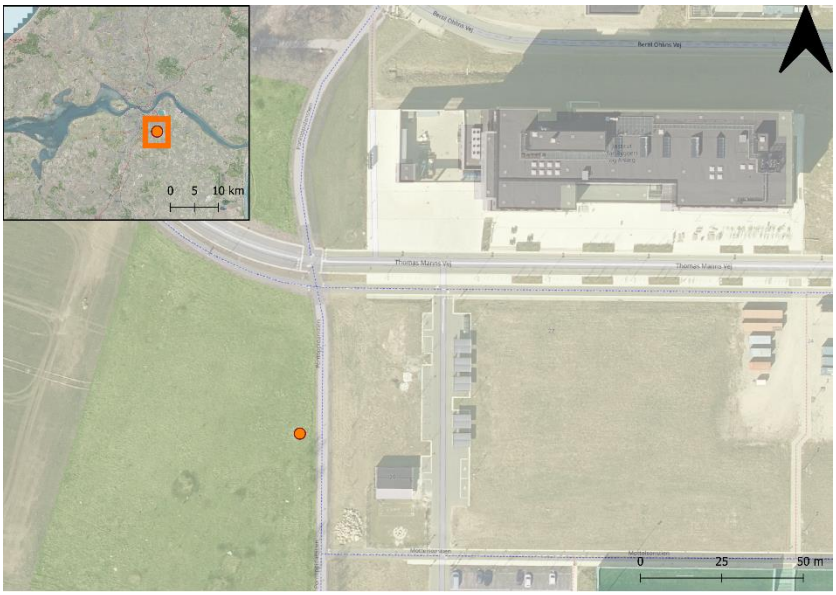

Figure 18 Location of experimental site at Thomas Mans Vej, Aalborg, the approximate spot where infiltration was performed is indicated by the orange circle.

Intact core samples (5cm diameter) and loose soil were collected after the infiltration experiment was finished and the soil was left to dry for a day. Loose soil samples were used to 1) texturally classify the soil using a sieving tower and shaker plates and 2) measure the air-dry water content. The small intact soil samples were used for 1) determining Ks under a constant head experiment 2)

measuring water contents at -100 and -300 cm suction (corresponding to pF 2 and ~2.5) with the help of a pressure plate/suction box and 3) to measure the dry bulk density, total porosity and organic matter content (via loss on ignition). Table 3 shows the resulting soil physical properties forming a "soil fingerprint" used to relate TMV to similar soils from the Danish soil library.

Table 3 TMV soil fingerprint and corresponding soil-relatives from Danish soil library (Hansen, 1976). Median, minimum and maximum values from 8 small intact soil samples.

	2-0.2 mm	*0.2-0.02 mm*	*0.02-0.002 mm*	*<0.002 mm*			
	Coarse sand [%]	**Fine sand [%]**	**Silt [%]**	**Clay [%]**	**OM [%]**	**pb [g/cm^3]**	**Θtot [cm^3/cm^3]**
TMV (grass)	58.0	36.4	2.8	2.8	2.1	1.52 (1.43-1.6)	0.424 (0.396-0.46)
Lundgaard 0-25	*63.1*	*26.6*	*3.8*	*4.3*	*2.2*	*1.5*	*0.434*
Studsgaard 0-22	*46.4*	*36.1*	*7.6*	*6.6*	*3.3*	*1.44*	*0.463*

3.3.2 Run 1 (unsaturated)

In (Cook & Broeren, 1994) the authors showed examples of how disk permeameters or infiltrometers can be used to obtain the Philip sorptivity. Figure 19a shows a plot of accumulated infiltration versus time with 2 distinct regions - I where the line is convexed and steady state has not been reached and II where the line is straight indicating steady state.

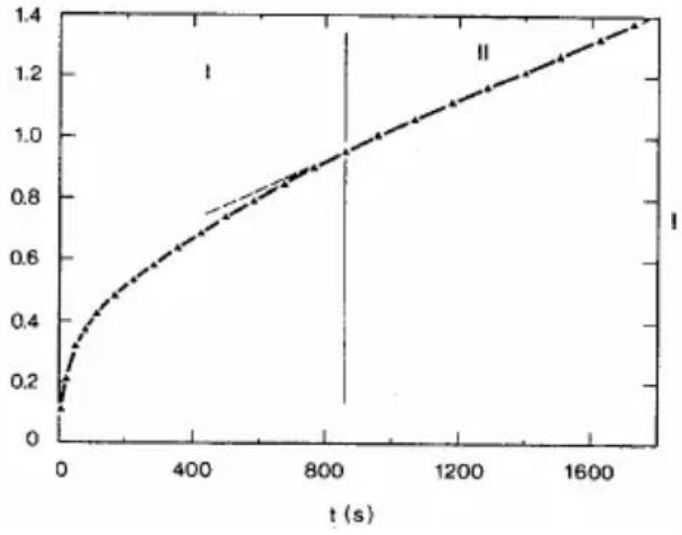

Figure 19a accumulated infiltration versus t - Region I shows flow prior to steady-state indicated by a curved line and Region II shows steady-state has been reached, indicated by a straight line. Figure by (Cook & Broeren, 1994).

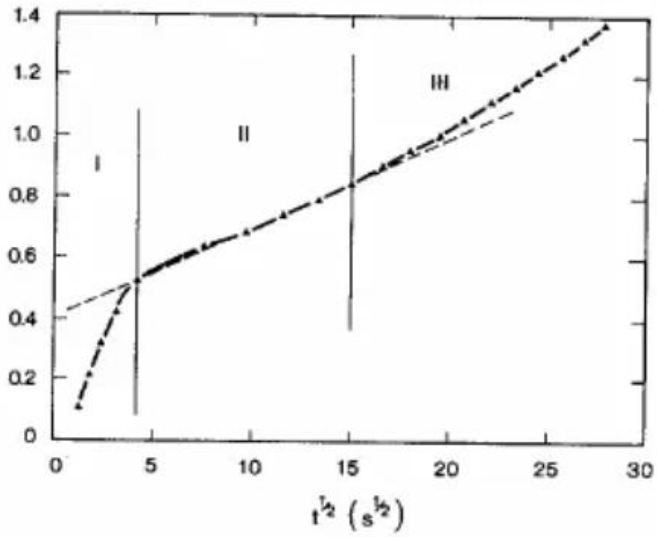

Figure 19a Accumulated infiltration versus √t - Region I shows adsorption of water into contact sand (used as a medium between soil and infiltrometer to ensure contact). Region II is where capillarity dominates the flow and region III is where gravity starts to have an effect. Sorptivity can be calculated by using the slope of Region II. Figure by (Cook & Broeren, 1994).

Figure 19b then shows a plot of accumulated infiltration versus √time for region I from Figure 19a where 3 regions are identified – I where water rapidly adsorbs to the sand medium used in the experiment between the soil and the permeameter, II where capillarity dominates as indicated by the straight line and III where gravity starts to have an effect and the line changes its slope.

If the initial soil conditions sufficiently dry and the experiment is carried out properly this should result in:

1. A plot of accumulated infiltration versus time showing two regions – unsteady state indicated by a convexed line and steady state indicated by a straight line.
2. A plot of accumulated infiltration versus √time for the unsteady state region where the part straight of the line indicates capillarity driven flow the slope of which is the Philip sorptivity.

Figure 20a shows the accumulated infiltration for TMV. Run 1 from can be divided into two regions, similarly to what is shown in (Cook & Broeren, 1994). Towards the 30th minute the line becomes straight.

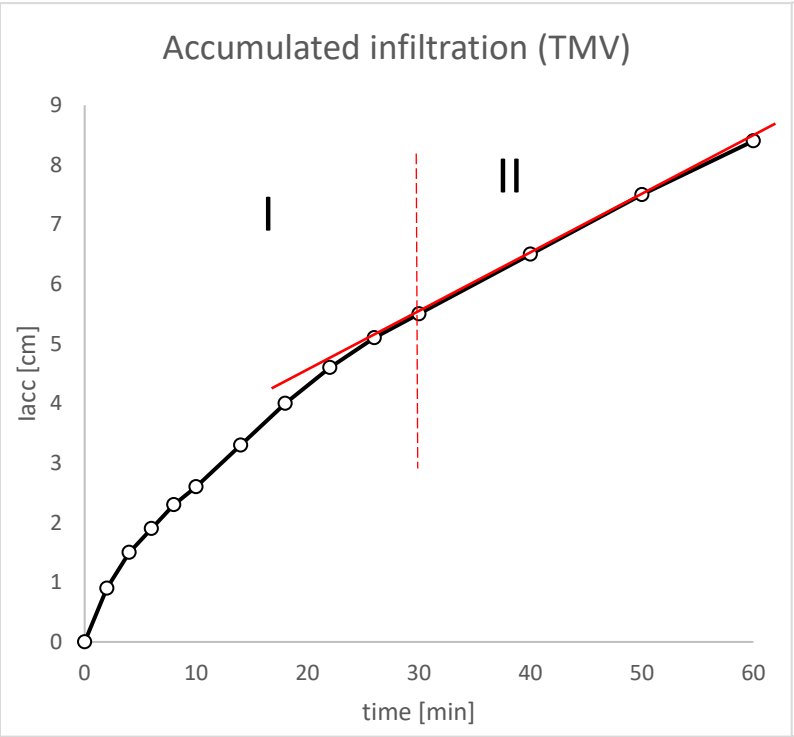

Figure 20a Accumulated infiltration versus time for Run 1. Region I shows unsteady state flow, indicating the effect of capillarity. Region II shows quasi-steady state as viewed by the straight segment of the curve. Division made by eye.

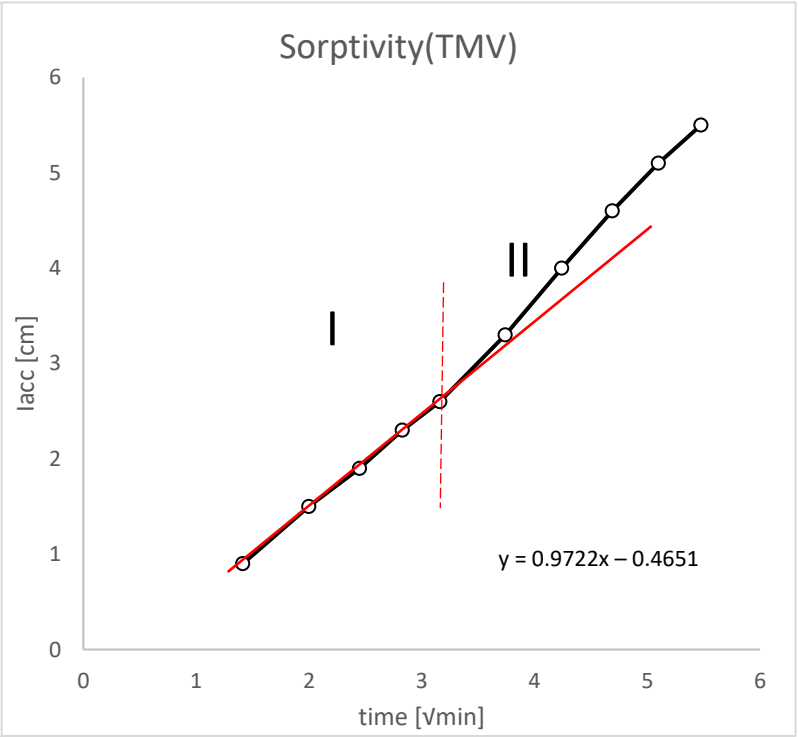

Figure 20b Accumulated infiltration versus time for Run 1. Region I is where capillarity is assumed to dominate and region II is where gravity starts to influence the flow. The slope of Region I is the sorptivity. Division made by eye.

Figure 20b shows a plot of accumulated infiltration versus √time for Region I from Figure 20a - the line is relatively straight from the beginning until little over minute 10. Then gravity starts to influence the flow and the capillary forces no longer dominate, as indicated by the divergence from the initial slope. Therefore, Region I with its first five points can be used to determine the sorptivity as the slope of the line - 0.972.

3.3.3 Run 2 (saturated)

Run 2 is used to estimate the saturated hydraulic conductivity. The first step is to plot the infiltration rate versus time to observe if the values are stable. This is shown in Figure 21.

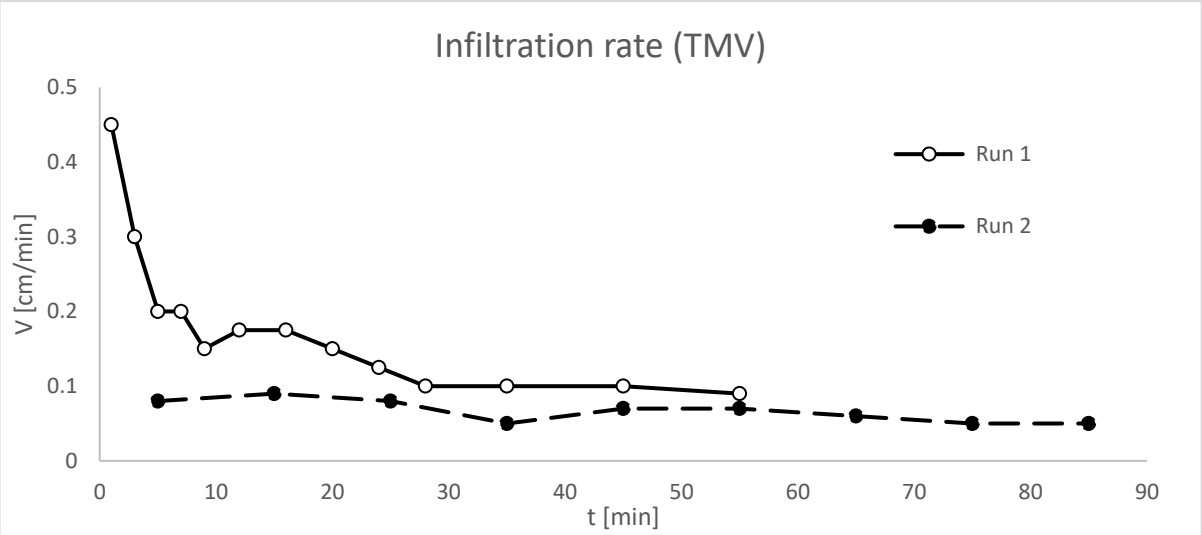

Figure 21 Infiltration rate versus time for Run 1 and 2. Steady state is already approached towards the end of Run 1 around the 30th minute. The line for Run 2 is stable indicating that Ks can be calculated.

It can be seen that the infiltration rate rapidly decreases over the course of Run 1 with the end point matching that in the beginning of Run 2. Over the course of Run 2 the infiltration rate slowly decreases and steady state. Obtaining Ks from the infiltration rate is detailed in appendix 9.4 and involves solving Darcy's law in a step-wise manner while estimating the hydraulic gradient in each step. As this is a falling head experiment the gradients drops with time. This is shown in Figure 22a along with the conductivity over Run 2 and the estimation of Ks - the mean of the last three measurements.

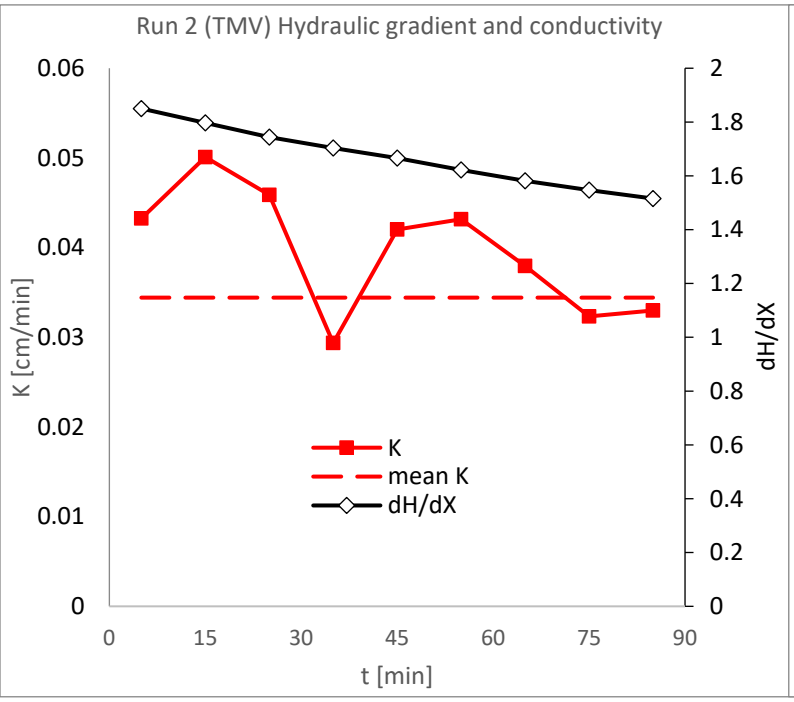

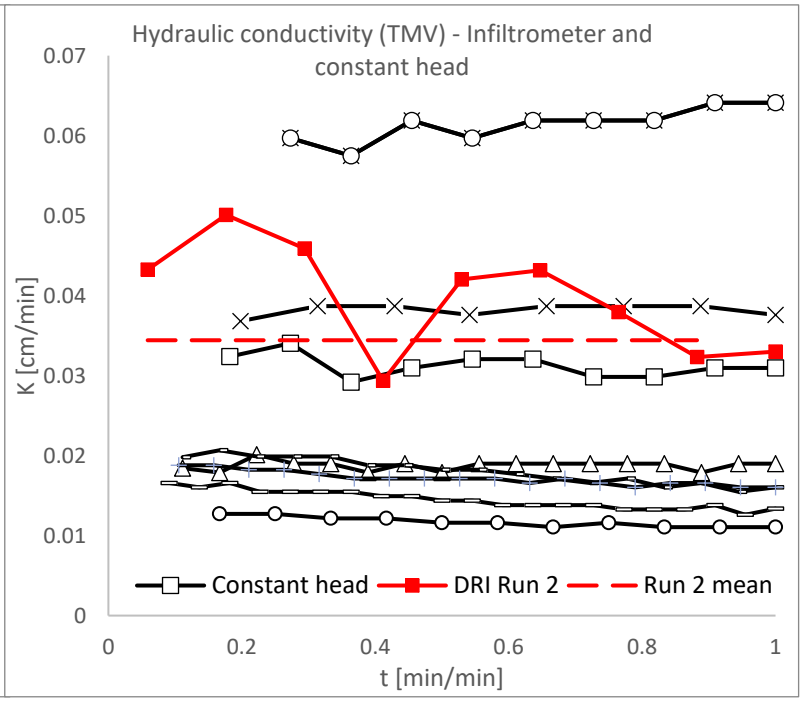

Figure 22 a) Hydraulic gradient and conductivity for Run 2. Gradient decreases over time as part of the falling head experiment, in black. Conductivity decreases over time, last two values are stable, in red. Dotted line is the mean of the final three measurements of K, assumed to be Ks. b) Hydraulic conductivity results from DRI and constant head on small intact samples. DRI values for Run 2 in red and values from the constant head experiments on the 8 intact soil samples in black.

Figure 22b shows the conductivity from Run 2 compared to the range of conductivities obtained from a constant head experiment on the small intact samples. The intact soil sample has a diameter of ~5 cm whereas the double ring infiltrometer's inner ring has a diameter of ~30cm. In essence the difference occurs due to soil heterogeneity – soils can vary highly from location to location even within the span of a few centimeters. Intact samples due to their small sampling size can produce both high and low results for Ks as is shown in Figure 22b but in this case show a lower value on average. The larger scale of the DRI on the other hand covers more ground and is less susceptible to spatial variability.

3.4 Constructing the Campbell retention and conductivity curves

Building the SWRC can be approached by dividing it into 4 segments:

- Segment 1 - straight line from pF 6 to pF 4.2. The water content at pF 6 can be obtained by air-drying soil in a room with ~50% relative humidity (Ravi et al., 2004). Gravimetric water content was obtained from loose soil that had been air-drying for several weeks by using rapid moisture analyzer. Gravimetric water content at pF 4.2 (permanent wilting point) can be estimated estimated from (Hansen, 1976) based on clay and organic matter content:

$$WC\ 4.2\ [\%\ weight] = 0.38Clay\% + 0.76OM\% + 0.38 \qquad \text{Equation 13}$$

  Conversion to volumetric water content is done by using the bulk density of the soil.
- Segment 2 – straight line from pF 4.2 to pF 3.2, the end of the wet zone and the upper limit of the Campbell model (Loll & Moldrup, 2000).
- Segment 3 – non-linear function from pF 3.2 to air entry ψe using the Campbell model. Here the missing component is the air entry potential ψe and there are three ways of obtaining this value. The first and simplest is to use literature values for similar soils like the ones in Table 2. In the of sandy soils the potential value ranges from 1.78 to 3.5 cm for sandy loam and sand, respectively. The second involves using the relationship between sorptivity and ψe, however it is considered a poor one. The third requires at least one water content measurement at a known soil-water potential i.e pF 2 and involves using Equation 1 and isolating ψe:

$$\psi e = \psi \left(\frac{\theta}{\theta s}\right)^{b} \qquad \text{Equation 14}$$

  Substituting θs with the median value from the intact samples 0.424 [cm^3/cm^3]; θ with the volumetric water content at pF 2– 0.227 [cm^3/cm^3]; ψ with the known soil-water potential of 100 [cm]; and b with the sorptivity-estimated value of 5.19 results in the following:

$$\psi e = 100 \times \left(\frac{0.227}{0.424}\right)^{5.19}$$

  If using one water content measurement in this case at pF 2 the result for ψe would be 3.9 [cm]. However, as there are two measured points ψe is best found by using the solver function in MS excel to minimize the difference between the two measured and modeled points (RMSE). This results in a ψe value of 3.54 [cm] for water contents at 2 and 2.5 pF of 0.227 and 0.175 [cm^3/cm^3]. In this case the difference is not large but having more calibration points is always preferable. When ψe is estimated by whichever approach the Campbell model can be used to plot the SWRC from air entry to pF 3.2.
- Segment 4 – straight vertical line from ψe to saturated water content θs.

These steps are summarized in Table 4 and the resulting SWRC is presented in Figure 23.

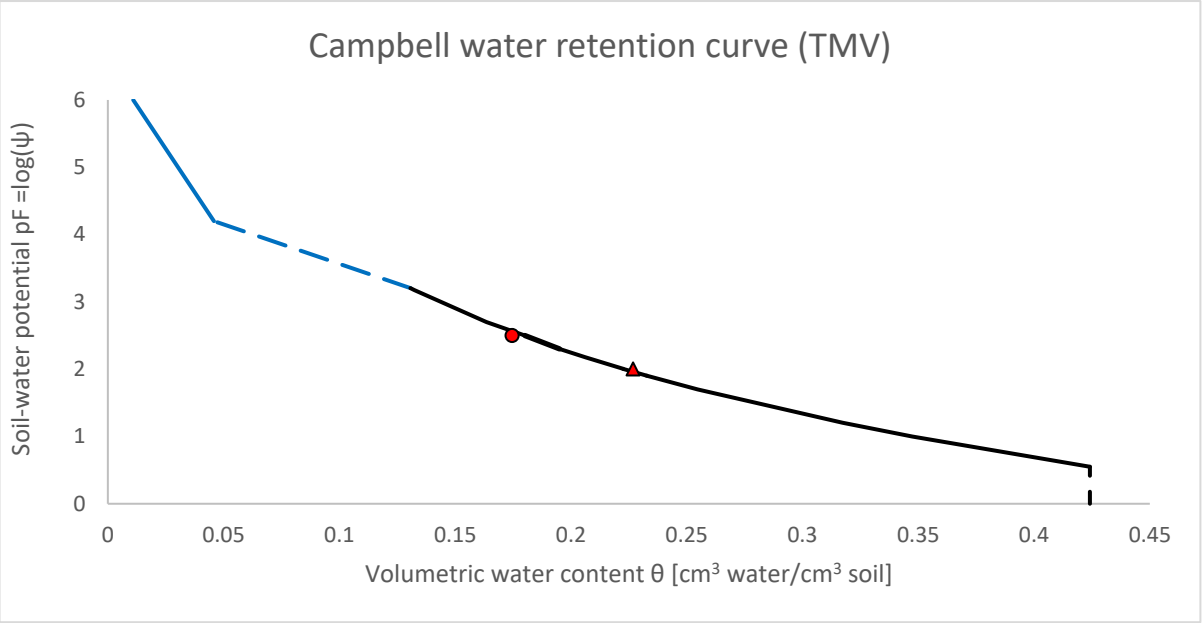

Figure 23 Campbell SWRC for TMV median Θ intact sample. Calibration points at pF2 and 2.5 shown in red triangle and circle, respectively. Segments 1 and 2 are shown in solid and dashed blue, respectively. Segments 3 and 4 are shown in solid and dashed black, respectively.

Table 4 Key points along the SWRC and how they are obtained.

Points [pF]	Method	Water content [cm^3/cm^3]	Reference
6.9	Assumed 0	0	(Vanapalli et al., 1998)
6	Measured from air-dried loose soil	0.011	(Ravi et al., 2004)
4.2	Estimated from clay and organic matter content	0.046	Equation 13 (Hansen, 1976)
2.5	Measured on small intact samples (median)	0.175	Appendix 9.3
2	Measured on small intact samples (median)	0.227	Appendix 9.3
0.55	Air entry value, Campbell model fit to pF 2 and 2.5 points	0.424	Equation 14 (Campbell, 1974)
"0"	Assumed equal to total porosity (median) from intact samples	0.424	Appendix 9.3 (Loll & Moldrup, 2000)

With the SWRC generated and all the hydraulic parameters estimated the Campbell hydraulic conductivity curve are present and thus the remaining step is to link the hydraulic conductivity to the water content using Equation 4. Figure 24 shows the result.

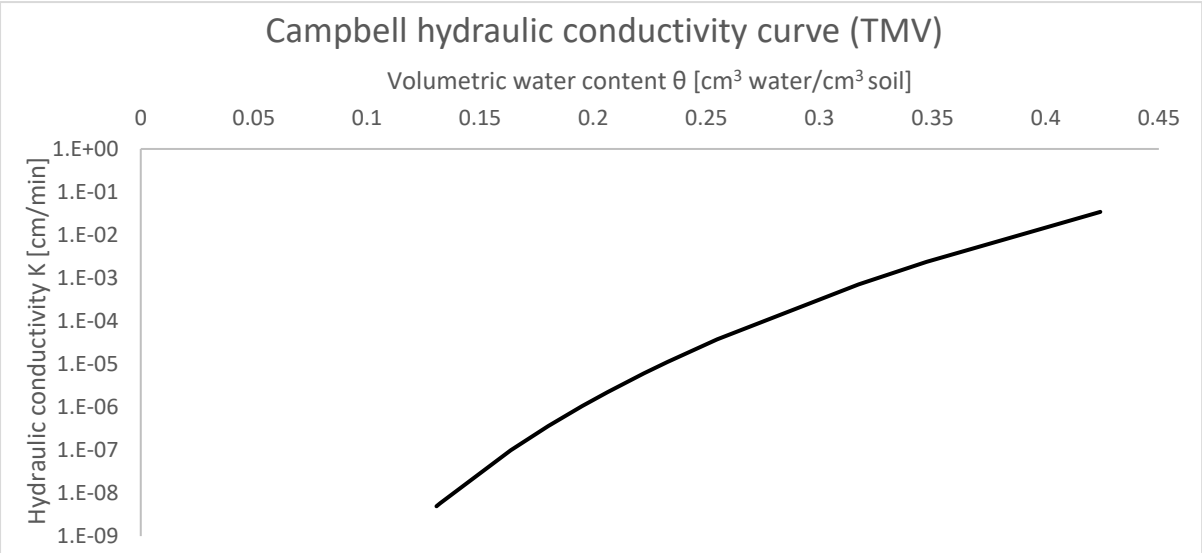

Figure 24 Campbell hydraulic conductivity curve for TMV. Generated using Equation 4, where Θ = 0.424 [cm³/cm³], b = 5.19, Ks = 0.034 [cm/min].

In the next section these results will be related to similar soils from the Danish and US soil libraries.

3.5 Comparison with similar Danish and American soils

3.5.1 Infiltration and sorptivity

The Philip model as shown in Equation 8 can be used to plot the accumulated infiltration versus time for different soil classes in the American soil library along with the results from Run 1. Only the first term of the equation is used as a comparison of the sorptivity is the goal of this plot. Three soils are chosen here – the closest according to texture and sorptivity estimation. The results can be seen in Figure 25.

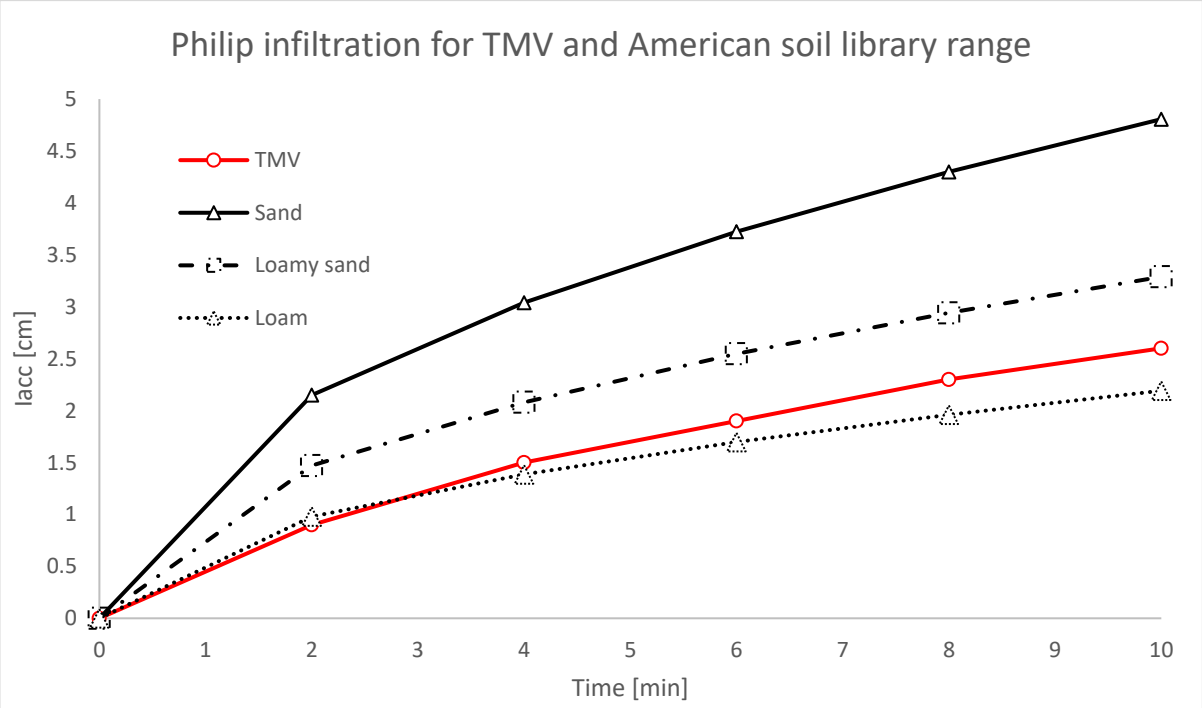

Figure 25 Accumulated infiltration versus time for TMV (experimental) and American soil library classes (modelled). TMV infiltration curve showed in red, as measured from Run 1. Modelled curves in black for the American soil library sand, loamy sand and loam, generated using the first term of Equation 8 with sorptivity values S = 1.52 , 1.04 , 0.693 [cm/√min], respectively. S value for TMV = 0.972 [cm/√min]

TMV is classified as sand according to texture and its calculated sorptivity from Run 1 is very similar to that of loamy sand, however the accumulated infiltration plot best matches that of loam. A possible explanation for this could be compaction although the site appeared rather pristine and even had to be "weeded out" before the experiment could be carried out.

3.5.2 Soil-water retention

The SWRC shown in Figure 23 is built using the median θs from the intact samples. It is worthwhile to visualize the maximum and minimum boundaries based on the gathered data, in a kind of a prediction or uncertainty band. The bands are constructed using the same method described previously in section 3.4. The upper band uses the maximum measured water contents on the small intact samples at pF 2.5 and 2 in combination with the maximum θs and vice-versa for the lower band. The b values are kept the same and ψe is calibrated for using the maximum and minimum parameter values instead of the median with the help of the solver function. Two more bands are formed by using soil-relatives from the American and Danish soil libraries. The results are shown in Figure 26. TMV falls within all bands, apart from θs values for the Danish soils band where Lundgaard and Studsgaard's porosities fall within the higher end of the measured values from the intact samples.

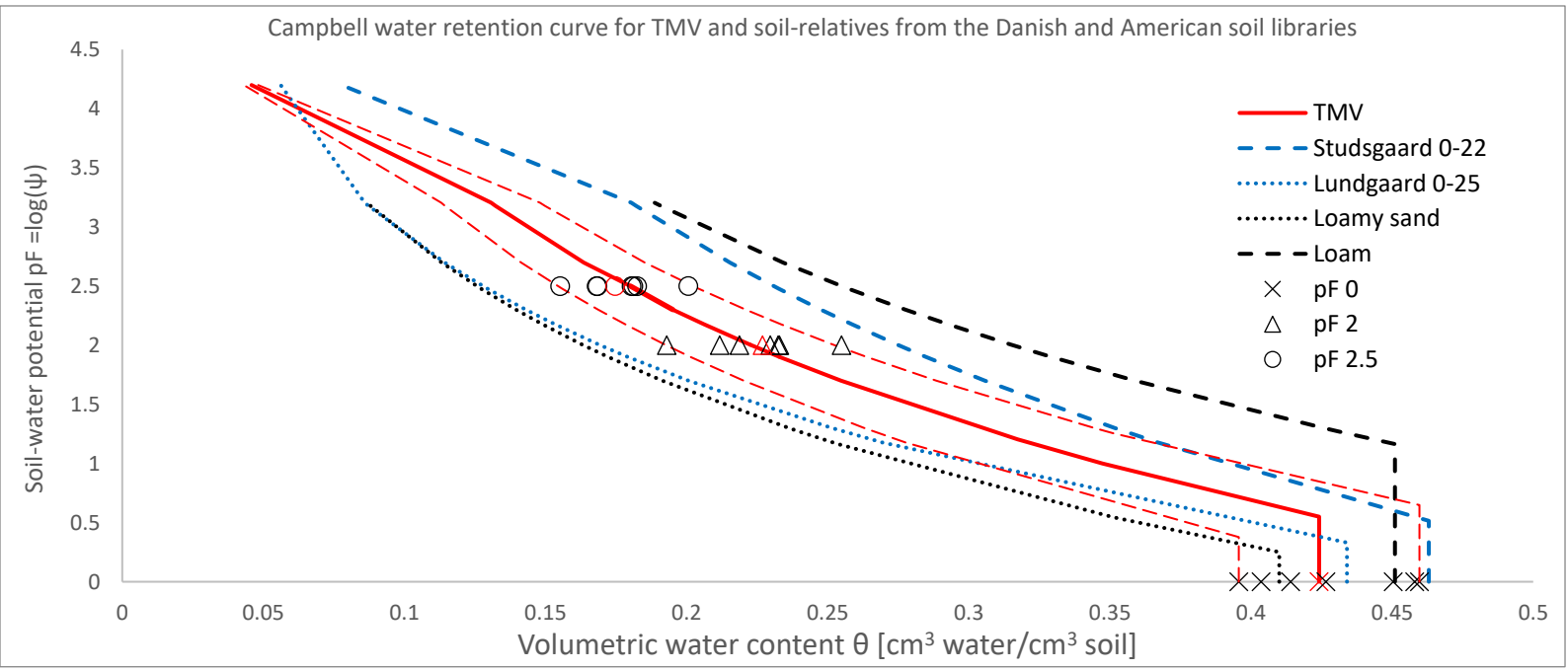

Figure 26 SWRC for TMV, shown in red. Includes uncertainty bands in dashed red for lowest and highest measured water contents. The soil-relatives from the Danish and American soil libraries shown in blue and black, respectively. Measured water contents on small samples at pF 2.5 and 2 and 0 indicated by circles, triangles and crosses, respectively, with median values in red used as calibration points for fitting the model. Table 5 lists all relevant soil parameters used to generate these curves.

3.5.3 Hydraulic conductivity

Similarly to the SWRC a prediction band can be formed for the hydraulic conductivity curve shown in Figure 24. The upper band is formed using the highest Ks from the constant head experiment in combination with the lowest θs values from the intact samples. The lower band is formed using the lowest Ks from the constant head experiment in combination with the highest θs values from the intact samples. Soil-relatives from the American and Danish libraries form two additional bands. The results are shown in Figure 27.

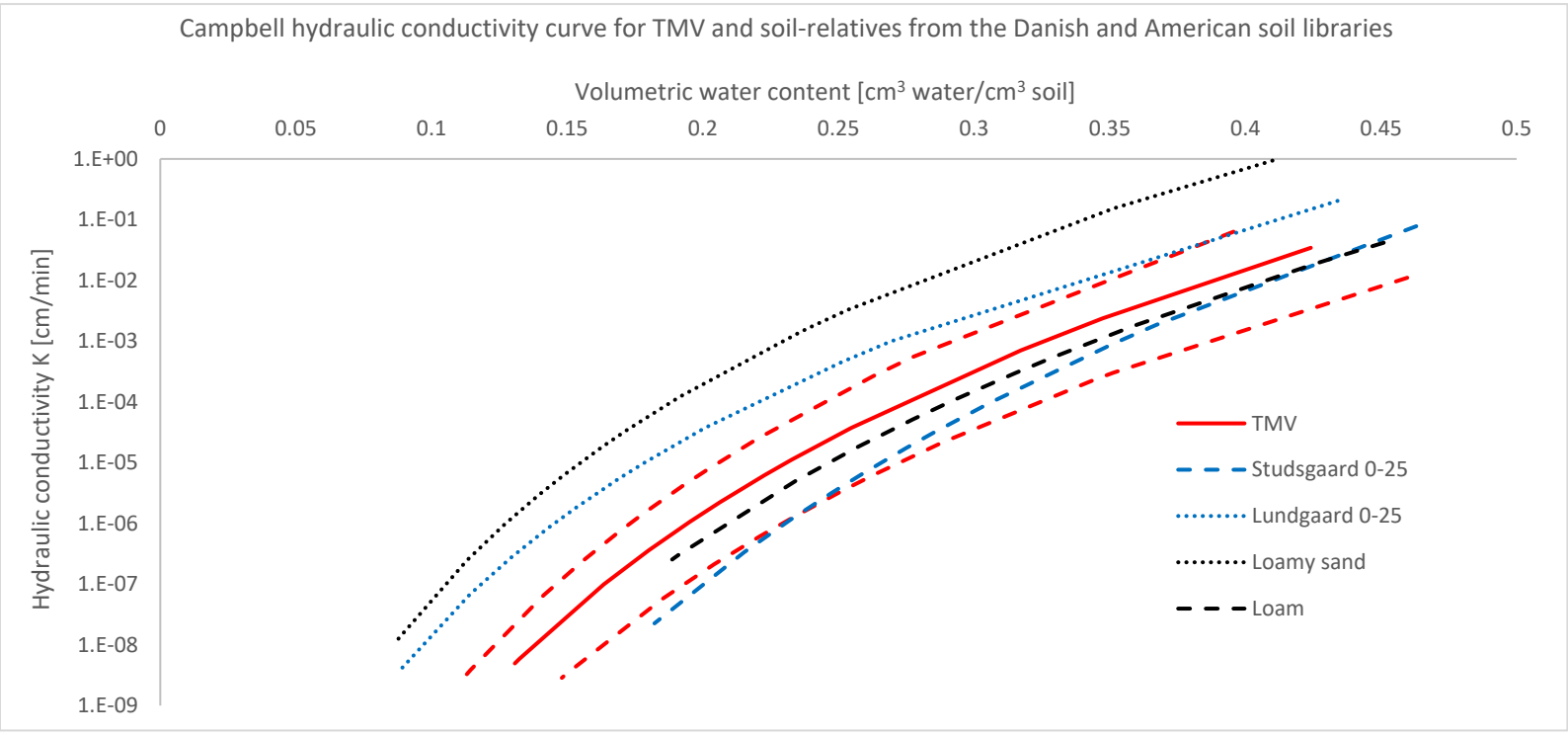

Figure 27 Hydraulic conductivity curve for TMV, shown in red. Includes uncertainty bands in red from lowest and highest values for ϑs and Ks. The soil-relative from the Danish and American soil libraries shown in blue and black, respectively. Table 5 lists all relevant soil parameters used to generate these curves.

Similarly to the SWRC TMV falls within all the bands, with Studsgaard topsoil layer and loam being closest to the average prediction.

3.5.4 Summary of parameter values

Table 5 shows the relevant hydraulic parameters used in the Philip and Campbell models for TMV and soil-relatives from the American and Danish soil libraries used in Figure 26 and Figure 27.

Table 5 Hydraulic properties for TMV and soils from Danish and American soil libraries used in Figure 26 and Figure 27. Median values with minimums and maximums in brackets.

	b	**ψe [cm]**	**θs[cm³/cm³]**	**Ks [cm/min]**	**S [cm/√min]**
TMV infiltration	5.19	3.54	0.424(0.396-0.46)	0.034	0.972
TMV small samples	4.75(4.4-5.28)	4.12(2.01-8.59)	-	0.016(0.011-0.063)	-
TMV band 1	5.19	4.45	0.460	0.011	-
TMV band 2	5.19	2.39	0.396	0.063	-
Lundgaard 0-25	4.13	3.38	0.434	0.204	-
Studsgaard 0-22	6.67	3.27	0.463	0.078	-
Loamy sand	4.38	1.78	0.410	0.938	1.040
Loam	5.39	14.6	0.451	0.0417	0.693
Clay	11.4	18.6	0.482	0.0077	0.268

4 Two-ring Two-run method test at six soil sites

In this chapter the Two-ring, Two-run method is tested at 3 locations with the purpose of creating the first steps towards a small database and testing the method on different soil types from urban to cultivated to forest. At Thomas Mans Vej and Gistrup the experiments were performed personally whereas the third location at St. Restrup was shared by students in the 7th semester of the 2020 Water and Environment course. As such some of the data available for TMV and Gistrup, for example a second measured point on the SWRC is not available for St. Restrup as the experiments there were carried out with a different purpose. Nevertheless, they are a valuable example of how the method can be applied with less information than what was shown in Chapter 3.

Figure 28 shows the locations of the three sites – Thomas Mans Vej, Gistrup and St. Restrup, all near Aalborg, Denmark.

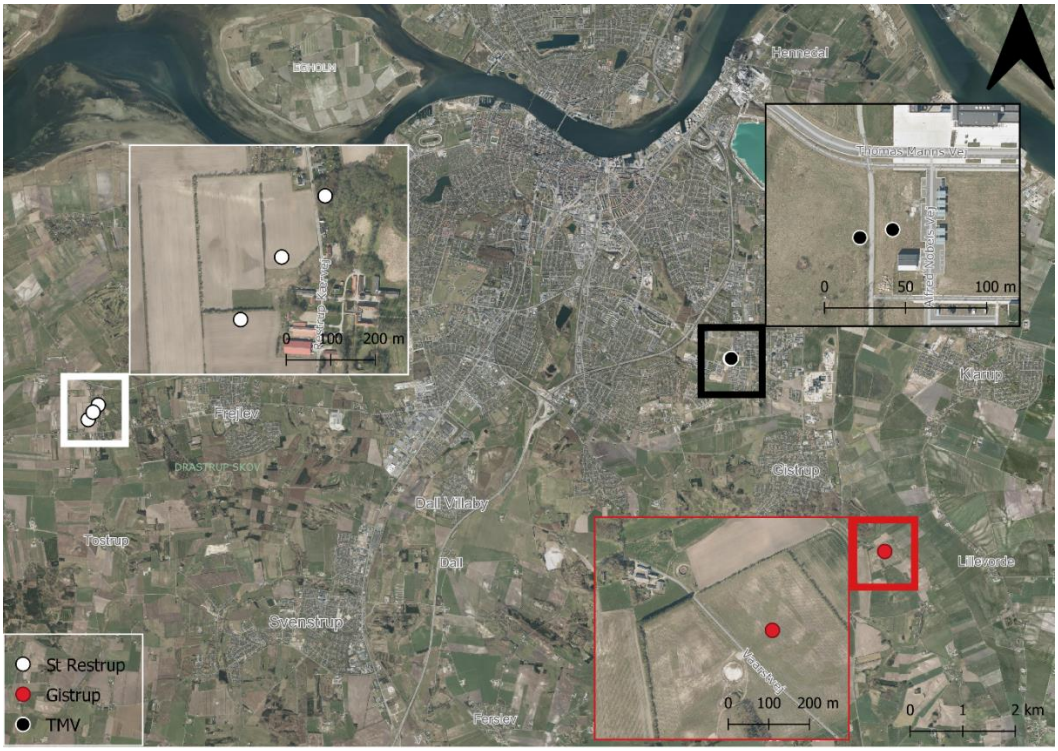

Figure 28 Experimental site locations - St Restrup in white, TMV in black and Gistrup in red.

The three locations differ in landuse:

- TMV represents urban soils, which have been impacted by human activity – in this case for aesthetic purposes as the location is next to a walking lane and the turf is kept grassy.
- The St. Restrup location comprises of three sites two of which are on agricultural fields used for growing maize and one is in an undisturbed forest.
- The Gistrup site is a former agricultural field which has been afforested by pine trees with the purpose of lessening the impact of agriculture on the local groundwater aquifer given that a layer of limestone is relatively close to the surface – within 1-5 meters. As an ex-agricultural field and current proto forest it falls somewhere between cultivated and forest currently more on the former side.

Given the geographical and landuse difference the three locations were expected to produce some variety, however texturally they all fall within the sand verging on loamy sand category of the USDA as shown in Figure 29.

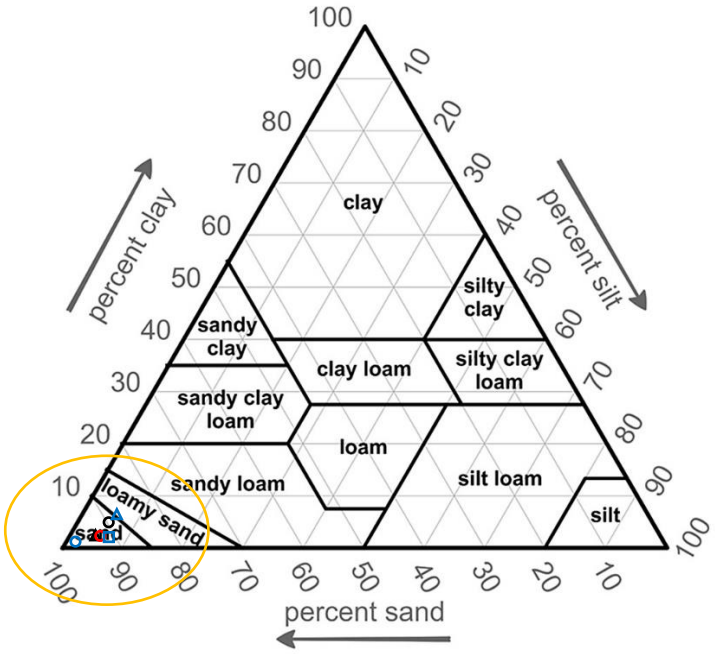

Figure 29 Location of soils in the USDA soil texture pyramid. TMV in black, Gistrup in red and St. Restrup in blue.

Even though all the soils are classified as sand where they differ is in their sand composition – coarse and fine – and in their level of compaction expressed by the bulk density and total porosity. Table 6 provides the relevant soil physical properties.

Table 6 Test sites soil fingerprint – texture, organic matter content, bulk density and total porosity

	2-0.2 mm	*0.2-0.02 mm*	*0.02-0.002 mm*	*<0.002 mm*			
	Coarse sand [%]	**Fine sand [%]**	**Silt [%]**	**Clay [%]**	**OM [%]**	**pb [g/cm^3]**	**Θtot [cm^3/cm^3]**
TMV (grass)	58.0	36.4	2.8	2.8	2.1	1.52 (1.43-1.6)	0.424 (0.396-0.46)
TMV 2 (grass)	26.7	62.2	5.5	5.5	3.1	1.43 (1.4-1.49)	0.46 (0.436-0.472)
Gistrup (pine sapplings)	32.0	62.2	2.8	2.8	2.7	1.4 (1.28-1.42)	0.472 (0.463-0.515)
St Restrup Forest	71.7	26.1	1.0	1.0	1.9	1.60	0.397
St Restrup Field 1 (maize)	25.3	63.0	5.7	5.7	2.4	1.45	0.453
St Restrup Field 2 (maize)	36.2	57.1	3.3	3.3	2.1	1.33 (1.28-1.37)	0.497 (0.483-0.518)

TMV 2 had just been mechanically mowed the previous day using a large commercial mowing machine. At Gistrup the limestone layer is relatively shallow– ~1-5 meters beneath the surface. St Restrup Forest and Field 1 results are based on one small intact sample hence the lack of STD.

4.1 Thomas Mans Vej and Gistrup sites

4.1.1 Soil physical properties

TMV 2 and Gistrup appear similar differing slightly in their fines composition with TMV 2 having a higher silt, clay and organic matter content. Gistrup also shows slightly higher spatial variability as seen by the larger range of bulk density and total porosity.

Table 7 TMV and Gistrup soil fingerprint – texture, organic matter content, bulk density and total porosity. Median values with minimum and maximum based on intact soil samples. Soil relative from (Hansen, 1976) in italic.

	2-0.2 mm	*0.2-0.02 mm*	*0.02-0.002 mm*	*<0.002 mm*			
	Coarse sand [%]	**Fine sand [%]**	**Silt [%]**	**Clay [%]**	**OM [%]**	**pb [g/cm³]**	**Θtot [cm³/cm³]**
TMV 2 (grass)	26.7	62.2	5.5	5.5	3.1	1.43 (1.4-1.49)	0.46 (0.436-0.472)
Gistrup (pine sapplings)	32.0	62.2	2.8	2.8	2.7	1.4 (1.28-1.42)	0.472 (0.463-0.515)
Ødum 0-45	21.3	49.6	14.7	11.7	2.3	1.48	0.436

4.1.2 Run 1

Figure 30a shows the accumulated infiltration for Run 1 at TMV and Gistrup. The difference between the sites is expressed in both higher total infiltrated water and lower time to achieve it for Gistrup. This results in a higher sorptivity as shown in Figure 30b. This is possibly due to the difference in fines content, however as hinted by the high variability preferential flow could also be a contributing factor.

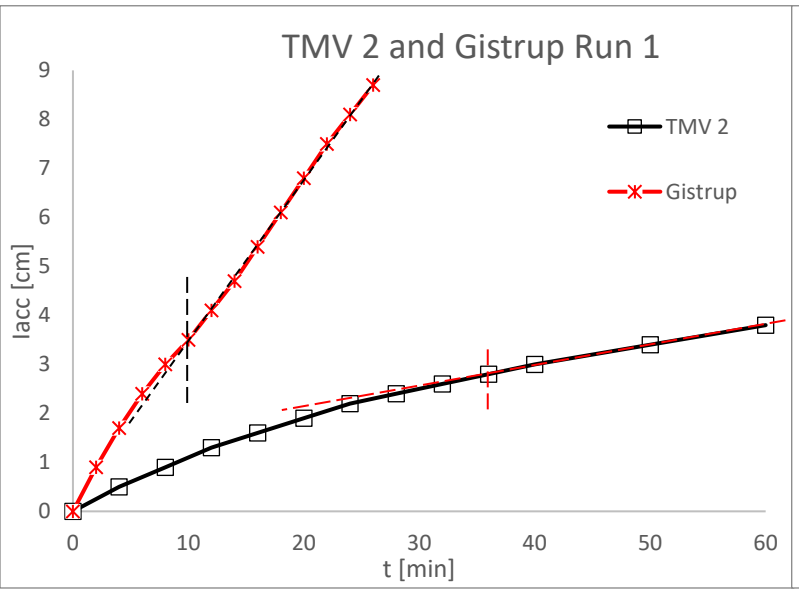

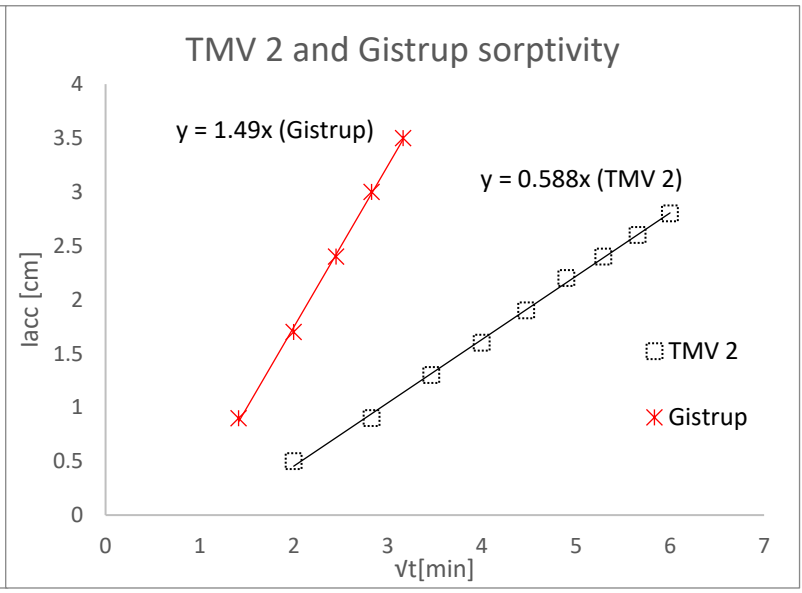

Figure 30 a) TMV 2 and Gistrup accumulated infiltration versus time for Run 1. Transition between unsteady and steady state indicated by eye. b) Accumulated infiltration versus √time for unsteady state region and resulting sorptivity.

Figure 31 and Figure 32 show the SWRC for the two sites and where they fall compared to loamy sand and loam from the American soil library and their soil-relatives from the Danish soil library. TMV 2 shows a very good match with its soil relative Ødum and both are close to the loam curve. The close fit is unusual as TMV 2 is a sandy soil and Ødum is classified as clayey topsoil (mull) and the clay and silt content of the two is quite different. The match could be attributed to possible compaction due to the removal of grass with a mower the previous day. Gistrup on the other hand behaves more like a sandy soil expressed by its proximity to both loamy sand and Lundgaard which is classified as sandy topsoil.

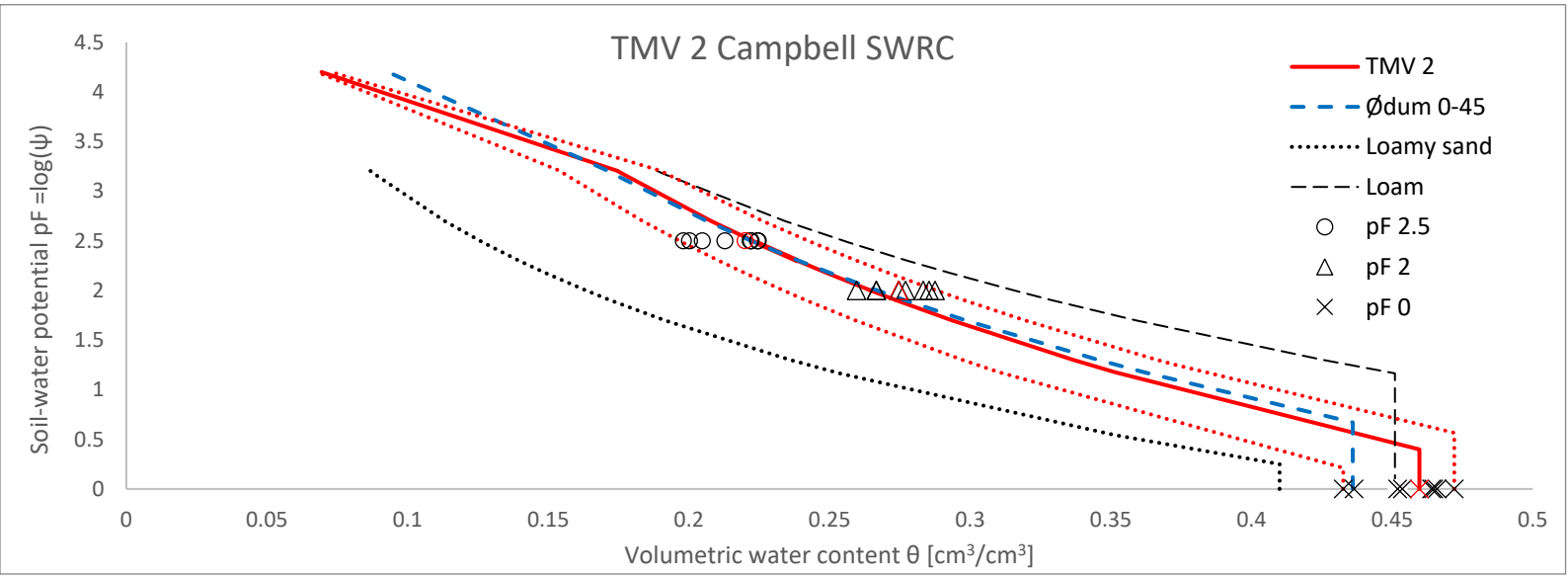

Figure 31 SWRC for TMV 2 in red. Uncertainty bands dashed red for lowest and highest measured water contents. American soil library soil band in black. SWRC for the soil-relative from the Danish soil library in blue. Circles, triangles and crosses show the measured water contents at pF 2.5, 2 and 0, respectively, with values in red used as calibration points for fitting the model. All parameter values listed in Table 8.

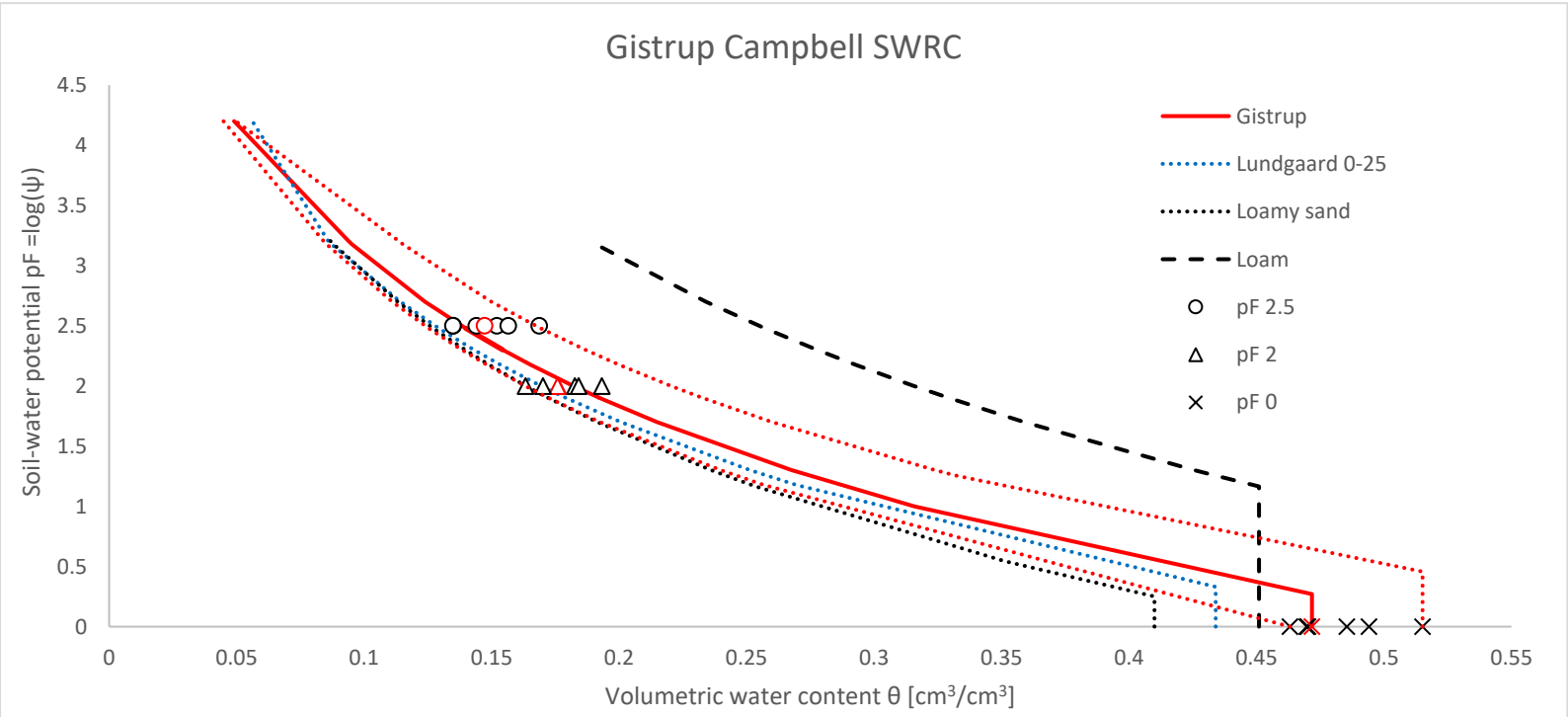

Figure 32 SWRC for Gistrup in red. Includes uncertainty bands in dashed red for lowest and highest measured water contents. The soil-relatives from the Danish and American soil libraries shown in blue and black, respectively. Measured water contents at pF 2.5 and 2 and 0 indicated by circles, triangles and crosses, respectively, with values in red used as calibration points for fitting the model. All parameter values listed in Table 8.

4.1.3 Run 2

Figure 33 shows Run 2 for both sites as a plot of hydraulic conductivity versus time. The hydraulic gradient is shown as a secondary axis showing the similarity between experimental conditions. The mean Ks calculated as the last 3 measurements of for each site is higher for Gistrup than TMV 2 by a considerable margin. Gistrup exhibits a Ks within the sandy soil range and TMV 2 falls within the loamy range according to the US soil library (see table Table 2). Another key difference is the large variability in the hydraulic conductivity measurements of Gistrup resulting in a less stable and therefore more uncertain estimate of Ks.

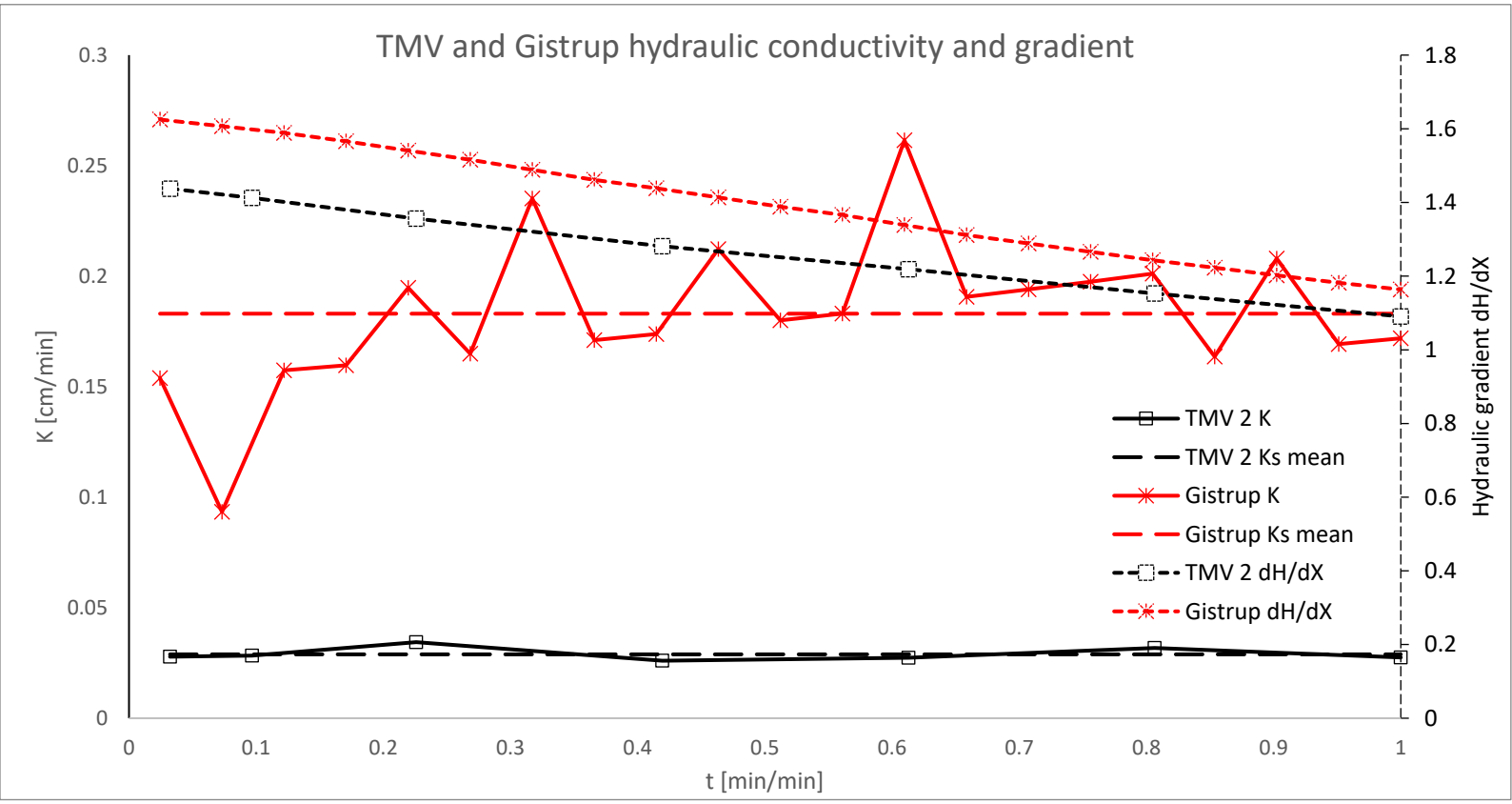

Figure 33 Hydraulic conductivity and gradient for TMV and Gistrup in black and red, respectively.

Figure 34 and Figure 35 show the Campbell HCCs for TMV 2 and Gistrup and their soil relatives. TMV 2 is close to the loam curve and far from the Ødum one unlike its close match on the SWRC. This could be attributed to Ødum's higher Ks compared to TMV 2 as the curves otherwise look similar in shape, apart from their anchoring position dependent on Ks and θs. A similar situation can be seen for Gistrup where the curve shape resembles that of Lundgaard albeit with a lower Ks value.

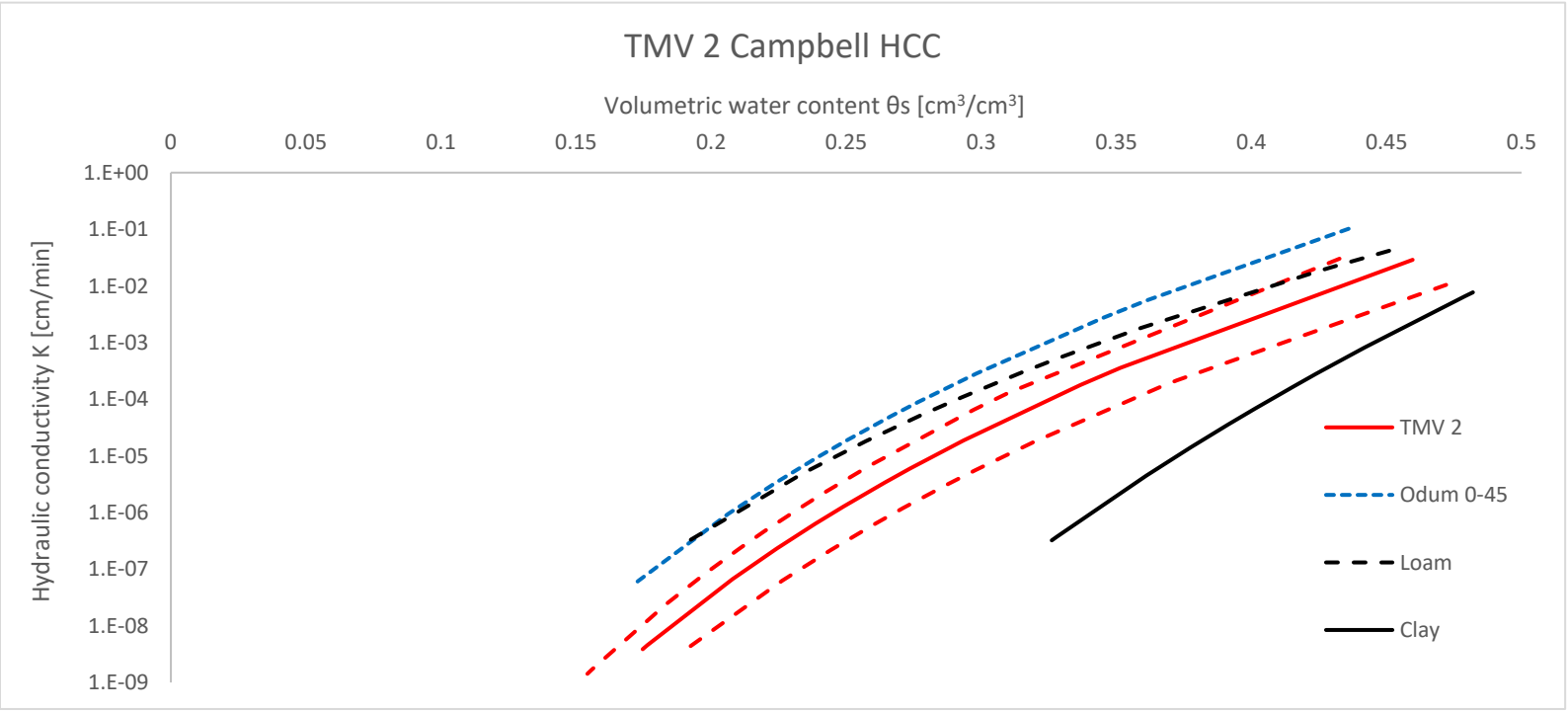

Figure 34 Hydraulic conductivity curve for TMV 2, in red. Includes uncertainty bands in red from lowest and highest values for ϑs and Ks. Soil-relatives from the Danish and American soil libraries shown in blue and black, respectively. All parameter values listed in Table 8.

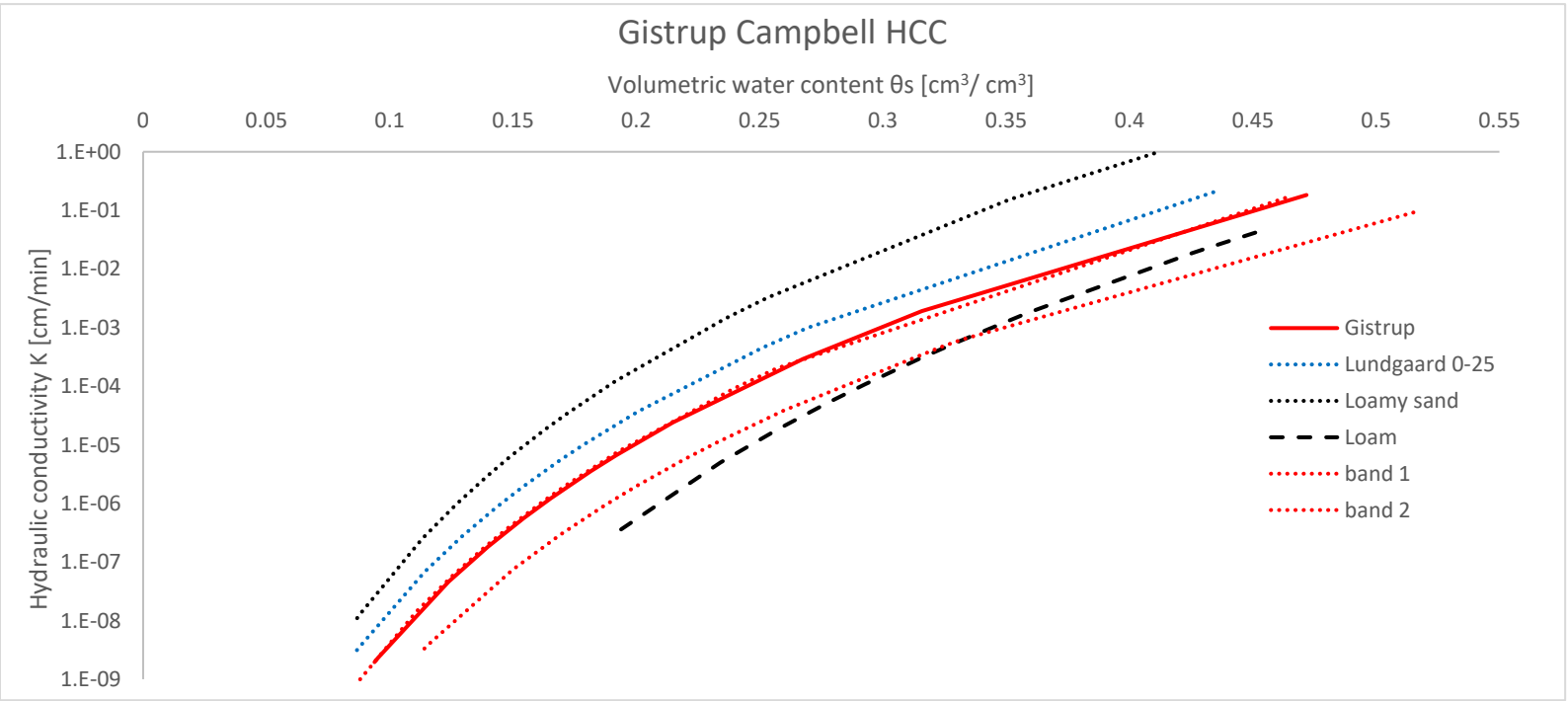

Figure 35 Hydraulic conductivity curve for Gistrup, shown in red. Includes uncertainty bands in red from lowest and highest values for ϑs and Ks. Soil-relatives from the Danish and American soil libraries shown in blue and black, respectively. All parameter values listed in Table 8.

4.1.4 Summary of parameter values for retention and conductivity.

Table 8 Hydrological properties for TMV 2 and Gistrup

	b	ψe [cm]	θs [cm^3/cm^3]	Ks [cm/min]
TMV 2	6.68	2.50	0.460	0.029
TMV 2 band 1	6.68	3.69	*0.472*	*0.010*
TMV 2 band 2	6.68	1.63	*0.433*	*0.030*
Gistrup	4.18	1.87	0.472	0.183
Gistrup band 1	*4.18*	*2.87*	*0.515*	*0.092*
Gistrup band 2	*4.18*	*1.27*	*0.463*	*0.282*
Lungaard 0-25	*4.08*	*2.14*	*0.434*	*0.204*
Ødum 0-40	*6.24*	*4.68*	*0.436*	*0.102*
Sand	*4.05*	*3.5*	*0.395*	*1.056*
Loamy sand	*4.38*	*1.78*	*0.410*	*0.938*
Loam	*5.39*	*14.6*	*0.451*	*0.0417*
Clay	*11.40*	*18.6*	*0.482*	*0.0077*

4.2 St. Restrup sites

4.2.1 Soil physical properties

The soils at the St. Restrup location vary significantly between one another as seen in Table 9 possibly due to the difference in land use. However, even in between the same land use the two agricultural fields differ in fines content, bulk density and total porosity. All three soils are sandy with the two fields showing similar composition of a larger fine sand fraction as opposed to the forest site which is very coarse. What's interesting is the lower OM % of the forest soil compared to the agricultural fields, as the it is usually the opposite (Osman & Osman, 2013) (Druckenbrod, 2012).

Table 9 St Restrup soil fingerprint – texture, organic matter content, bulk density and total porosity. Soil relative based on texture and bulk density shown in italic.

	2-0.2 mm	*0.2-0.02 mm*	*0.02-0.002 mm*	*<0.002 mm*			
	Coarse sand [%]	**Fine sand [%]**	**Silt [%]**	**Clay [%]**	**OM [%]**	**pb [g/cm^3]**	**Θtot [cm^3/cm^3]**
Forest	71.7	26.1	1.0	1.0	1.9	1.60	0.397
Lundgård 25-55	*67.6*	*24.7*	*3.1*	*3.3*	*1.3*	*1.51*	*0.447*
Field 1 (maize)	25.3	63.0	5.7	5.7	2.4	1.45	0.453
Borris 0-40	37.2	48.4	6.9	5.3	*2.2*	*1.50*	*0.420*
Field 2 (maize)	36.2	57.1	3.2	3.2	2.1	1.33 (1.28-1.37)	0.497 (0.483-0.518)
Tylstrup 0-28	*12.0*	*75.7*	*6.2*	*3.7*	*2.3*	*1.39*	*0.441*

4.2.2 Run 1

Figure 36 shows Run 1 and the resulting sorptivities for the three sites at St. Restrup. The sites are quite unique when compared to each other with the Forest showing very high infiltration capacity as it absorbs the same amount of water as Field 2 in a third of the time. Within the same landuse the difference is notable possibly explained by Field 1's higher fines content and higher bulk density. The resulting sorptivities exceed the sandy range for the Forest and Field 2 sites and Field 1 is within the loamy range (see table Table 2).

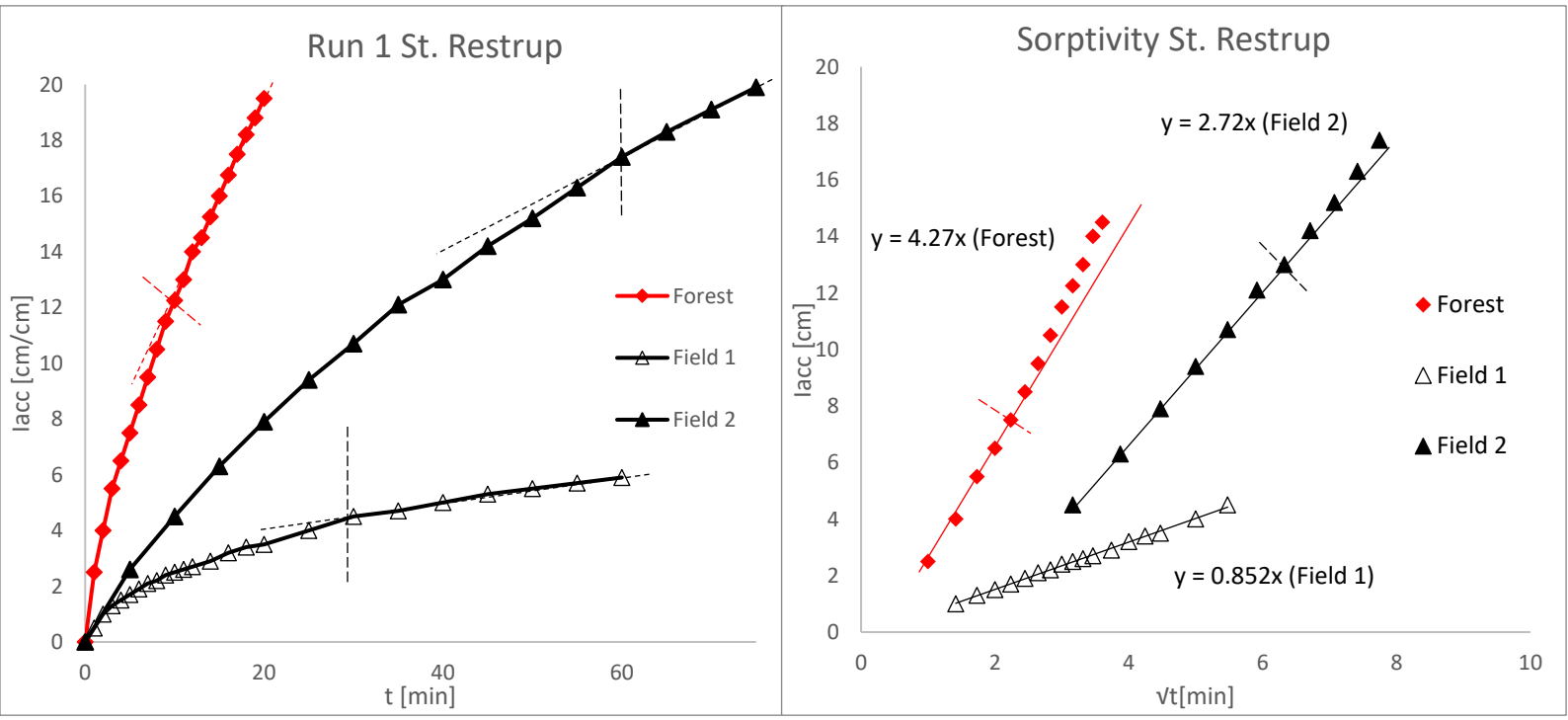

Figure 36 a) St. Restrup accumulated infiltration versus time for Run 1. Transition between unsteady and steady state made by eye. b) Accumulated infiltration versus √time for unsteady state region and resulting sorptivity.

Figure 37 shows the SWRCs for St. Restrup. For the Forest site the curve apart from its high air entry value resembles that of Lundgaard and sand. Field 1 exhibits strange characteristics mainly due to its very low air entry value which is a result of a high b value characteristic of a very slow infiltrating soil. Furthermore, the measured water content at pF 2 was unrealistically low (see appendix 9.3) and therefore considered erroneous so the Field 2 water content was used instead. Field 2 resembles loamy soils in its wet end and sandy soils in its dry end.

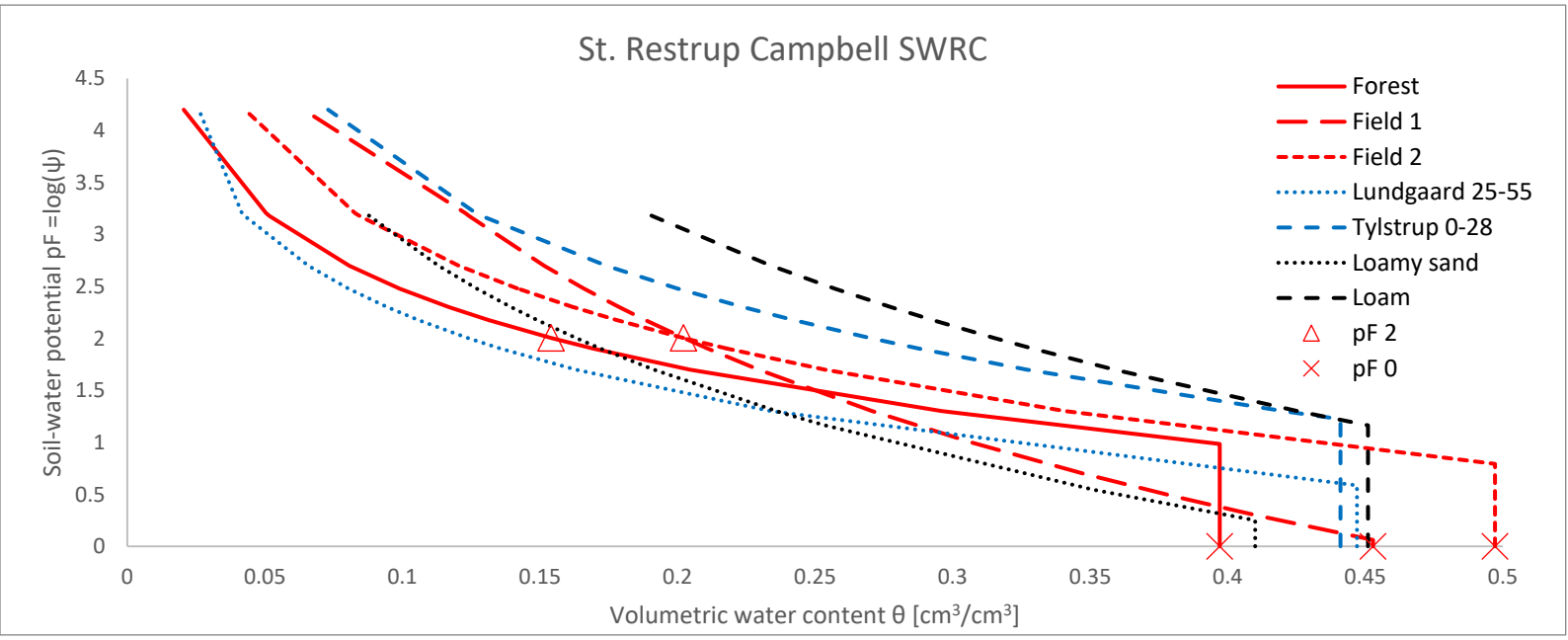

Figure 37 SWRC for St Restrup Forest Field 1 and 2, in red. Soil-relatives from the Danish and American soil libraries in blue and black, respectively. Measured water contents at pF 2 and 0 shown in triangles and crosses, respectively. All relevant parameter values listed in

4.2.3 Run 2

Figure 38 shows Run 2 for the St. Restrup sites as a plot of hydraulic conductivity versus time. As hinted by Run 1 and the infiltration capacity the Forest site has the highest conductivity followed by Field 2 and Field 1. The Forest site is very unstable and therefore its Ks value falls within the sandy range but perhaps cannot be considered as saturated. Field 2 shows less variance and lower Ks falling within a loamy soil range. Field 1 is interesting as it exhibits a hydraulic conductivity within the clay spectrum even though it is a sandy soil and having the highest hydraulic gradient of all sites.

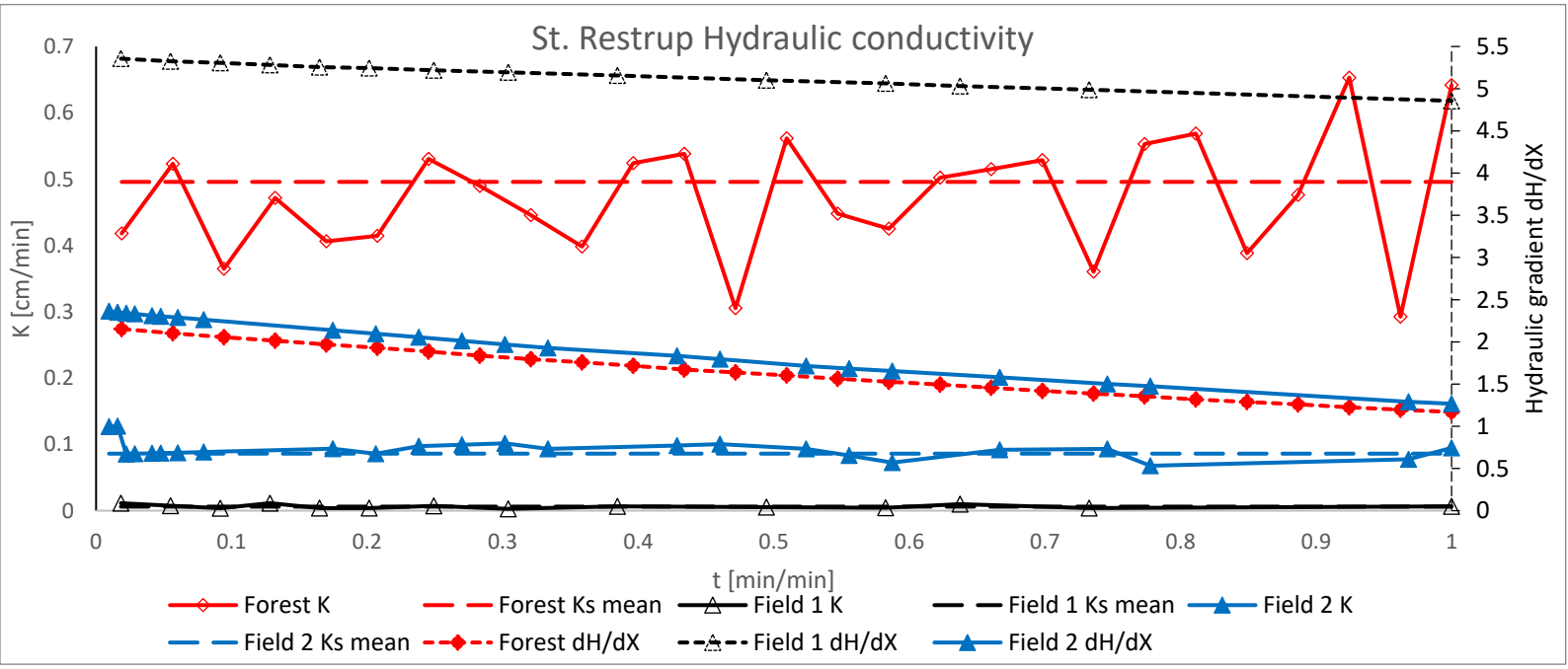

Figure 38 Hydraulic conductivity and gradient for St. Restrup Forest, Field 1 and 2 in red, black and blue, respectively.

Figure 39 shows the Campbell HCCs for St. Restrup and their soil relatives. The Forest site resembles sand in the wet range but has a considerably higher conductivity in the dry range. Field 1 site's curve is shaped similarly to that of Borris and loam, however due to its very low Ks falls closer to the clay curve. Field 2 shows the same tendency of behaving like loam in the wet range and loamy sand in the dry range.

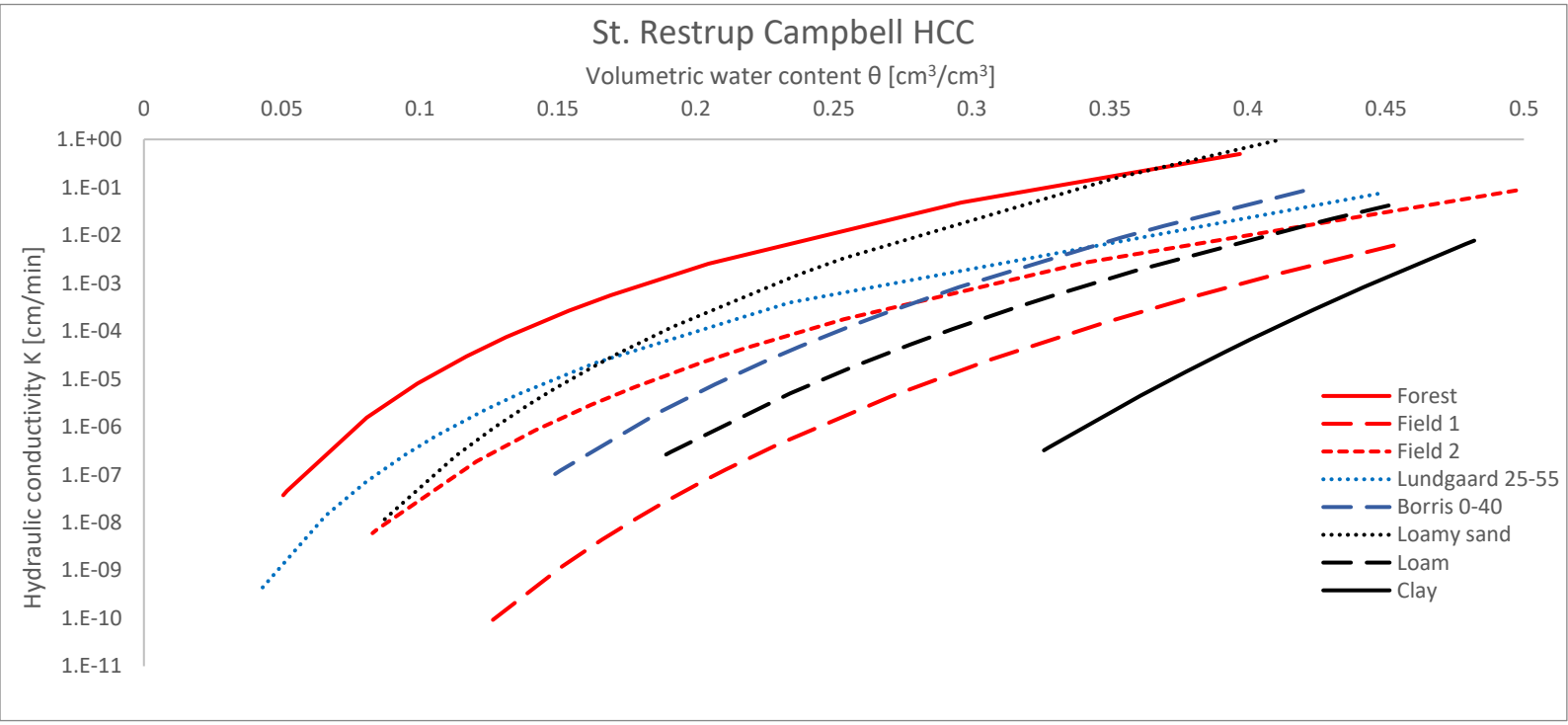

Figure 39 Hydraulic conductivity curve for St. Restrup in red. The soil-relatives from the Danish and American soil libraries shown in blue and black, respectively. All relevant parameter values listed in

4.2.4 Summary of parameter values for retention and conductivity

Table 10 Hydrological properties for St Restrup

	b	ψe [cm]	θs [cm³/cm³]	Ks [cm/min]
Forest	2.48	9.67	0.397	0.496
Field 1	5.55	1.15	0.453	0.006
Field 2	3.10	6.22	0.497	0.086
Lungaard 0-25	4.08	2.14	0.434	0.204
Borris 0-40	5.07	8.39	0.420	0.084
Tylstrup 0-28	3.66	16.75	0.441	0.114
Loamy sand	4.38	1.78	0.410	0.938
Loam	5.39	14.6	0.451	0.0417
Clay	11.40	18.6	0.482	0.0077

4.3 All sites compared

4.3.1 Infiltration and sorptivities

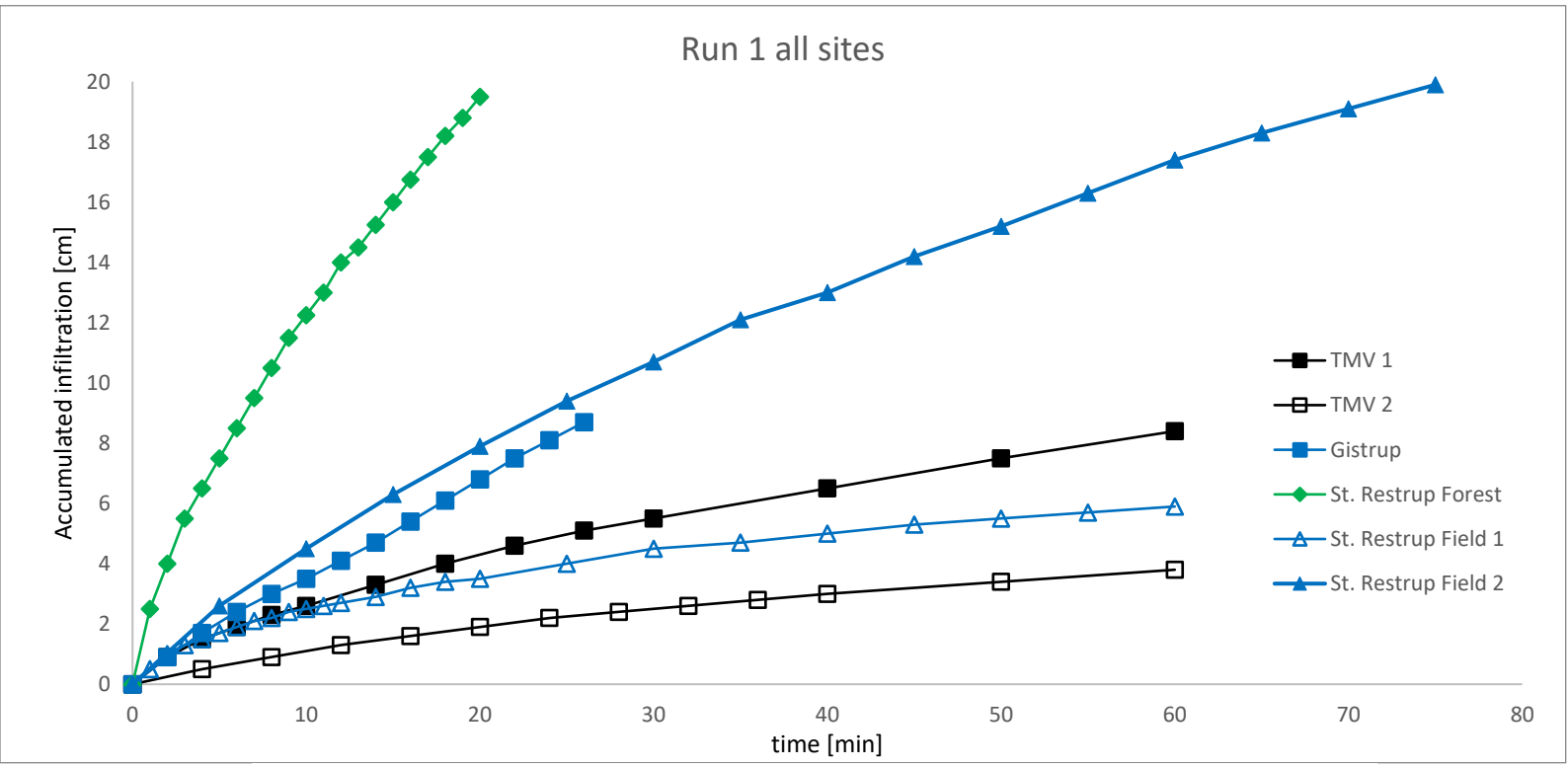

Figure 40 Run 1 - Accumulated infiltration versus time for all sites.

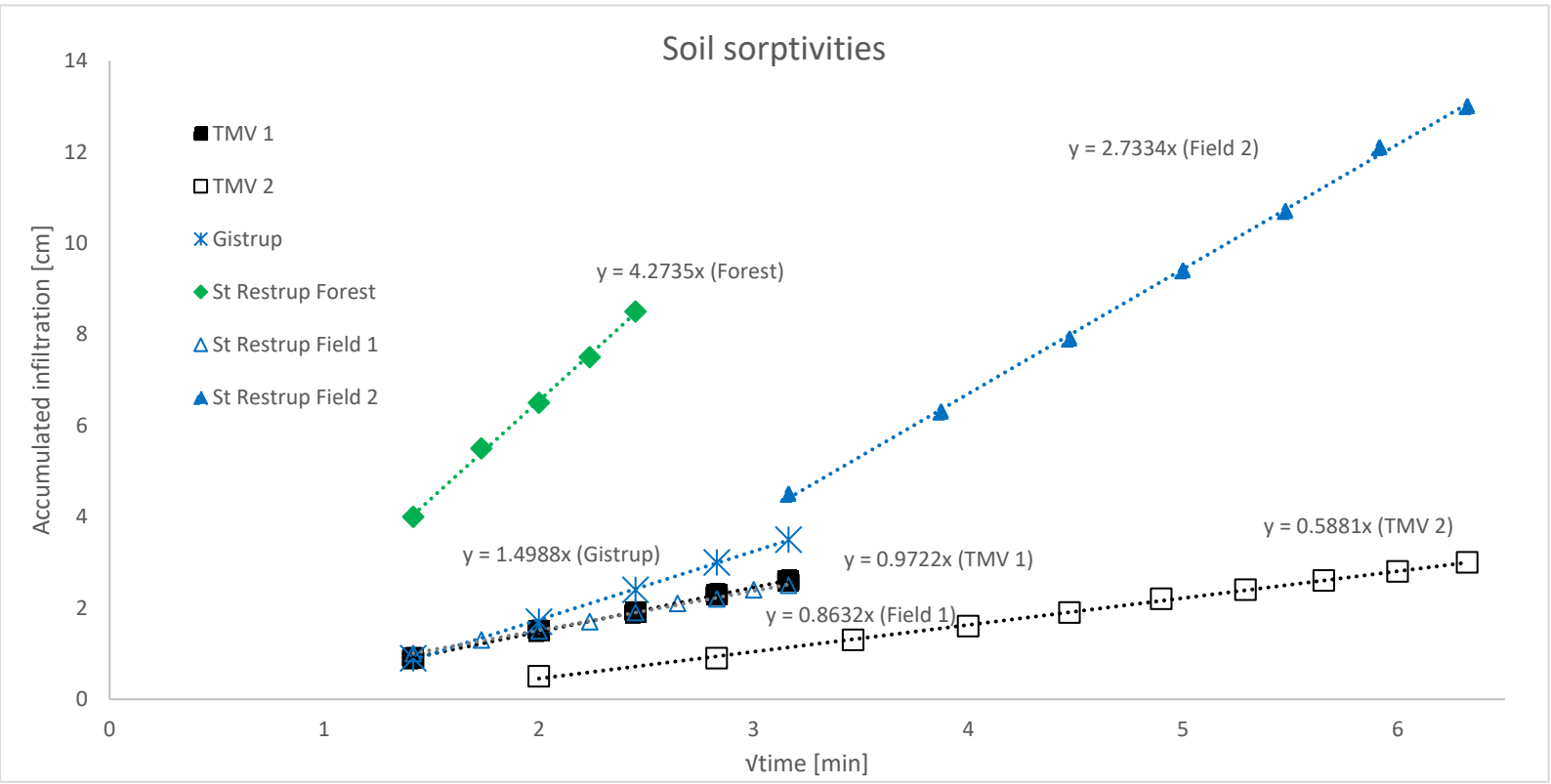

Figure 41 Run 1 – soil sorptivities for all sites.

4.3.2 The Twin Campbell curves

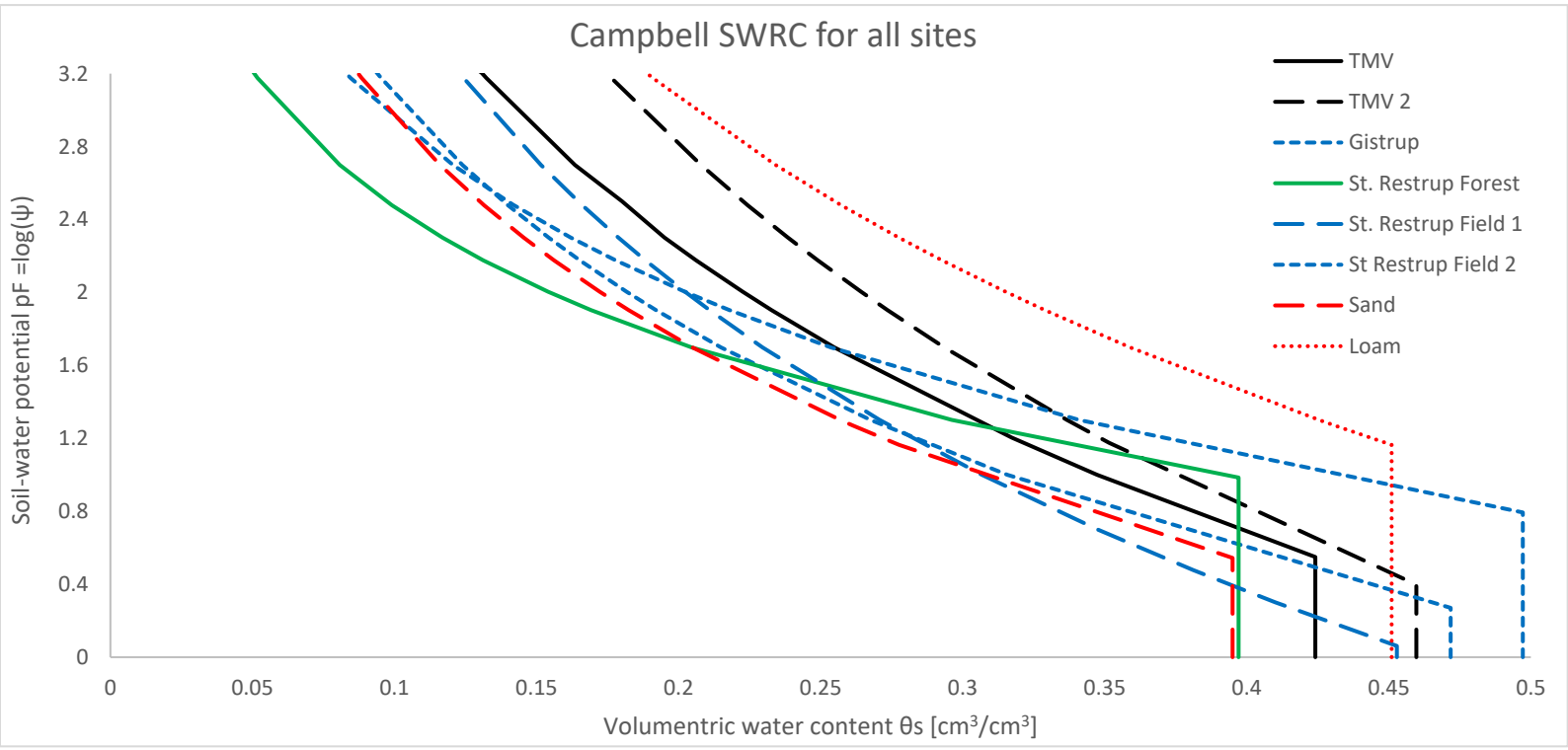

Figure 42 Campbell soil-water retention curves for all soils.

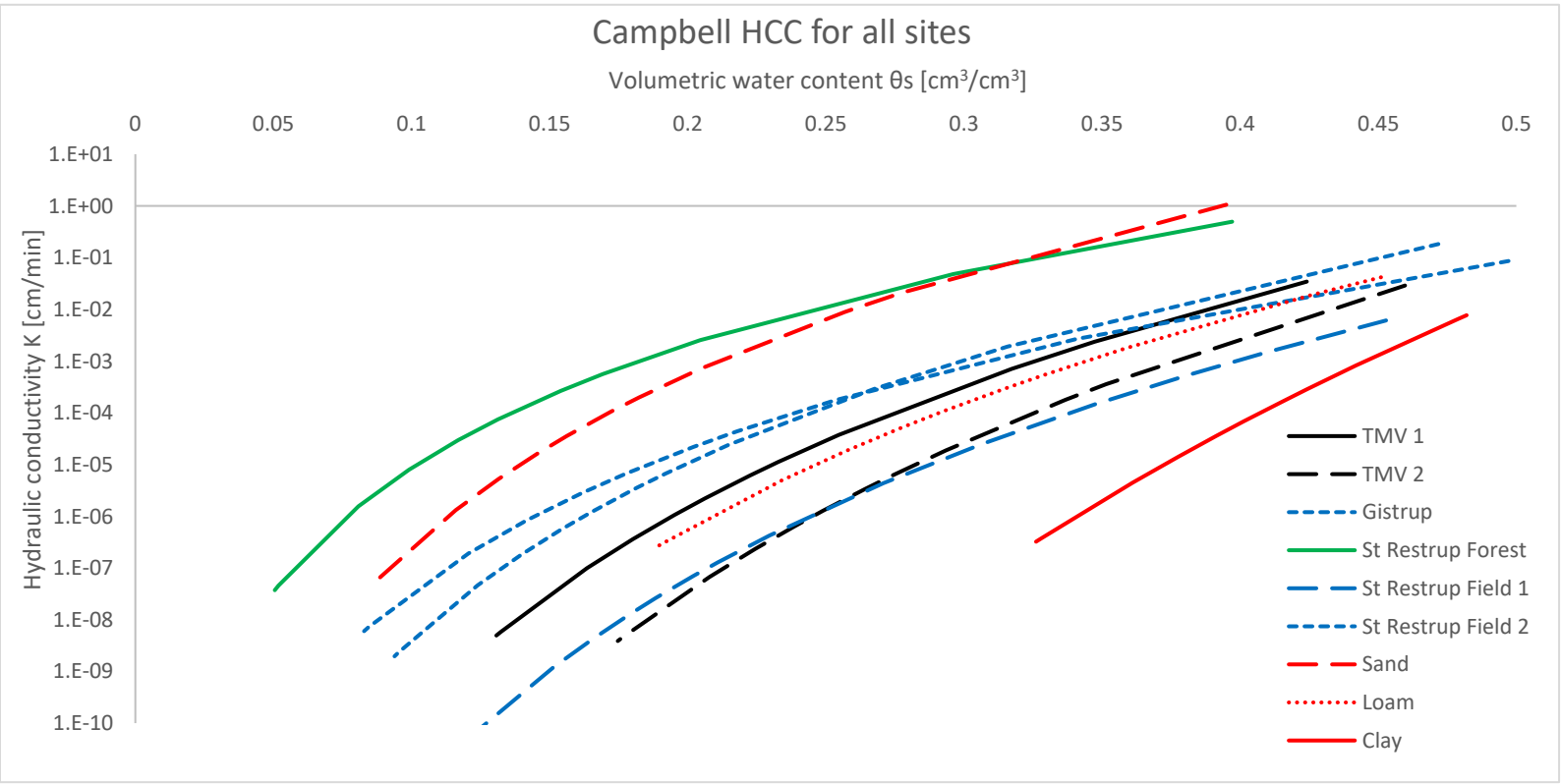

Figure 43 Campbell hydraulic conductivity curve for all soils.

4.3.3 Summary of parameter values

Table 11 Hydrological properties for all sites

	b	ψe [cm]	θs [cm^3/cm^3]	Ks [cm/min]	S [cm/√min]
TMV (grass)	5.19	3.54	0.424 (0.396-0.46)	0.034	0.972
TMV 2 (grass)	6.68	2.50	0.46 (0.436-0.472)	0.029	0.588
Gistrup (pine sapplings)	4.18	1.87	0.472 (0.463-0.515)	0.183	1.49
St. Restrup Forest	2.48	9.67	0.397	0.496	4.27
St. Restrup Field 1 (maize)	5.55	1.15	0.453	0.006	0.852
St. Restrup Field 2 (maize)	3.10	6.22	0.497 (0.483-0.518)	0.086	2.72
Sand	4.05	3.5	0.395	1.056	1.520
Loam	5.39	14.6	0.451	0.0417	0.693
Clay	11.4	18.6	0.482	0.0077	0.268

5 Applying the full Philips equation on Run 1 infiltration data

The curves presented in chapter 3 and 4 based on the new method have the key assumption that the two runs can be neatly distinguished by the driving force behind the infiltration – suction or gravity. Given this assumption the Philip two-term equation can therefore be divided into a one term equation. In reality this might not be the case based on the initial conditions namely the soil-water potential. Therefore, it is within the realm of possibility that Run 1 is influenced by gravity and Run 2 is influenced by suction and measured sorptivities and hydraulic conductivities are skewed. One way of investigating the effect this would have is to fit the two-term Philip equation on Run 1 and investigate if the values for S from the two-term fit are vastly different from the one-term fit used in Chapters 3 and 4 and more importantly what is the change to the twin curves.

5.1 Concept for determining S from 2-term Philips equation

Chapter 2 introduced the two-term Philips equation as

$$I = S\sqrt{t} + At \qquad \text{Equation 8}$$

which was later in Chapter 3 separated into the one-term Philips equation

$$I = S\sqrt{t} \qquad \text{Equation 15}$$

where it was used to determine the sorptivity was determined from early Run 1 infiltration data. If the two-term equation is to be used on the same infiltration data a value for the A parameter must be chosen. As stated previously in chapter 2 the A parameter represents gravity-driven flow and is therefore related to the hydraulic conductivity having the same dimensions of [L/T]. A has been shown to range anywhere from 0.3 to 0.5 Ks and theoretically up to ~1Ks for very long infiltration experiments. For the purposes of this evaluation a value of 0.33Ks has been chosen following the SWIG database method (Rahmati et al., 2018). With this is mind the two-term Philips equation can be expressed as:

$$I = S\sqrt{t} + 0.33Ks \times t \qquad \text{Equation 16}$$

Rearranging and isolating the sorptivity results in:

$$S = (I - 0.33Ks \times t)/\sqrt{t} \qquad \text{Equation 17}$$

The procedure for determining S from the two-term fit is essentially the same as the one-term fit explained in chapter 3: plotting $I - 0.33Ks \times t$ versus $\sqrt{t}$ and looking for where the plot diverges from a straight line. The value for Ks used is the one determined from the last few points of Run 2. Figure 44 shows the resulting plots compared to the ones from Chapters 3 and 4.

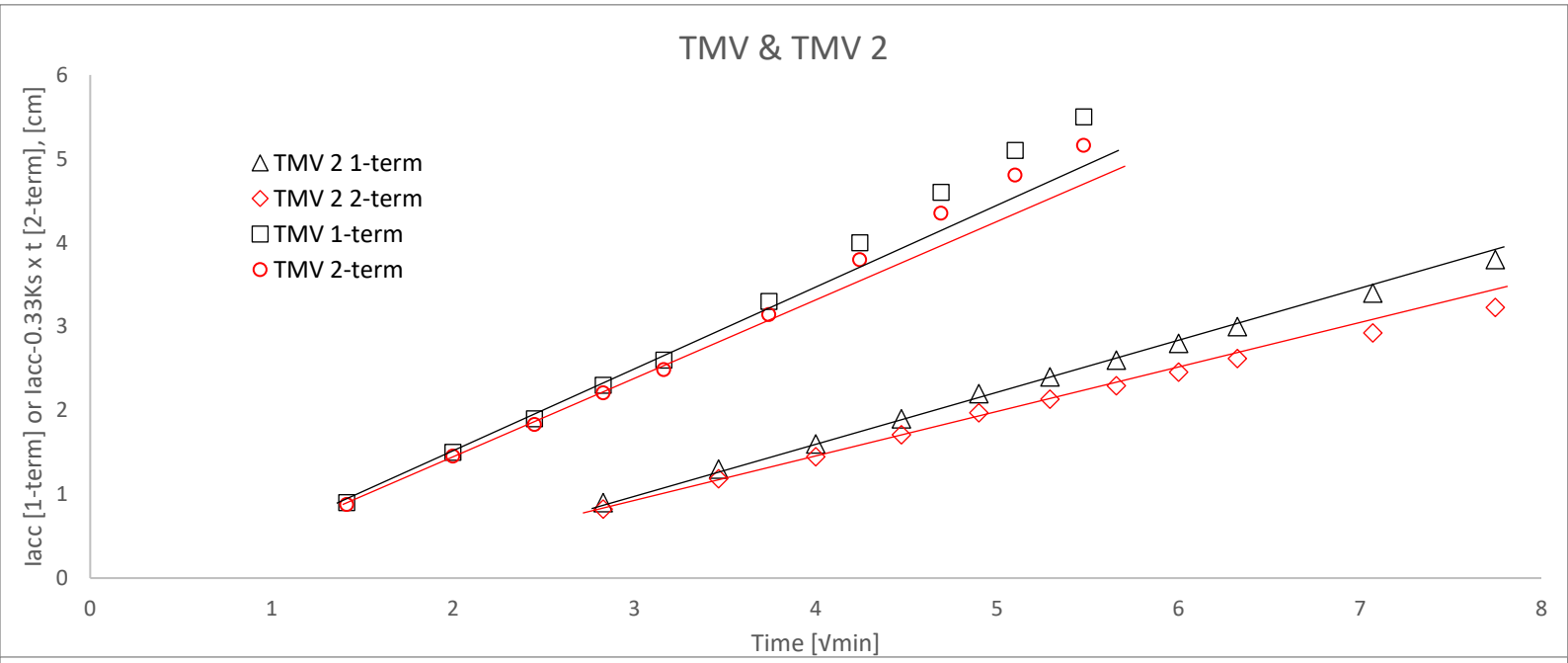

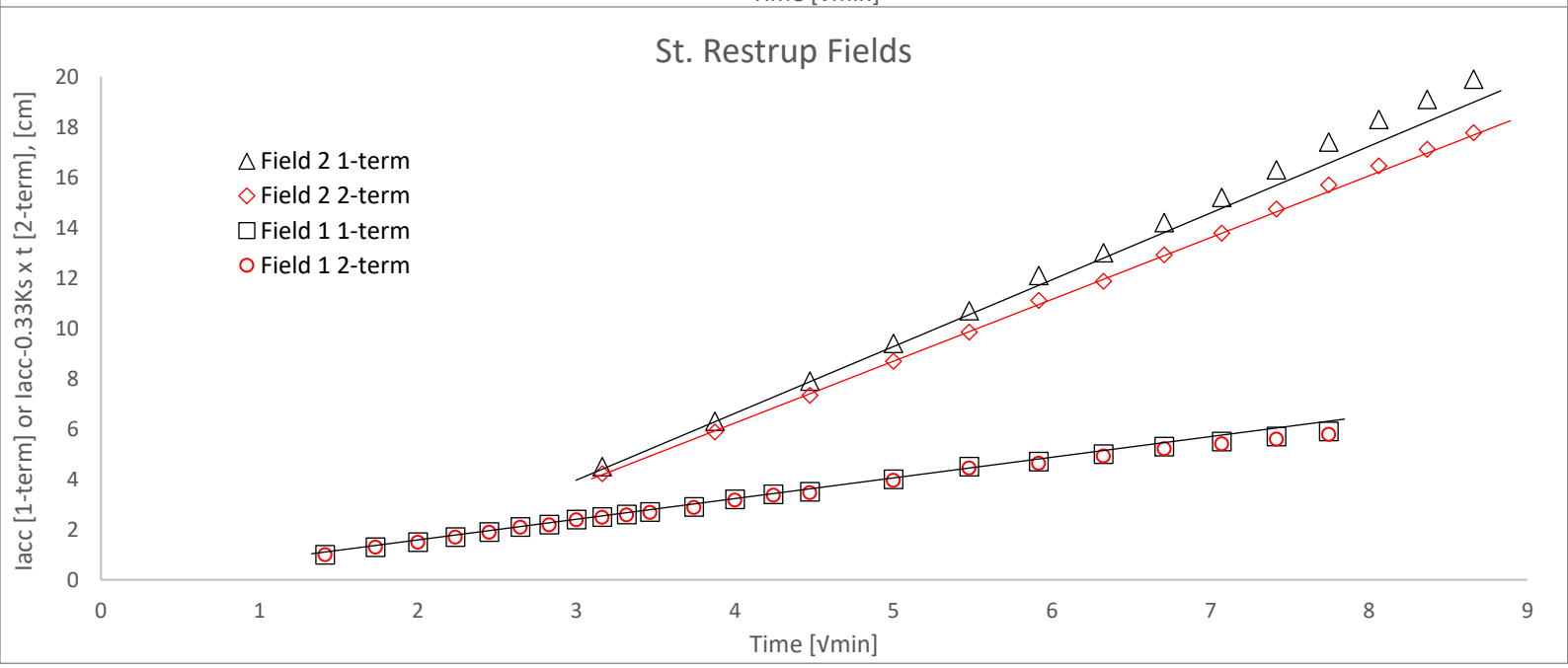

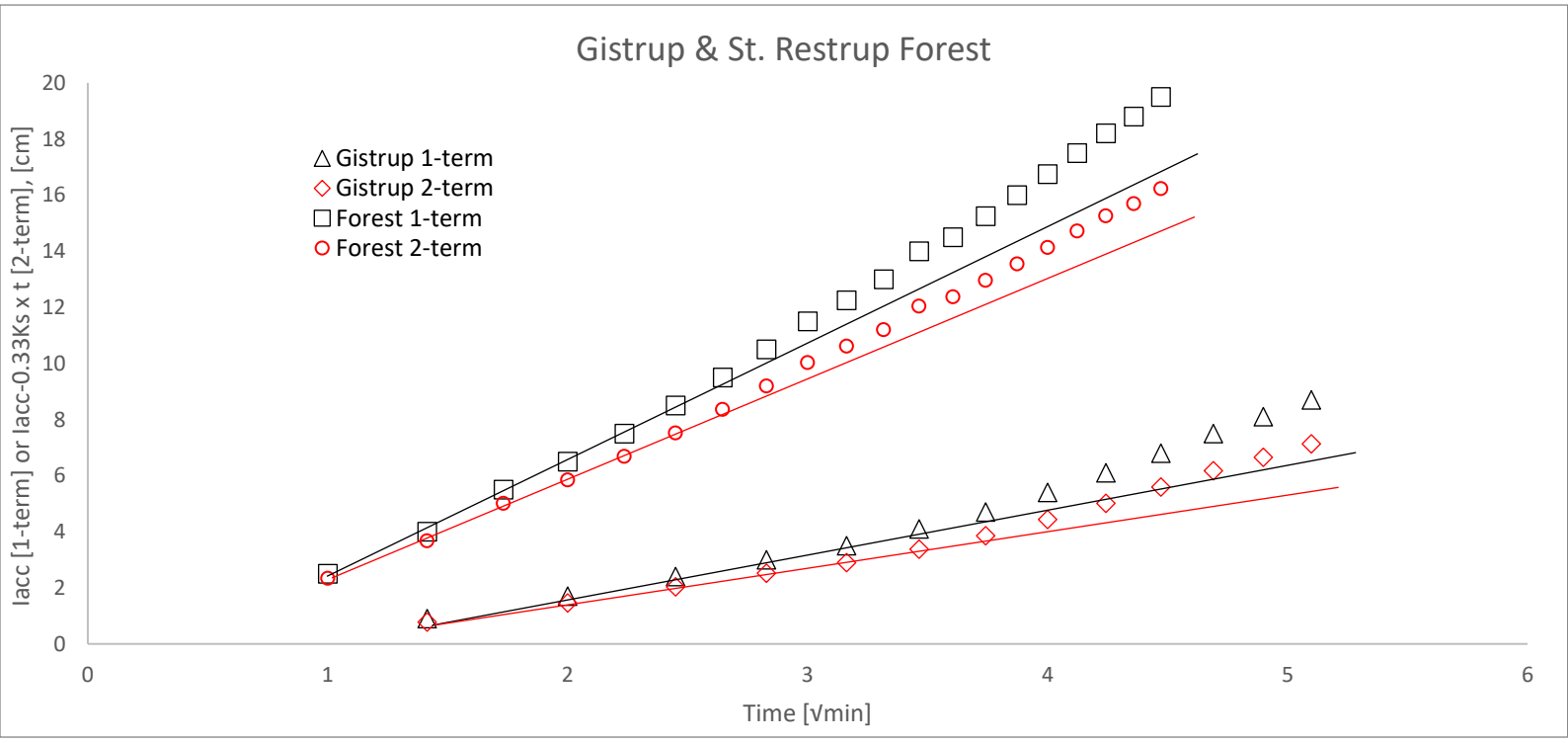

Figure 44 One- and Two-term accumulated infiltration versus time for Run 1 in black and red, respectively. a) TMV sites b) St. Restrup fields 1 and 2 c) Gistrup and St. Restrup Forest

5.2 Comparing S by 1-term and 2-term Philips determination

As it can be seen in all cases the slope of the plot changes and is always gentler for the two-term plot compared to the one-term. One aspect that does not seem affected is the number of points which can be included in the calculation of the slope. Table 12 shows a comparison S and b values from the one- and two-term approaches.

Table 12 Comparison of S and b from one- and two-term Philip determination.

	1-term S	2-term S	% change	1-term b	2-term b	% change	Ks [cm/min]
TMV	0.972	0.920	5	5.19	5.34	**3**	0.034
TMV 2	0.588	0.507	14	6.68	7.19	**7**	0.029
Gistrup	1.49	1.22	18	4.18	4.63	**10**	0.183
Forest	4.27	3.64	15	2.48	2.68	**8**	0.496
Field 1	0.852	0.842	1	5.55	5.58	**1**	0.006
Field 2	2.72	2.46	10	3.10	3.26	**5**	0.086

Figure 44 and Table 12 show that the difference between the one- and two-term fit in regards to the sorptivity ranges from 1 to 18% and generally scales with the magnitude of Ks. At first this seems substantial, however the resulting change to the b values and therefore the SWRCs is far smaller – up to 10% in the case of Gistrup. Figure 45 shows the changes to the Gistrup and St. Restrup Forest curves being the two with the highest changes in b.

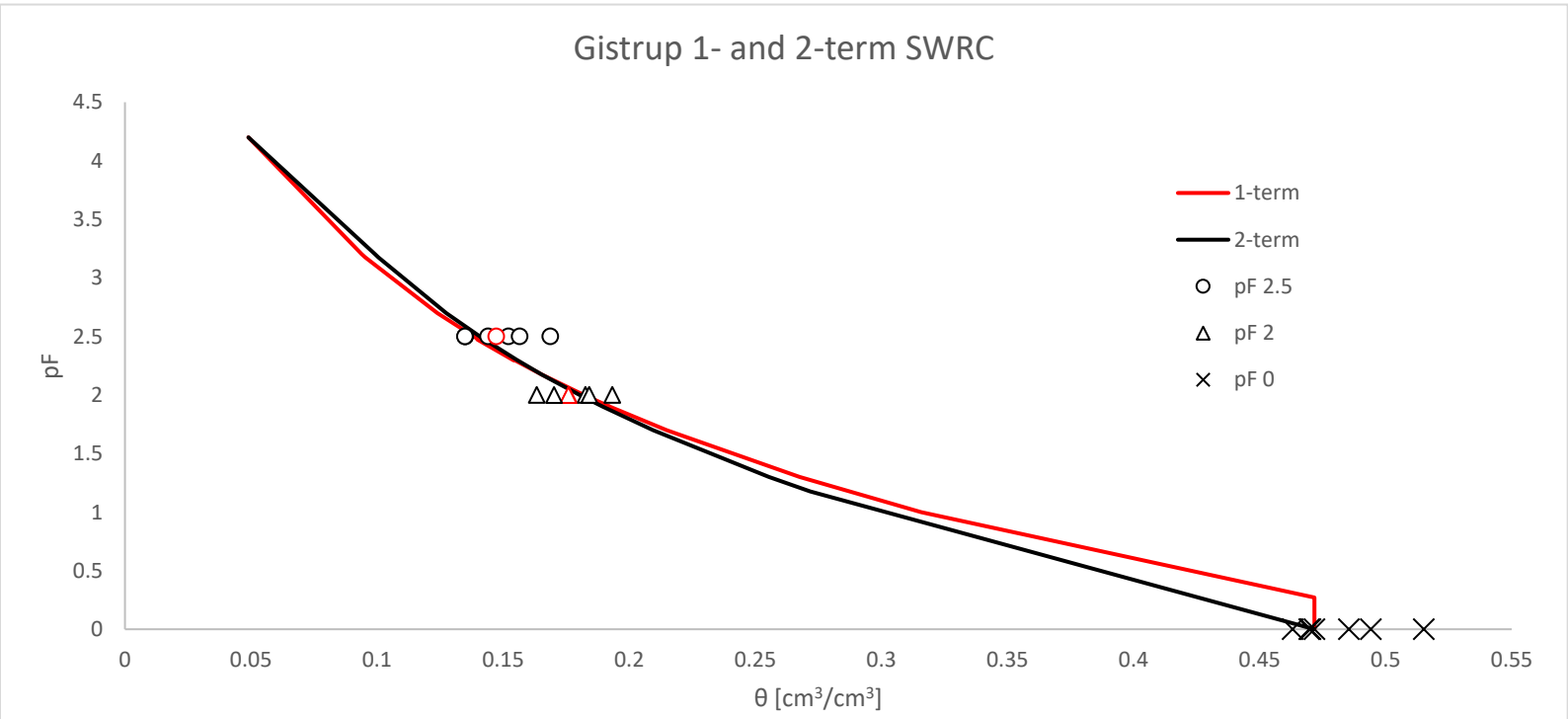

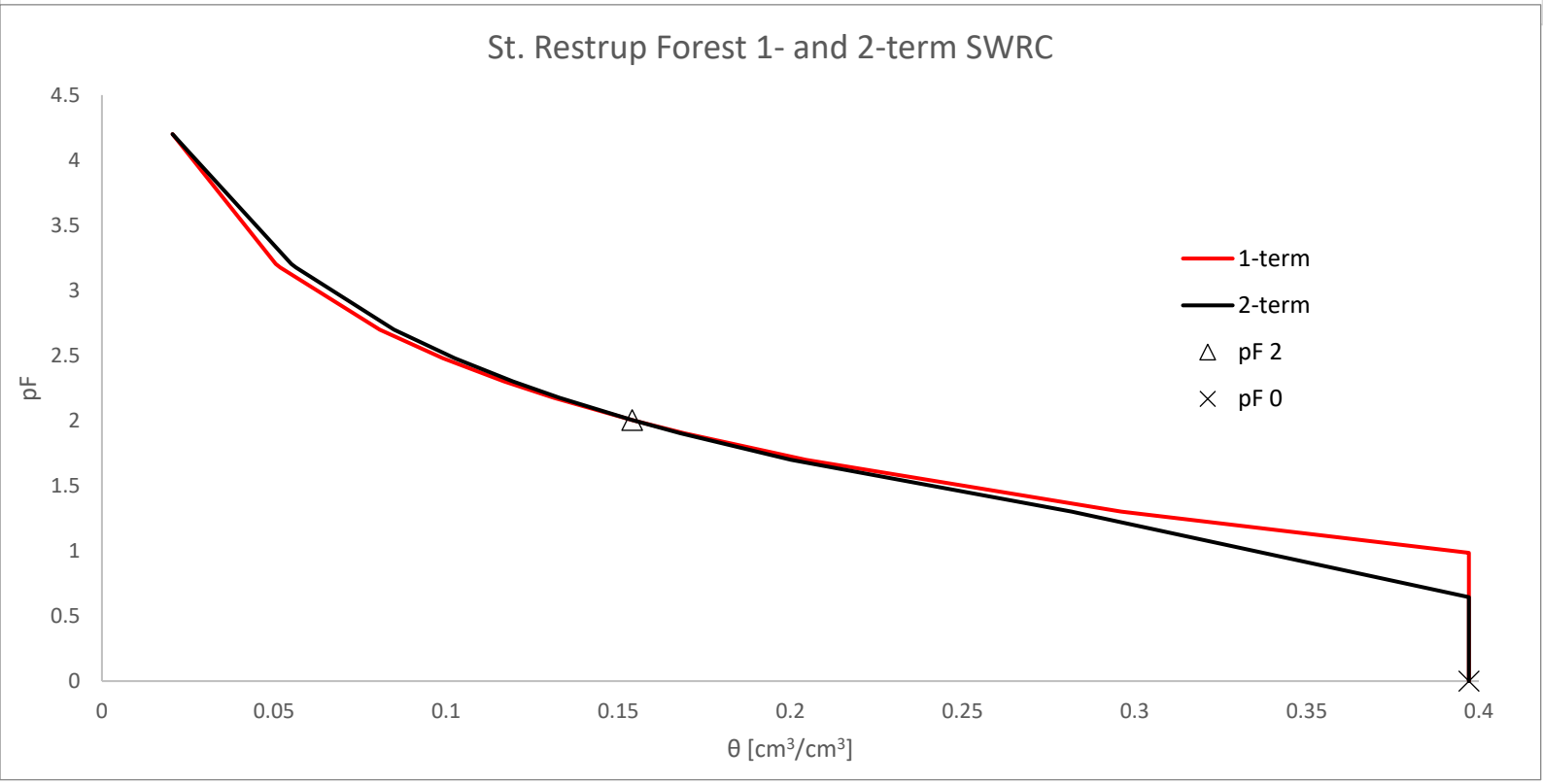

Figure 45 Gistrup and St. Restrup Forest SWRCs using the 1- and 2-term approach for determining S and b. Measured water contents at pF 2.5 and 2 and 0 indicated by circles, triangles and crosses, respectively, with values in red used as calibration points for fitting the model.

As it can be seen the change to the SWRCs is minimal – a higher b value calls for a lower ψe if the curve is to fit through the same calibration points. This results in a lower water content prior to those points and a higher one after. The HCC were not shown as the change to the SWRC is not considered important in either site. However, this might not be the case in soils with a higher Ks value as the trend in Table 12 suggests.

Given that the two-term approach is introducing the influence of Run 2 in Run 1 by incorporating Ks into the determination of S it is worthwhile to briefly reexamine the estimates Ks from Run 2. Figure 46 show the hydraulic conductivity for Run 2 for all sites.

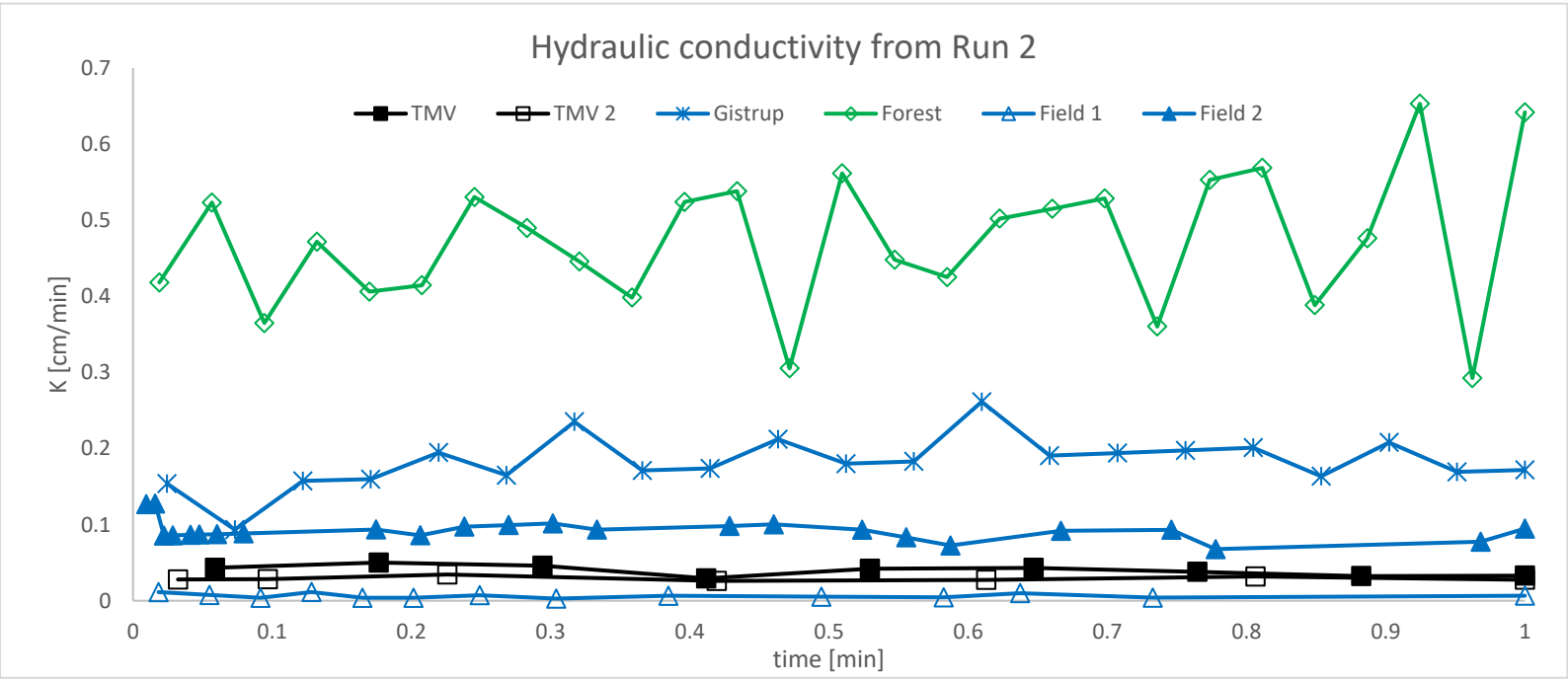

Figure 46 Hydraulic conductivity versus time from Run 2 for all six sites.

It can be clearly observed that for the Forest Ks value is very likely wrong as fluctuations are observed until the very end, indicating that steady state has not been reached. This is important to keep in mind when comparing the two approaches for determining S. It is hard to draw conclusions based on the presented data which approach is more valid. The one-term Philips determination completely negates the effect of gravity and assumes suction-dominated flow for early Run 1 which can lead to error especially in coarse soils where the suction-dominated period can be so short that it leads to insufficient points for determining S. The two-term Philips determination on the other hand is likely the better choice for such cases, however it introduces two new uncertainties – the relationship between A and Ks assumed in this project to be A = 0.33Ks and therefore the underlying robustness of the Ks determination.

It can perhaps be better to view the two approaches as resulting in a field-scale prediction band of S and b where the 1-term determination gives the lower end of the b spectrum and the 2-term determination gives the higher end.

Appendix 9.6 also presents a third alternative – combining the Run 1 and 2 into a single dataset and fitting the two-term Philip equation on that.

In the next chapters these prediction bands will come in handy when determining the “true” values of the hydraulic parameters and validating the method via inverse modelling.

6 HYDRUS-1D for the Two-ring Two-run method with built-in moisture sensors

6.1 Sensor setup and data

In this chapter the use inverse modelling with the help of built-in soil moisture sensors as a way of validating the Two-ring Two-run method at field scale will be investigated. Three sets of sensors (METER's EC-5) were inserted underneath the DRI excavation at Gistrup – two at ~15 cm depth and one at ~30 cm depth as shown in Figure 47. The infiltration test was then carried out as per procedure (Eijkelkamp, 2015) and the data, water contents at the given depths throughout the experiment, is used in HYDRUS-1D - a software for simulating one dimensional water flow in variably saturated media.

Figure 47 Sensor setup at the Gistrup site.

The time at the start of the experiment when water was poured in the inner and outer rings of the infiltrometer was noted down. From this time forward the sensor data is considered as shown in Figure 48.

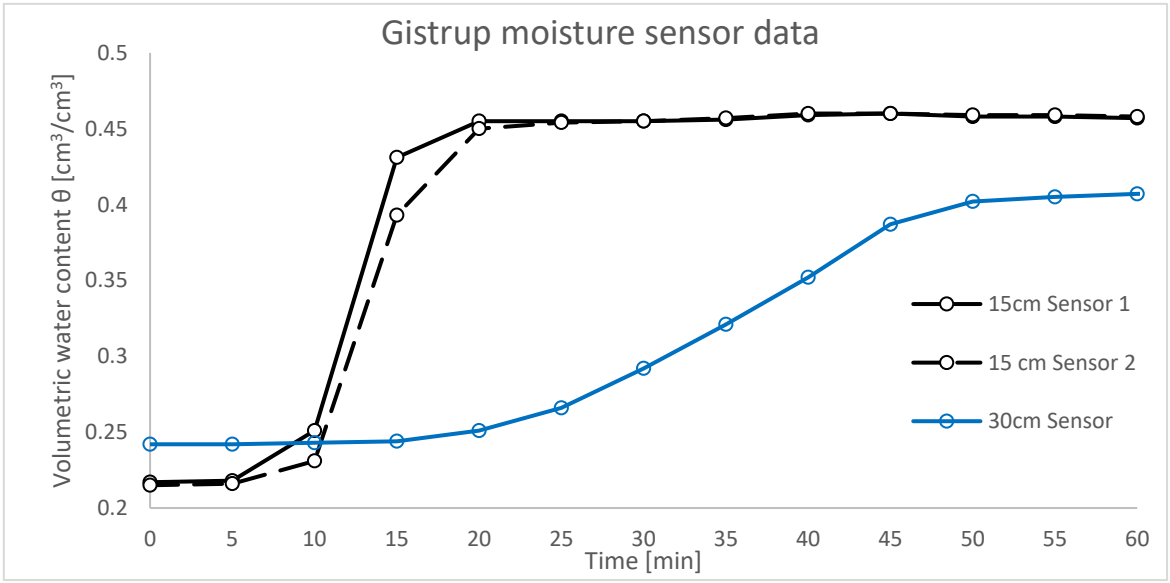

Figure 48 Soil water content during Gistrup Run 1, as read by the in-built moisture sensors. Water content at ~15 cm depth in black (duplicate sensors) and ~30cm in blue.

Several things can be observed here:

- The initial water contents at the two depths are different – ~0.216 [cm^3/cm^3] at 15cm and ~0.242 [cm^3/cm^3] at 30cm. This could be attributed to soil heterogeneity or simply the same soil which is drier towards the surface and is progressively wetter with depth.
- The two sensors at the 15 cm depth show similar values for initial and final (saturated) water content as well as a steep raise in water content from minute 10 to 20 when the wetting front hits the sensor area.
- The 30 cm sensor shows a less steep slope for the wetting front which could be a result of dispersion of the front, different soil characteristics or a faulty installation.

6.2 Relating the van Genuchten and Campbell retention models

Before setting up the HYDRUS simulation of Run 1 the van Genuchten (vG) and Campbell models must be linked as HYDRUS accepts only vG parameters as input and this project has focused on the Campbell model.

As described in Chapter 2 the vG model can be mathematically expressed as:

$$\theta = \theta r + \frac{\theta s - \theta r}{[1 + (\alpha * \psi)^n]^m} \quad \text{Equation 2}$$

Where θr is the residual water content or the water content under a very dry condition; α, n and m are empirical constants where α is the inverse of air-entry potential 1/ψe, n is related to the width of the pore-size distribution and m is assumed equal to 1-1/n.

For ease of modelling and relating vG to the Campbell model in this project θr is assumed to be 0, thus Equation 2 is simplified to:

$$\theta = \frac{\theta s}{[1 + (\alpha * \psi)^n]^{1-1/n}} \quad \text{Equation 18}$$

With the two assumptions of θr = 0 and m = 1-1/n the four-parameter vG model is reduced to a two-parameter model like the Campbell one:

$$\theta(\psi) = \theta s \frac{\psi e^{1/b}}{\psi} \quad \text{Equation 1}$$

and a comparison between the two can now be made.

As already mentioned the vG α parameter is directly related to the Campbell air entry ψe: α = 1/ ψe. *As a side note* (Quirijn & Everton Alves Rodrigues, 2018) *argue that this relationship is erroneous and that α is not related to air entry and is "merely a scaling parameter relative to the matric potential axis". However, for the purposes of this project the above relationship is considered valid.*

The vG n it is a parameter that relates to the pore-size distribution of the soil much like the Campbell b. However, in this case the relationship is not as straight-forward as with the vG α and air entry. Table 13 shows average vG parameters for the 12 soil texture groups of the USDA pyramid, courtesy of (Carsel & Parrish, 1988). Using these n values and correlating them to the Campbell b values from the US soil library as seen in Table 2 (excluding the loam texture class, as it is not listed) results in the following relationship:

Table 13 Average vG parameters for the 12 USDA soil texture classes. Data from (Carsel and Parrish, 1988)

Soil texture	θ_r [$cm^3\ cm^{-3}$]	θ_s [$cm^3\ cm^{-3}$]	α_{vG} [cm^{-1}]	n [-]
Sand	0.045	0.43	0.145	2.68
Loamy sand	0.057	0.41	0.124	2.28
Sandy loam	0.065	0.41	0.075	1.89
Loam	0.078	0.43	0.036	1.56
Silt	0.034	0.46	0.016	1.37
Silt loam	0.067	0.45	0.020	1.41
Sandy clay loam	0.100	0.39	0.059	1.48
Clay loam	0.095	0.41	0.019	1.31
Silty clay loam	0.089	0.43	0.010	1.23
Sandy clay	0.100	0.38	0.027	1.23
Silty clay	0.070	0.36	0.005	1.09
Clay	0.068	0.38	0.008	1.09

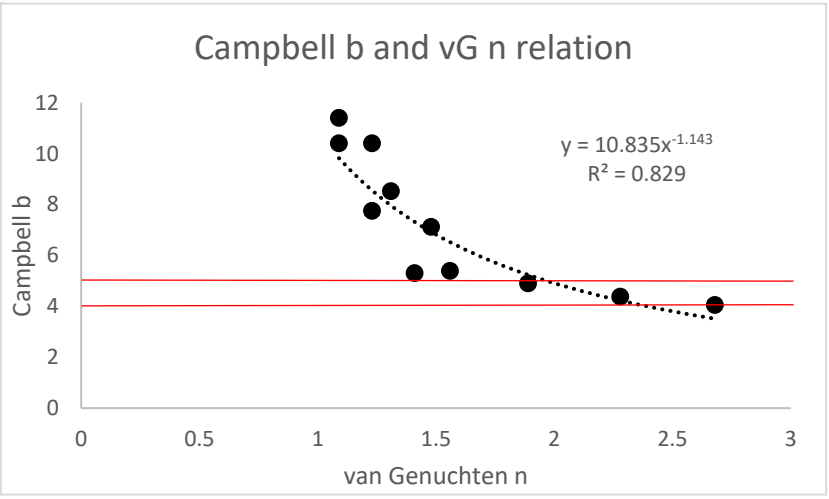

Figure 49 Campbell b and VG n relationship, based on Campbell b data from (Clapp & Hornberger, 1978) *and vG n data (Carsel and Parrish, 1988). Red lines indicate the sandy soil range.*

Figure 49 shows that n and b are inversely related – the higher the b the lower the n. For example, sandy classes with a b values in the range of 4-5 correspond to vG n in the range of ~1.9 to 2.7.

6.3 HYDRUS-1D setup for Gistrup

In this section some of the more relevant HYDRUS setup features and parameters will be briefly discussed.

6.3.1 Geometry and time

First and foremost the depth of the soil profile is defined as the total length of soil through which the water flows. In this case 100cm was chosen with the intention of having the lower boundary sufficiently far away from the depth of interest – 15 cm. The data from the lower sensor has not been used for two reasons - 1) due to the lack of knowledge about the soil at the depth, as intact or loose soil samples were only collected at ~15 cm and 2) as the name suggests HYDRUS-1D simulates one-dimensional flow and so fits with the DRI which is assumed to facilitate such flow within its confines, however the further the investigated area is from the insertion depth the higher the likelihood of 2D/3D flow as in this case with the lower sensor being at 30cm and the insertion depth of the ring being 11 cm. As only one set of data can be used Sensor 1 from Figure 48 was chosen as it appears that it is the first to experience the wetting front and has a steeper slope.

Next the simulation time was set at 20 minutes corresponding to the time it takes for soil around Sensor 1 to become saturated according to Figure 48. The minimum and maximum timesteps were respectively set as $5x10^{-4}$ [min] and 0.01 [min].

6.3.2 Soil hydraulic parameters

The parameters in HYDRUS that can be input are θr, θs, α, n and Ks.

- θr is set to 0.
- θs is assumed equal to the highest Sensor 1 measurement – 0.460 [cm^3/cm^3].
- vG α is set to 0.5, the inverse of the Gistrup's air entry of 1.87 [cm].
- vG n is set to 2.1 using the relationship from Figure 49 and on Gistrup's Campbell b of 4.18.

Regarding Ks some additional attention is required. Figure 50 shows the hydraulic conductivity for Run 2 at Gistrup where the Ks value is based of the last 3 measurements and the constant head Ks measurements on the small intact samples.

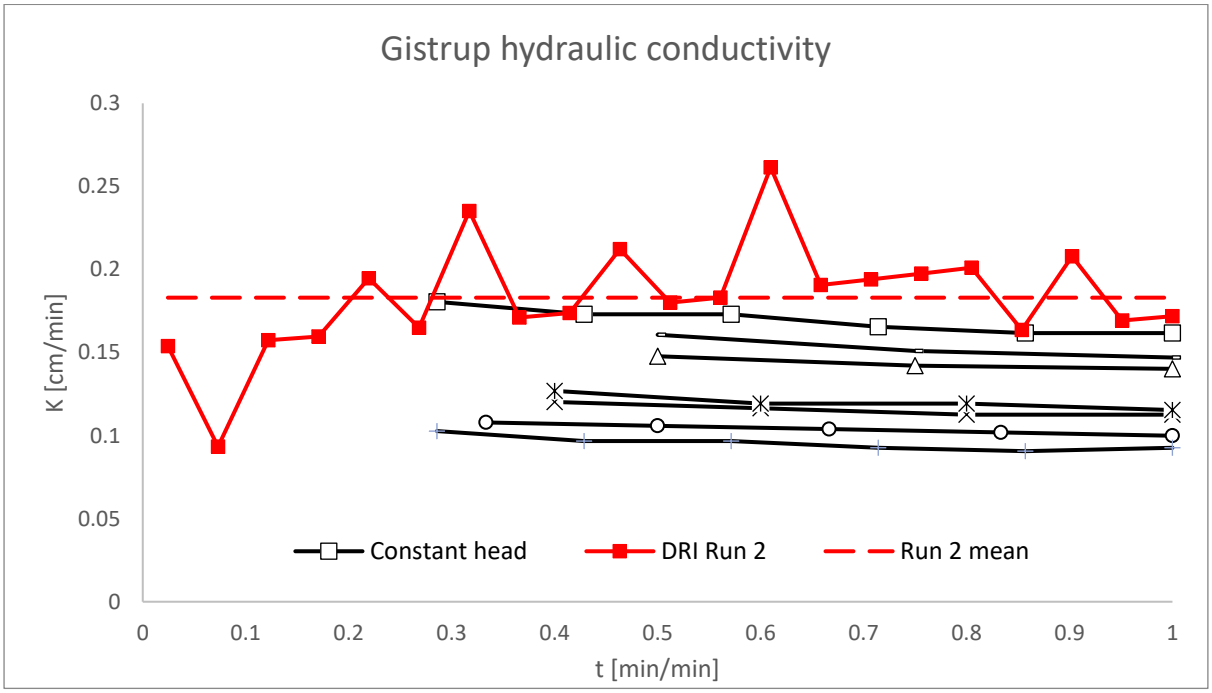

Figure 50 Gistrup Hydraulic conductivity results from DRI and constant head on small intact samples. DRI values for Run 2 in red and constant head on the 7 intact soil samples in black.

Run 2 appears highly fluctuating ranging from ~0.1 to ~0.25 [cm/min]. Furthermore, the initial readings are higher than the final ones and unlike TMV and TMV 2 they are not within the range of measured Ks from the constant head. It can be assumed that Run 2 was not carried out sufficiently long to ensure field-saturation and that the Ks value of 0.183 [cm/min] is an overestimation. Therefore, the median intact sample Ks value of 0.118 [cm/min] is used instead of the DRI Ks.

6.3.3 Boundary conditions and profile information

Next the upper and lower boundary conditions for the soil column are chosen. The upper boundary condition is set as variable pressure head and the input for that is the water level measurements during Gistrup Run 1 (see in Appendix 9.1). The lower boundary is set to free drainage requiring no additional inputs.

The initial conditions of the soil column can be set as water contents or pressure heads. As the sensors measure water content that is option is selected and the initial value throughout the entire column is set as 0.216 [cm^3/cm^3] corresponding to the value at t = 0 [min] in figure Figure 48.

6.4 Interpreting HYDRUS results

Figure 51 shows the results from the HYDRUS simulation, the setup of which is explained in the previous section.

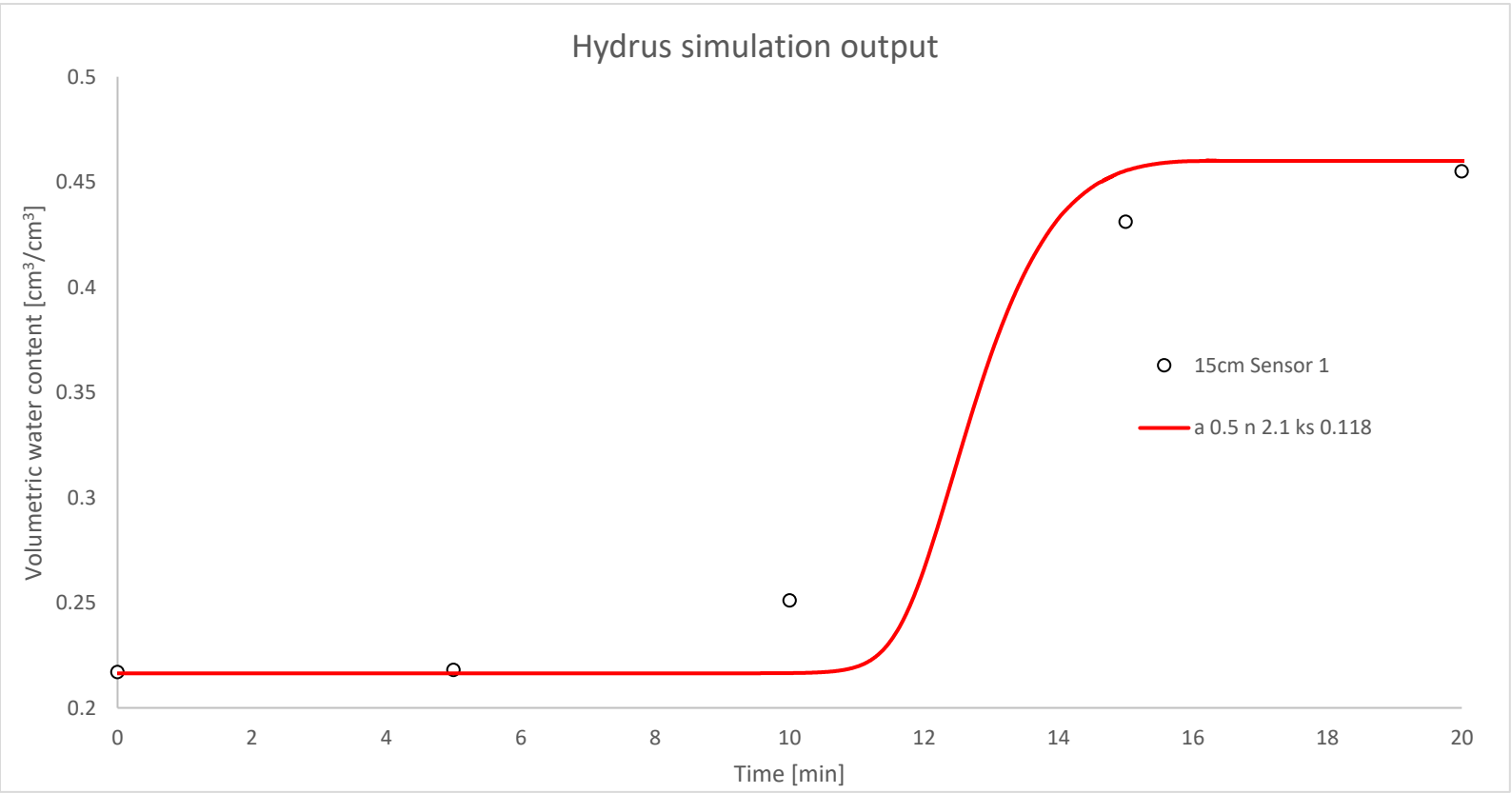

Figure 51 Hydrus simulation outputs for Gistrup in red and sensor measurements in black.

Sensor 1 first picks up the wetting front at minute 10. This does not necessarily mean that that is the exact time at which the wetting front reaches the sensor as the minimum measurement frequency is 5 minutes. Due to this resolution at the next measurement at minute 15 the soil is already very close to sensor-saturation and at minute 20 it is considered saturated. The initial Gistrup setup misses the 10- and 15-minute points and therefore the parameters must be changed to produce a better fit than the initial guess-values. However, before any changes are made to the vG parameters some attention needs to be brought to how each individual parameter affects the twin curves for the new soil, as well as the output from HYDRUS.

6.4.1 Influence of van Genuchten α

Figure 52 shows how altering the vG α parameter influences the SWRC, the subsequent change in the HCC and the effect on the output from HYDRUS.

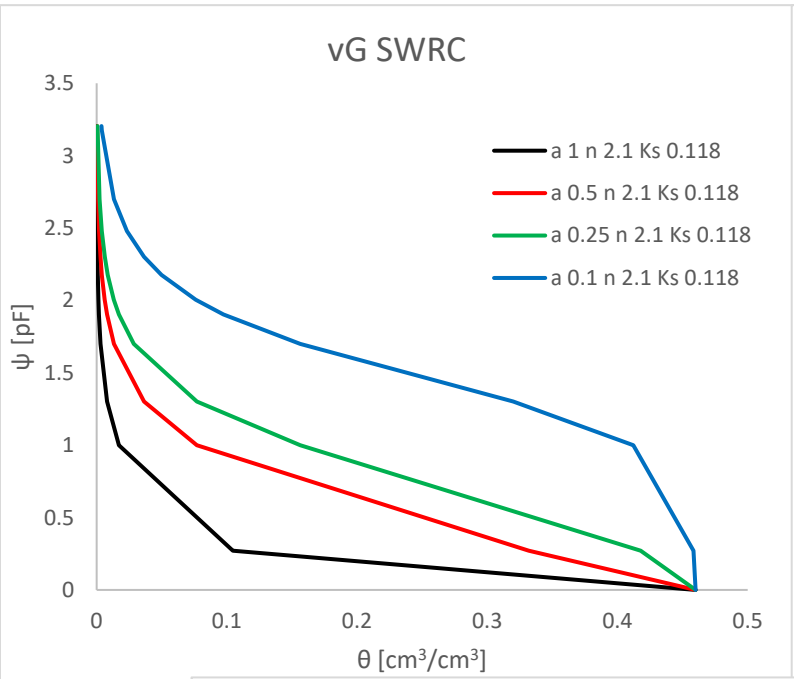

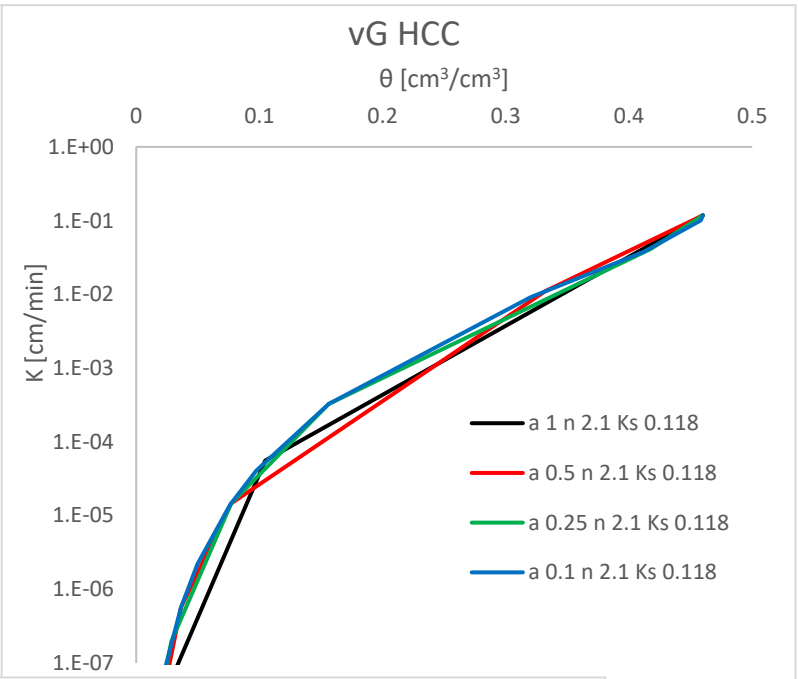

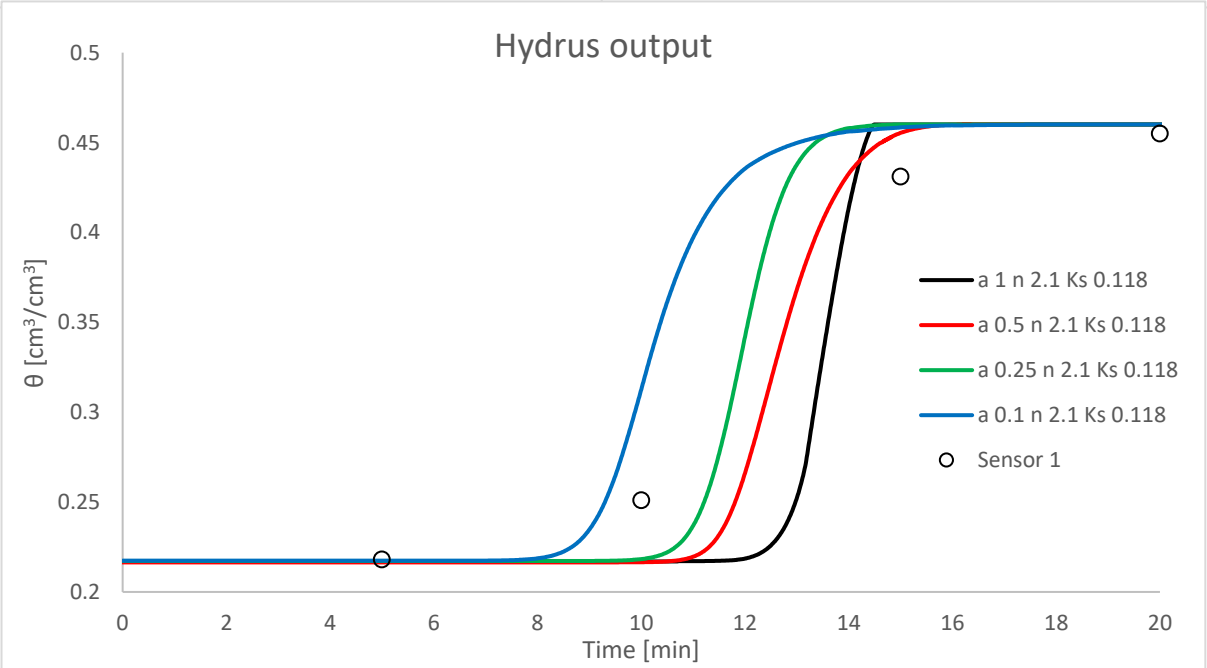

Figure 52 Effect of the vG alpha on the twin curves and HYDRUS output.

It can be seen that increasing alpha from 0.5 to 1 results in a lower air entry pulling the SWRC down. Decreasing alpha from 0.5 to 0.25 and 0.1 results in a higher air entry and pulls the SWRC up. The effect on the HCC is difficult to tell especially in the wet end, however as the soils dry a lower α suggests higher conductivity values for a given water content. The effect of increasing alpha on the HYDRUS output curve is that it takes longer for the wetting front to reach the 15cm depth and the slope is slightly steeper. The opposite is observed as alpha decreases – the wetting front hits the sensor faster and takes longer to reach saturation, as expressed by the gentler slope.

6.4.2 Influence of van Genuchten n

Figure 53 shows how changing the vG n parameter influences the twin curves the effect on the output from HYDRUS.

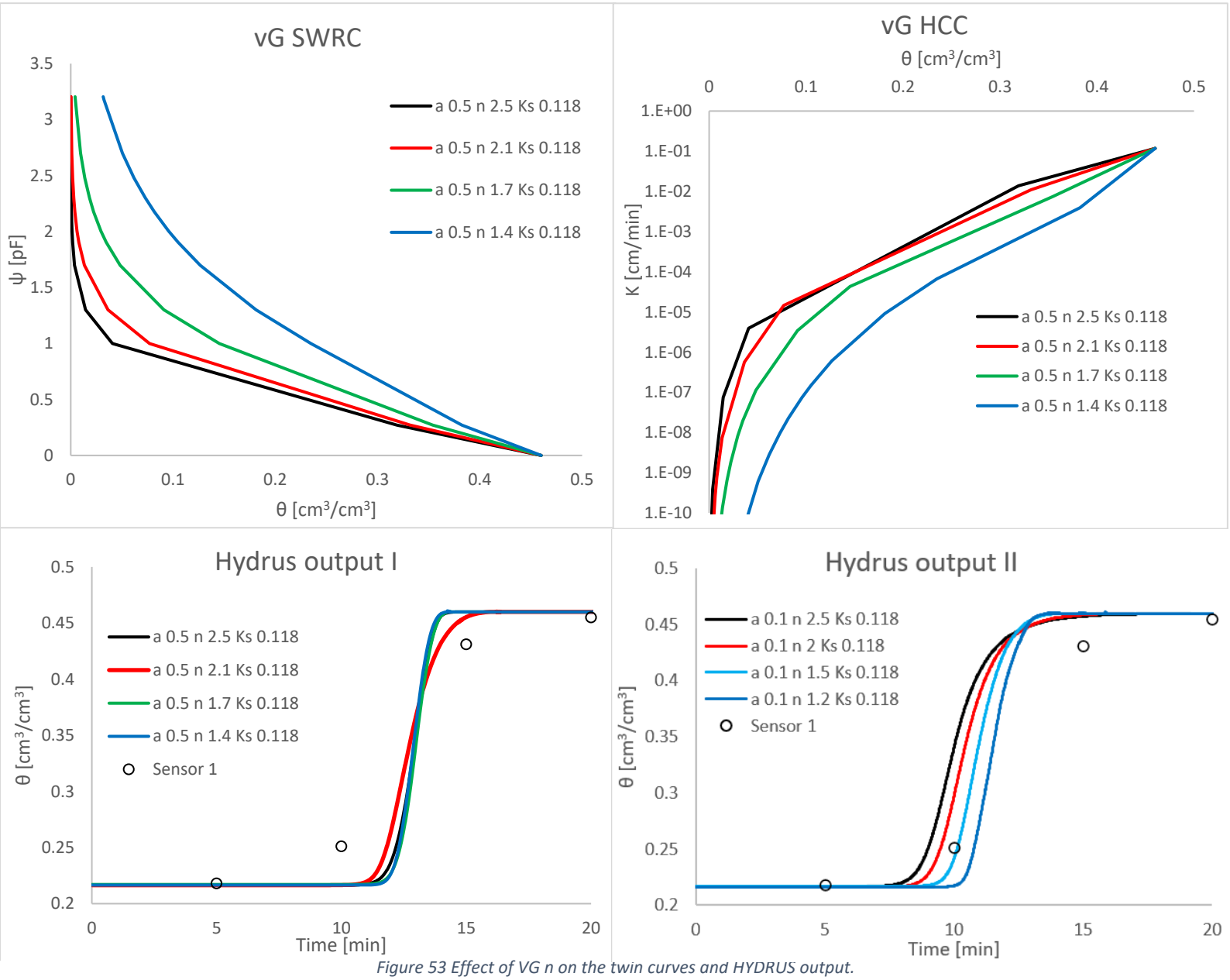

Figure 53 Effect of VG n on the twin curves and HYDRUS output.

Increasing n pulls the whole SWRC to the left resulting in a "drier" soil profile given the same soil-water potential. The effects on the HCC are more profound than in the case of the alpha parameter – as n decreases the curve is pulled down as n is a pore size-distribution index a higher value means larger and therefore more conductive pores and vice versa. No noticeable change was observed for the HYDRUS by changing n given the set alpha and Ks values. By changing the alpha from 0.5 to 0.1 there was an observed difference - increasing n results in a gentler HYDRUS curve where the wetting front hits the sensor earlier and takes a longer time to reach saturation. The effect is similar to a low alpha value but more pronounced at the wet end.

6.4.3 Influence of saturated conductivity Ks

Figure 54 shows how changing Ks influences the HCC and the effect on the output from Hydrus. The SWRC remains unchanged by Ks and is therefore not relevant.

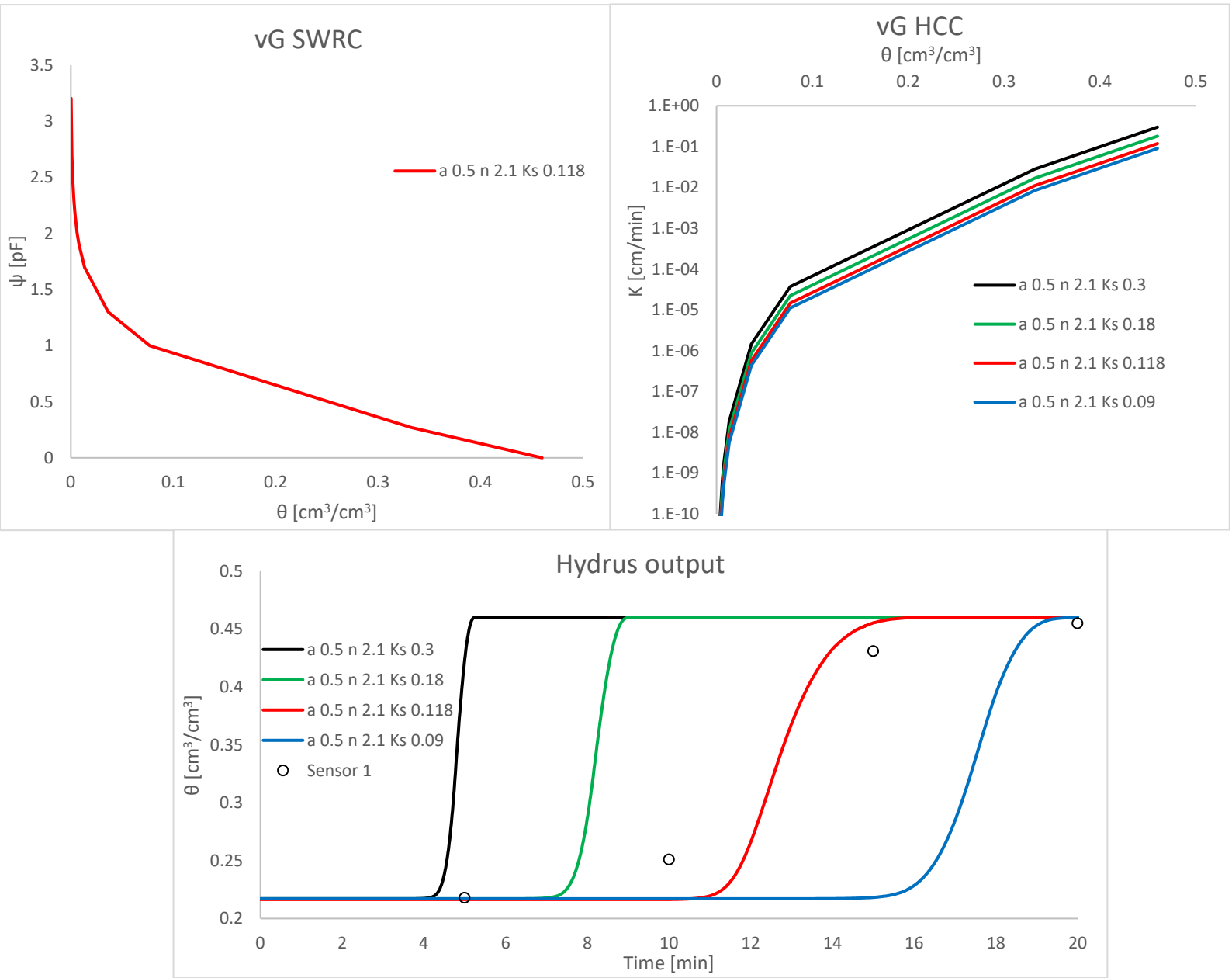

Figure 54 Effect of Ks on the HCC and HYDRUS output.

Changing Ks only affects the initial anchoring of the HCC where the shape remains the same – the high Ks the higher the position of the curve and vice versa. In HYDRUS however Ks is a very sensitive parameter and decreasing it results in more time for the wetting front to hit the sensor and reach saturation as indicated by the gentle slope of the curve. On the other hand, increasing Ks results in rapid water flow where the wetting front hits the sensor early on and the curve rises steeply to saturation.

6.4.4 Insight from parameter influence

Figure 52, Figure 53 and Figure 54 all show how a single parameter affects the twin curves and resulting HYDRUS output. Knowing this it can be said that the curve in shown in Figure 51 would

produce a better fit if the wetting front hits the 15cm depth earlier and reaches saturation in a more gradual manner, hence a gentler slope is required. This can be achieved by reducing α, reducing Ks or increasing n.

In order to fit the HYDRUS output to the sensor data more than a single parameter will needs to be calibrated. If one assumes field capacity equal to 0.2 [cm^3/cm^3] which is the most frequent measurement of the sensor over several months then the vG α and n need to be changed simultaneously to ensure that the resulting simulation not only fits the sensor measurement but the combination of parameters also results in a soil with a the selected water content at pF 2. A manual fit of the parameters then becomes challenging. Fortunately HYDRUS has the option of calibrating these parameters based on an input such as water content measurements at a given depth in a given time as provided by the sensors.

6.5 Inverse modelling

6.5.1 Input data for inverse solution

Two types of input data for the inverse solution are used:

- Water contents at a given depth at a given time provided by from Sensor 1 as shown in figure Figure 48
- One measured point along the SWRC at pF 2 following the assumption that the initial conditions are at field capacity

The frequency of sensor measurement is one reading every 5 minutes which is the highest resolution for this type of water content sensor. Combined with an accuracy of 0.03 [cm^3/cm^3] and the specific locations of the points at minute 10 and 15 which are very close to the initial and final measurements makes the data somewhat uncertain and lacking the fine resolution required for inverse modelling. Therefore, it was deemed necessary to construct more "measurement" points between minute 10 and 15 in order to estimate the breakthrough time of the curve and its corresponding and water content. Figure 55 shows the additional points at minutes 11, 12, 13 and 14, estimated through interpolation.

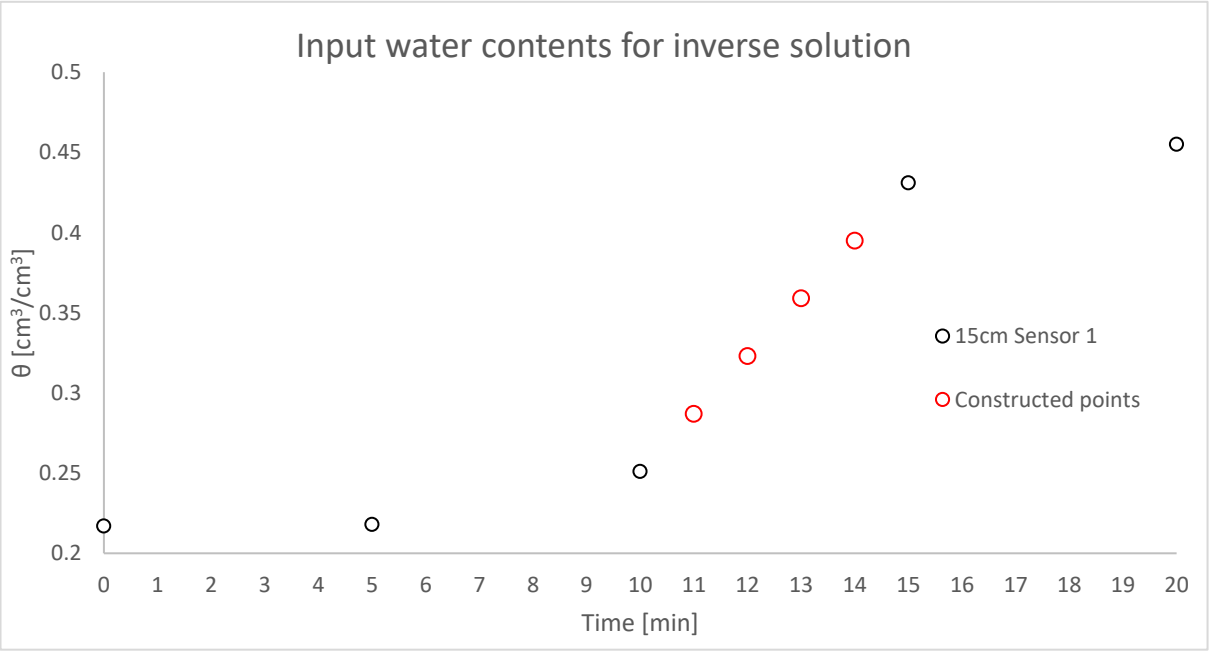

Figure 55 Water contents used for inverse modelling - sensor measured points in black and constructed points in red, obtained via interpolation between points at minutes 10 and 15.

Table 14 shows the exact values of the data used for the inverse solution.

Table 14 Data for inverse modelling - constructed points in italic.

Time [min]	Water content [cm^3/cm^3]
5	0.218
10	0.251
11	*0.287*
12	*0.323*
13	*0.359*
14	*0.395*
15	0.431
20	0.455

Additionally, one more point is entered – the water content of 0.2 [cm^3/cm^3] corresponding to a soil-water potential of -100 [cm].

6.5.2 Parameter constraints

When HYDRUS fits the solution to the measured data points it does so by changing the hydraulic parameters until a good match is found. If these parameters are unrestricted the software can present an unrealistic solution which is to say that even though it might fit the objective the resulting soil would be too far from what is plausible onsite. For example, it is known that Gistrup is a sandy soil and therefore if the solution proposes a clayey soil as the best fit then that is likely false. Therefore, the parameters α, n and Ks must be constrained within a given range of plausible values.

Starting with alpha and knowing it is the inverse of air entry the Danish soil library can be used as it is based on local soils. Taking the inverse of the first and third quartiles of air entries provides the upper and lower alpha values – 0.5 and 0.1. This equates to air entries ranging from ~-1 to -10 [cm].

The vG n is related to the Campbell b the range of which is provided by the intact samples: 4.18 to 8.47. Following the relationship in Figure 49 this results in a rough VG n range of 1.2 to 2.2.

The Ks range is again obtained from the small intact samples, on which the constant head experiment was performed as shown in Figure 50. The upper boundary is 0.16 [cm/min] and the lower is 0.09 [cm/min].

This setup is seen in Figure 56 as is in the HYDRUS interface.

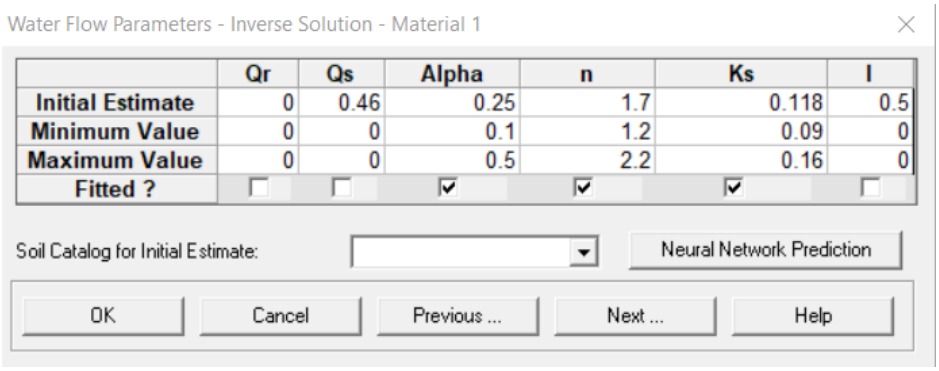

Figure 56 Hydrus hydraulic parameter setup - initial estimates and constrains.

6.5.3 Best fit and resulting retention and conductivity curves

Figure 57 shows the results from the HYDRUS setup described in the previous section.

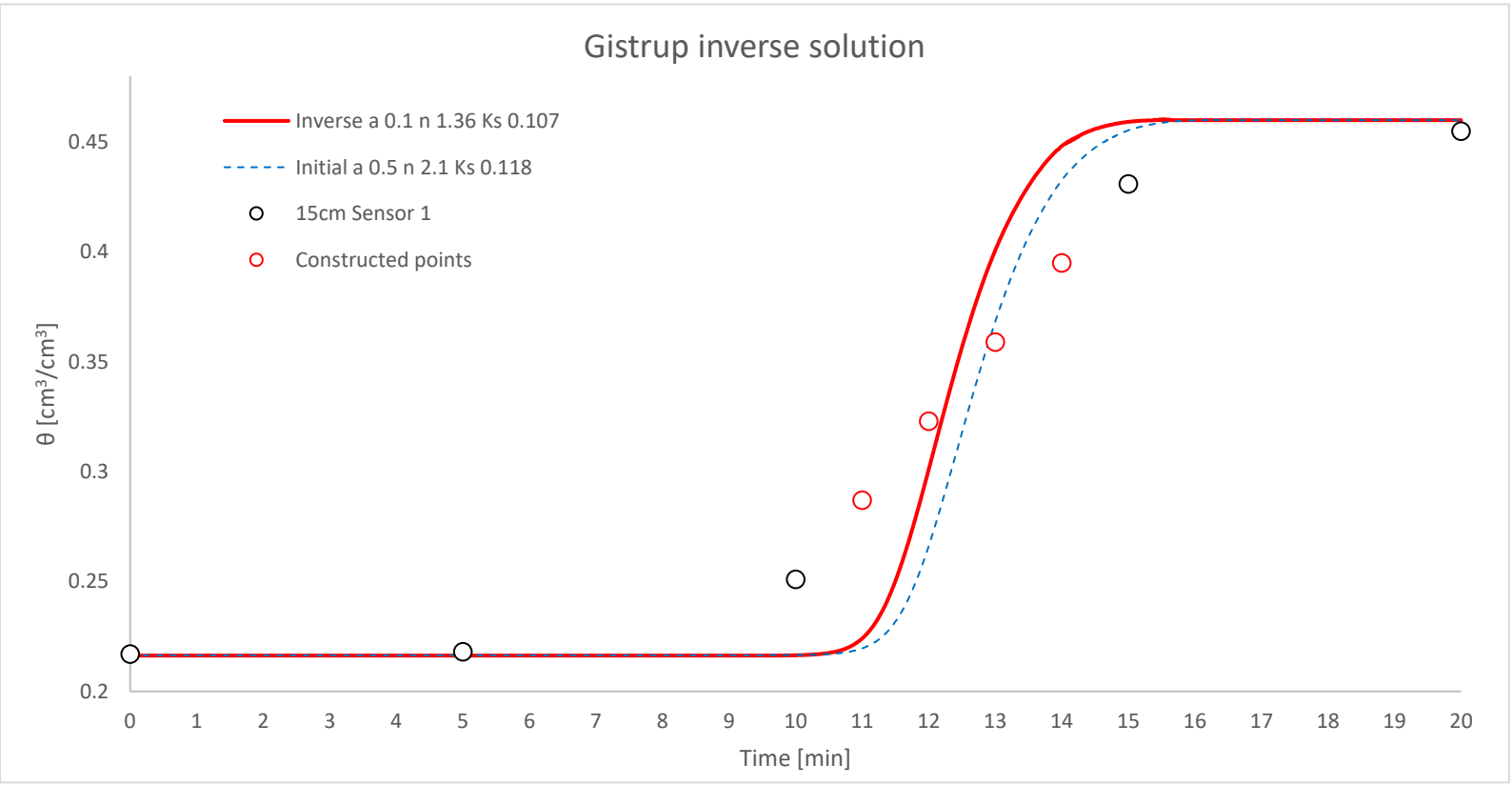

Figure 57 Gistrup inverse modelling results – sensor measurements in black (with constructed points in red), inverse fit in red and the initial guesstimate from Figure 51 in dashed blue.

The inverse solution produces a good fit around the estimated breakthrough time of the curve, however it misses both real measurements at minutes 10 and 15 on which the estimate is based on. Comparing the initial guesstimate to the inverse solution shows that the software reduced the α and Ks, as expected from the parameter insight in the previous chapter. On the other hand the value of n decreased instead of increasing in order to fulfil the set requirement for water content at pF 2. In other words, to balance the reduction in α. Regardless, this is the outcome under the assumed initial conditions, inputs and constraints. Figure 58 shows a comparison of the twin curves for Gistrup, one set based on the parameters from the Two-ring Two-run method and the other from the inverse fit.

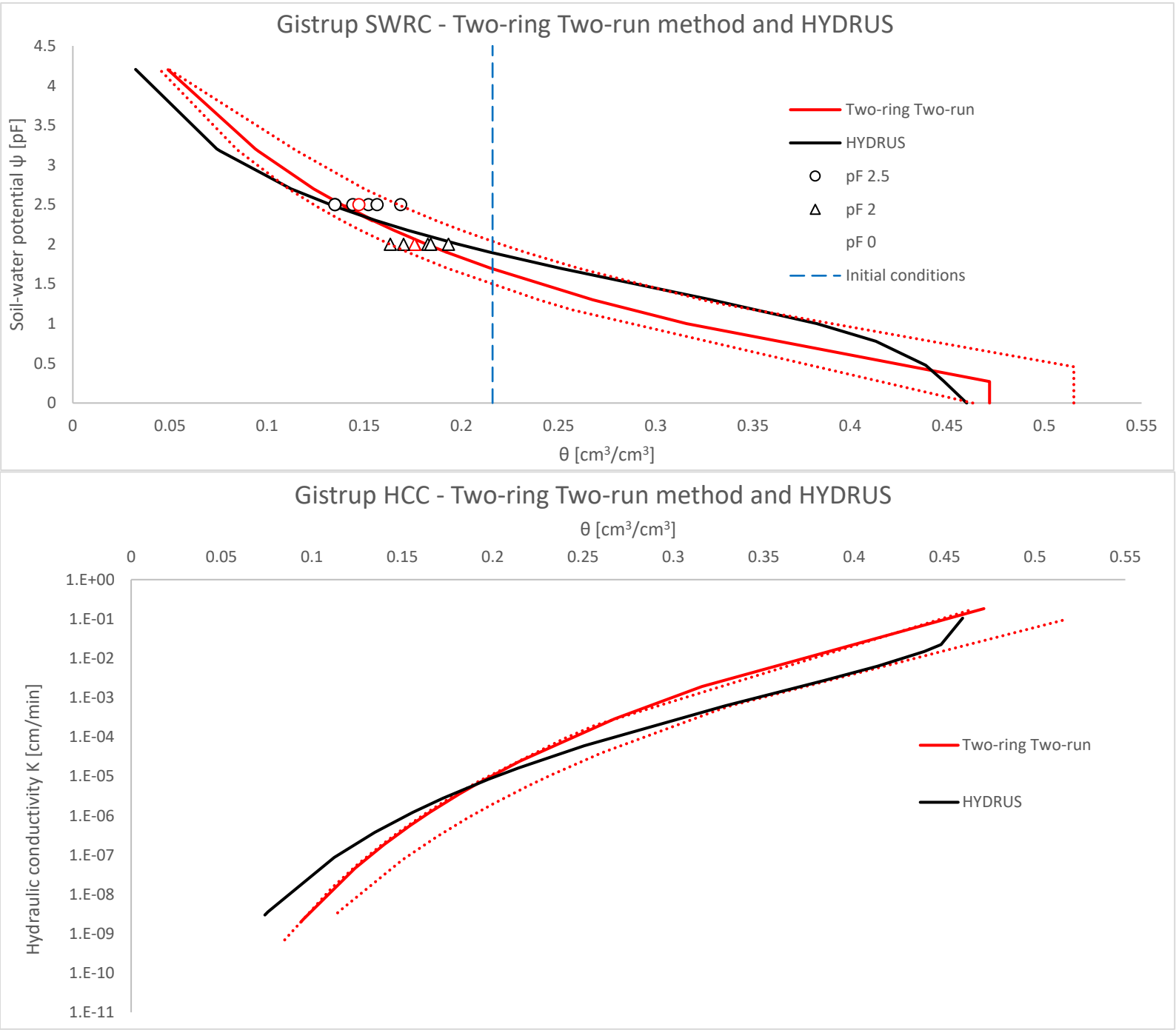

Figure 58 Twin curves for Gistrup, 2-ring 2-run with prediction bands in red and inverse solution from HYDRUS in black. Initial conditions, in water content from the sensor readings, shown in blue.

While not a perfect fit the HYDRUS parameters produce a curve which fall within the prediction band of the new method curve, at least in the wet end. The mismatch towards the drier end may be explained by the assumption that the residual water content in the vG model was assumed to be 0 which is the parameter that has an increasing shape-effect towards the dry end of the SWRC. It is considered a "good enough" result and enough to show that the Two-ring Two-run method shows promise but requires more precise validation, namely a more high-resolution sensor with more measurements.

There is, however one final consideration regarding inverse modelling that should be mentioned and that is regarding the logic behind the given constraints. It can be seen from Figure 57 that HYDRUS

chose the lowest limit for α, which can be viewed as indication that the given constraints are too narrow. The constraints for α were chosen based on its relationship to air entry and the air entry values from the Danish soil library. However, if another source for α is used such as the ROSETTA software introduced in (Schaap et al., 2001) it becomes clear that the relationship between α and ψe is not kept as is shown in Table 15.

Table 15 Hydraulic paramters for USDA textural classes in the ROSETTA software, data obtained from (Schaap et al., 2001)

soil texture rosetta	**Θs** [cm^3/cm^3]	**a** **[1/cm]**	**n**	**1/a = ψe** **[cm]**
sand	0.375	0.035	3.17	**28**
loamy sand	0.390	0.035	1.75	**29**
sandy loam	0.387	0.027	1.45	**37**
loam	0.399	0.011	1.47	**90**
silt	0.489	0.007	1.68	**152**
silt loam	0.439	0.005	1.66	**196**
sandy clay loam	0.384	0.021	1.33	**47**
clay loam	0.442	0.016	1.41	**63**
silty clay loam	0.482	0.008	1.52	**119**
sandy clay	0.385	0.033	1.21	**30**
silty clay	0.481	0.016	1.32	**62**
clay	0.459	0.015	1.25	**67**

As a final thought therefore the HYDRUS inverse setup was repeated with this in thought and the constraints were relaxed to include the range for sandy soils shown in Table 15. The Ks range was also increased with 20% to account for the uncertainty of the Ks value obtained from the experiment. The results are shown in Figure 59 and the resulting twin curves are shown in Figure 60.

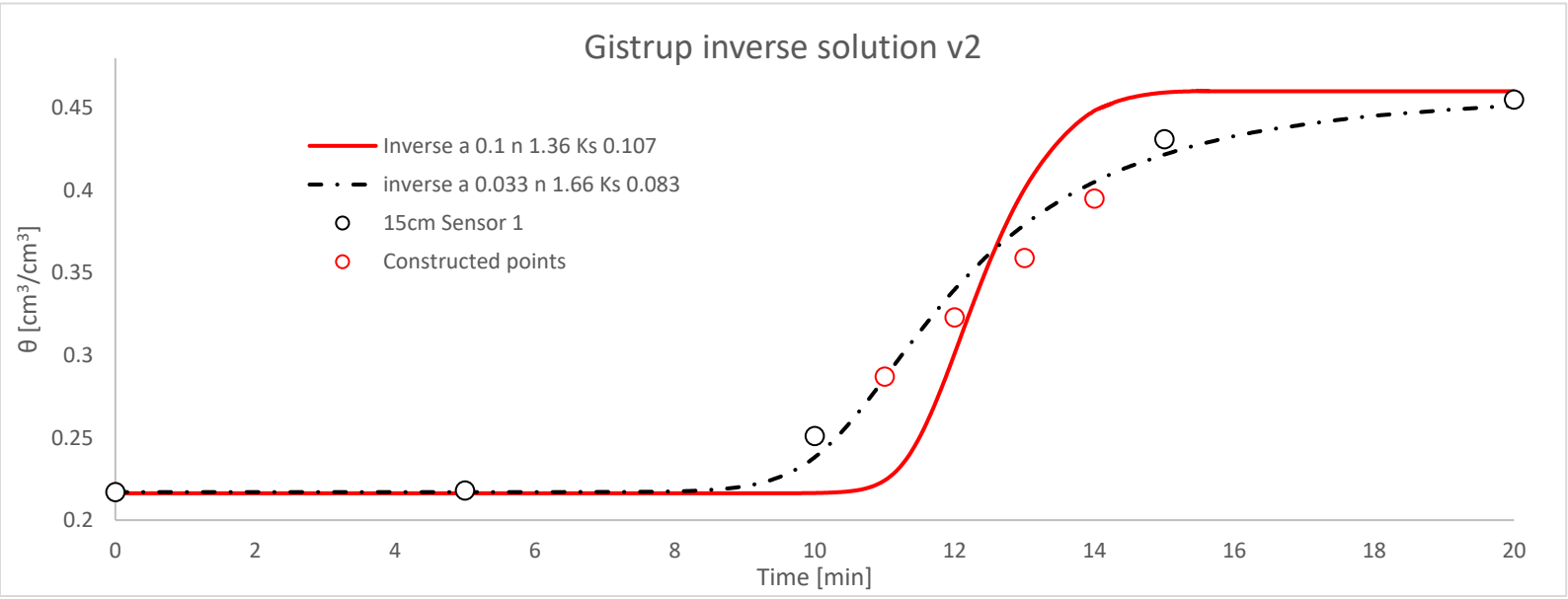

Figure 59 Gistrup inverse modelling results with relaxed parameter constraints – sensor measurements in black (with constructed points in red), original inverse fit in red and the relaxed parameter fit in dashed black.

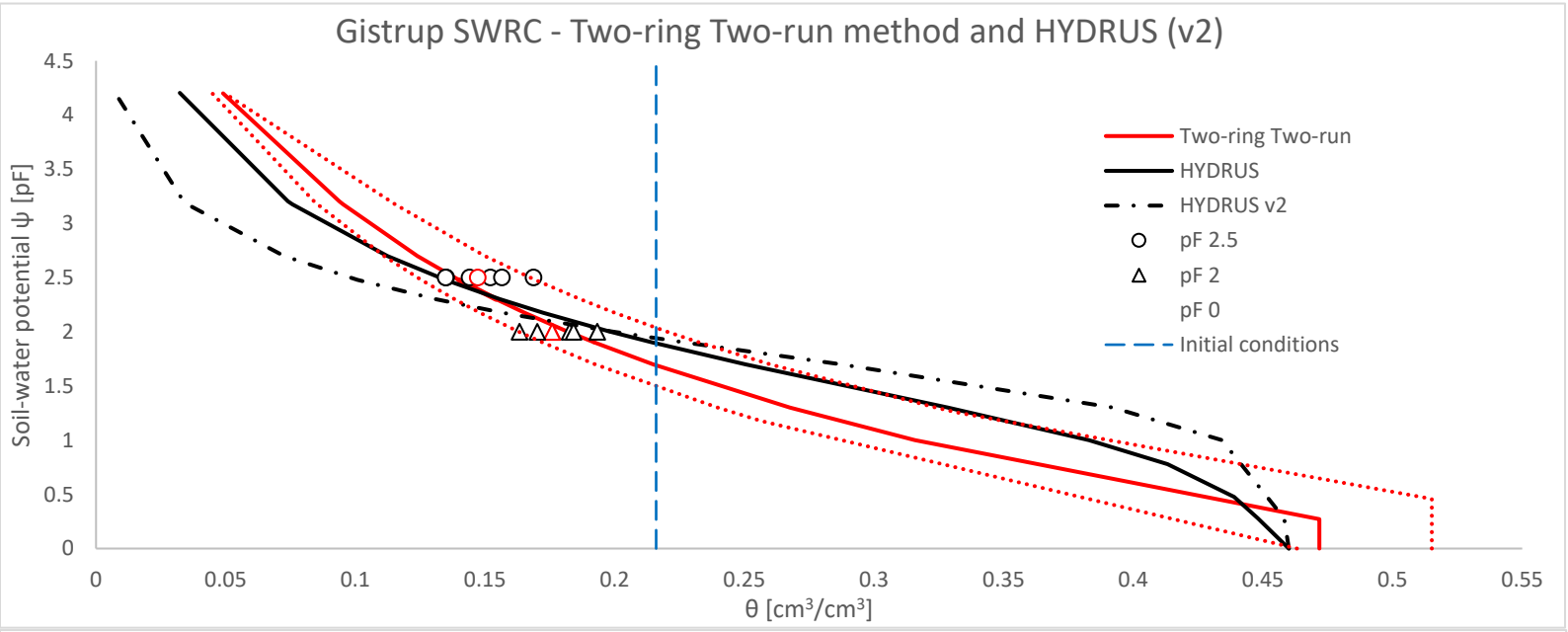

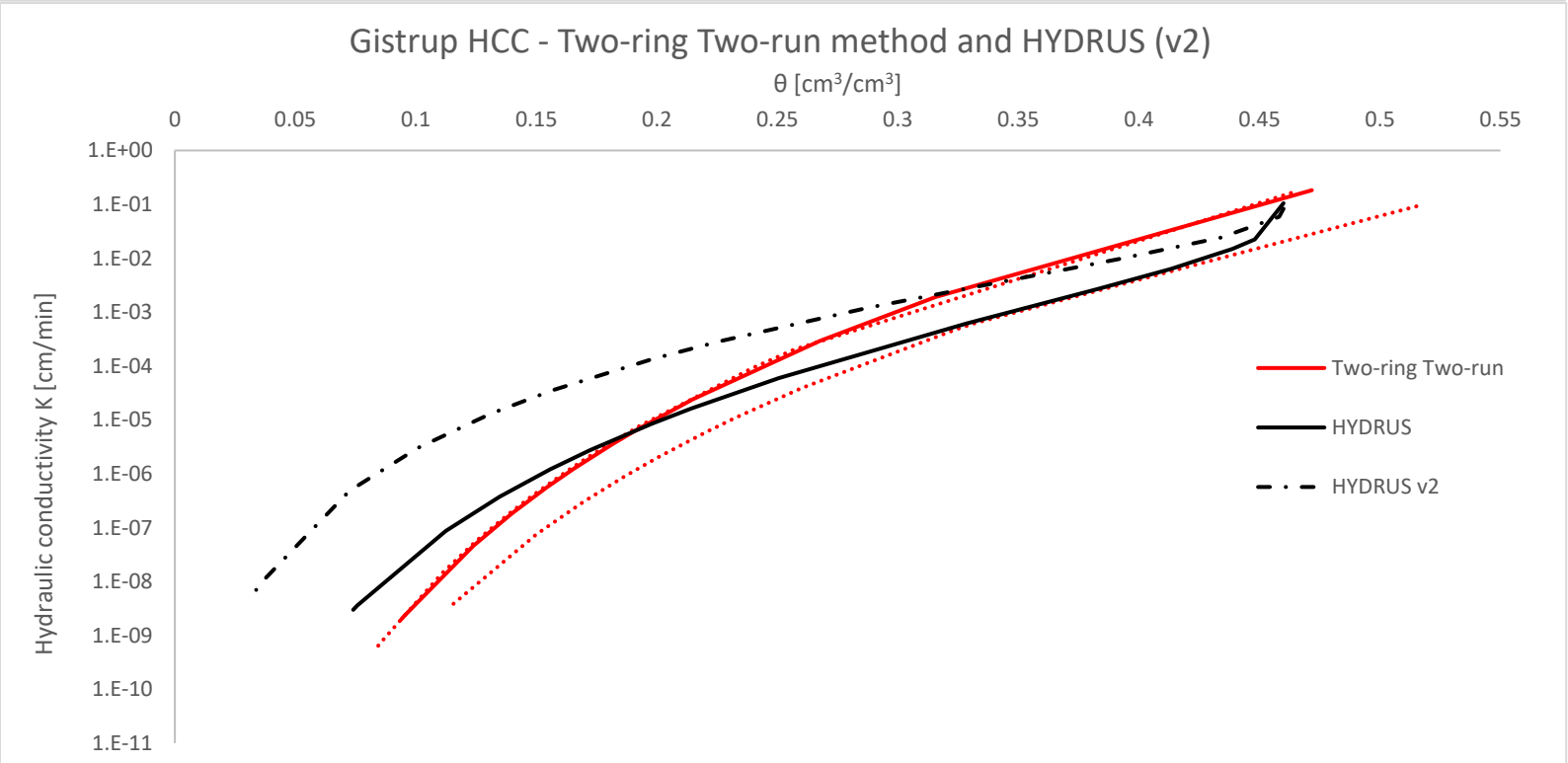

Figure 60 Twin curves for Gistrup, Two-ring Two-run with prediction bands in red and inverse solution from HYDRUS in black (original) and dashed black (relaxed parameters). Initial conditions, in water content from the sensor readings, shown in blue.

As it can be seen from figure Figure 59 the relaxed constrains result in a much better fit to the sensor measurements. However, as seen in Figure 60 this translates into a larger deviation from the estimation of the twin curves by the Two-ring Two-run method with the v2 simulated Gistrup soil parameters falling between the loamy sand and sandy loam texture classes, as listed in Table 15. This is unlikely as the fines of Gistrup were under 10%, and it is classified as sand, rather than loamy sand or sandy loam. Therefore, these last results (v2) should hardly be and were produced and shown purely out of interest – what would the "perfect" Gistrup fit according to HYDRUS while disregarding some of the assumptions for the parameter constraints.

7 Conclusion

This project introduced the Two-ring Two-run method as an easy and quick way to estimate the key unsaturated soil parameters needed to generate the Campbell curves for retention and conductivity. The twin curves are required for any modelling of water flow through soil and therefore are the subject of interest of many fields that deal with soil and water. The novelty of the method was to use the traditionally disregarded initial stages of infiltration facilitated by a double ring infiltrometer estimate the Campbell b and air entry parameters. The two main assumptions of the method presented in Chapter 3 are 1) in the initial stages of infiltration suction forces dominate and gravitational flow can be disregarded and 2) there is a strong enough link between the Philip sorptivity and the Campbell b to obtain one from the other. In Chapter 4 the method was tested at six soil sites including urban, forest and cultivated, all distinct from one another in both physical and hydrological senses. Chapter 5 addressed assumption 1 of the method and showed how gravity could affect the initial stages. The real validation was done in Chapter 6 where the twin curves generated from the new method were compared to curves obtained through inverse modelling using HYDRUS 1-D with the help of in-built moisture sensors. This similar scale comparison showed that the new method holds promise but requires more validation than the one showed in this case.

If the method is to be further developed these few points can be used as a starting point:

1. Further validation – the inverse modelling of the Gistrup site resulted in curves that were close to the ones estimated by the method, however it should be noted that the fit of the HYDRUS model to the measured water contents was sub-optimal with the measured water contents lacking high enough resolution to be considered good inputs for inverse modelling. Further validation should be carried out ideally using higher resolution sensors or in less coarse soils so that a measuring interval of 5 minutes is sufficient.
2. Refining and automation – some of the effects of human error can be seen in, for example, taking manual readings of the water level during infiltration which can lead to too frequent and/or inaccurate measurements. Given how important the initial stages of infiltration are for determining the sorptivity and inferring Campbell b from it is crucial that the early-stage infiltration is documented properly. This can be easily solved with a degree of automation i.e a pressure transducer or a water level meter.
3. Application on different soil types – as shown in Chapter 4 the six test sites were all classified as sandy soils and a possible shortcoming of the method is that it was not tested on any other soil type.

8 Reference list

Alagna, V., Bagarello, V., Di Prima, S., & Iovino, M. (2016). Determining hydraulic properties of a loam soil by alternative infiltrometer techniques. *Hydrological Processes*, *30*(2), 263–275. DOI 10.1002/hyp.10607

Angulo-Jaramillo, R., Bagarello, V., Iovino, M., & Lassabatere, L. (2016). Unsaturated Soil Hydraulic Properties. In *Infiltration Measurements for Soil Hydraulic Characterization* (pp. 181–287). Springer International Publishing. DOI 10.1007/978-3-319-31788-5_3

Angulo-Jaramillo, R., Bagarello, V., Iovino, M., Lassabatere, L., Angulo-Jaramillo, R., Bagarello, V., Iovino, M., & Lassabatere, L. (2016). Saturated Soil Hydraulic Conductivity. In *Infiltration Measurements for Soil Hydraulic Characterization* (pp. 43–180). Springer International Publishing. DOI 10.1007/978-3-319-31788-5_2

Bodhinayake, W., Si, B. C., & Noborio, K. (2004). Determination of Hydraulic Properties in Sloping Landscapes from Tension and Double-Ring Infiltrometers. *Vadose Zone Journal*, *3*(3), 964–970. DOI 10.2136/vzj2004.0964

Bordoni, M., Bittelli, M., Valentino, R., Chersich, S., & Meisina, C. (2017). Improving the estimation of complete field soil water characteristic curves through field monitoring data. *Journal of Hydrology*, *552*, 283–305. DOI 10.1016/j.jhydrol.2017.07.004

Bouma, J. (1989). *Using Soil Survey Data for Quantitative Land Evaluation* (pp. 177–213). Springer, New York, NY. DOI 10.1007/978-1-4612-3532-3_4

Brooks, R., & Corey, A. (1964). Hydraulic properties of porous media. *Hydrology Papers, Colorado State University*, *3*(March), 37 pp.

Buckingham, E. (1907). Studies on the Movement of Soil Moisture. *Bureau of Soils---Bulletin No. 38*, 61.

Campbell, G. S. (1974). A simple method for determining unsaturated conductivity from moisture retention data. *Soil Science*, *117*(6), 311–314. DOI 10.1097/00010694-197406000-00001

Carsel, R. F., & Parrish, R. S. (1988). Developing joint probability distributions of soil water retention characteristics. *Water Resources Research*, *24*(5), 755–769. DOI 10.1029/WR024i005p00755

Clapp, R. B., & Hornberger, G. M. (1978). Empirical equations for some soil hydraulic properties. *Water Resources Research*, *14*(4), 601–604. DOI 10.1029/WR014i004p00601

Cook, F. J., & Broeren, A. (1994). Six methods for determining sorptivity and hydraulic conductivity with disc permeameters. *Soil Science*, *157*(1), 2–11. DOI 10.1097/00010694-199401000-00002

Dane, J. H., & Clarke Topp, G. (Eds.). (2002). *Methods of Soil Analysis: Part 4 Physical Methods, 5.4*. Soil Science Society of America. DOI 10.2136/sssabookser5.4

Darcy, H. (1856). Les fontaines publiques de la ville de Dijon : exposition et application des principes à suivre et des formules à employer dans les questions de distribution d'eau. *Recherche*, 647.

Degré, A., van der Ploeg, M. J., Caldwell, T., & Gooren, H. P. A. (2017). Comparison of Soil Water Potential Sensors: A Drying Experiment. *Vadose Zone Journal*, *16*(4), vzj2016.08.0067. DOI 10.2136/vzj2016.08.0067

Druckenbrod, D. L. (2012). *Effect of Forest Age on Soil Organic Matter at Mount Vernon, VA*.

Eijkelkamp. (2015). *Double Ring Infiltrometer Manual*. Double Ring Infiltrometer. https://en.eijkelkamp.com/products/field-measurement-equipment/double-ring-

infiltrometer.html

Eijkelkamp. (2021). *Manual Art . no . 0909 Tension infiltrometer Soll preparatlon :* https://en.eijkelkamp.com/products/field-measurement-equipment/tech-specs-tension-infiltrometer.html

Fan, G., Han, Y., & Song, M. (2012). Experimental study on the reasonable inbuilt-ring depth of soil one-dimensional infiltration experiment in field. *IFIP Advances in Information and Communication Technology*, *368 AICT*(PART 1), 427–436. DOI 10.1007/978-3-642-27281-3_48

Fernández-Gálvez, J., Pollacco, J. A. P., Lassabatere, L., Angulo-Jaramillo, R., & Carrick, S. (2019). A general Beerkan Estimation of Soil Transfer parameters method predicting hydraulic parameters of any unimodal water retention and hydraulic conductivity curves: Application to the Kosugi soil hydraulic model without using particle size distribution data. *Advances in Water Resources*, *129*, 118–130. DOI 10.1016/j.advwatres.2019.05.005

Gardner, W. R. (1958). Some steady-state solutions of the unsaturated moisture flow equation with application to evaporation from a water table. *Soil Science*, *85*(4), 228–232. DOI 10.1097/00010694-195804000-00006

Gill, L., Knappe, J., Morrissey, P., Gill, L., Knappe, J., & Morrissey, P. (2019). A comparison of falling head vs constant head percolation tests using field results and numerical modeling to determine the hydraulic conductivity of soils. *EGUGA*, 5298.

Gonzalez-Sosa, E., Braud, I., Dehotin, J., Lassabatère, L., Angulo-Jaramillo, R., Lagouy, M., Branger, F., Jacqueminet, C., Kermadi, S., & Michel, K. (2010). Impact of land use on the hydraulic properties of the topsoil in a small French catchment. *Hydrological Processes*, *24*(17), n/a-n/a. DOI 10.1002/hyp.7640

Hansen, L. (1976). Soil Types at the Danish State Experimental Stations. *Statens Forsøgsvirksomhed i Plantekultur*, 742–758.

Hopmans, J. W. (2011). *Richards Equation - an overview | ScienceDirect Topics*. https://www.sciencedirect.com/topics/earth-and-planetary-sciences/richards-equation

Iiyama, I. (2016). Differences between field-monitored and laboratory-measured soil moisture characteristics. *Soil Science and Plant Nutrition*, *62*(5–6), 416–422. DOI 10.1080/00380768.2016.1242367

Jang, J., Narsilio, G. A., & Santamarina, J. C. (2011). Hydraulic conductivity in spatially varying media-a pore-scale investigation. *Geophysical Journal International*, *184*(3), 1167–1179. DOI 10.1111/j.1365-246X.2010.04893.x

Ket, P., Oeurng, C., & Degré, A. (2018). Estimating Soil Water Retention Curve by Inverse Modelling from Combination of In Situ Dynamic Soil Water Content and Soil Potential Data. *Soil Systems*, *2*(4), 55. DOI 10.3390/soilsystems2040055

Lai, J., Luo, Y., & Ren, L. (2010). Buffer Index Effects on Hydraulic Conductivity Measurements Using Numerical Simulations of Double-Ring Infiltration. *Soil Science Society of America Journal*, *74*(5), 1526–1536. DOI 10.2136/sssaj2009.0450

Lai, J., Luo, Y., & Ren, L. (2012). Numerical Evaluation of Depth Effects of Double-Ring Infiltrometers on Soil Saturated Hydraulic Conductivity Measurements. *Soil Science Society of America Journal*, *76*(3), 867–875. DOI 10.2136/sssaj2011.0048

Lai, J., & Ren, L. (2007). Assessing the Size Dependency of Measured Hydraulic Conductivity Using Double-Ring Infiltrometers and Numerical Simulation. *Soil Science Society of America Journal*,

71(6), 1667–1675. DOI 10.2136/sssaj2006.0227

Lassabatere, L., Angulo-Jaramillo, R., Goutaland, D., Letellier, L., Gaudet, J. P., Winiarski, T., & Delolme, C. (2010). Effect of the settlement of sediments on water infiltration in two urban infiltration basins. *Geoderma*, *156*(3–4), 316–325. DOI 10.1016/j.geoderma.2010.02.031

Lassabatère, L., Angulo-Jaramillo, R., Soria Ugalde, J. M., Cuenca, R., Braud, I., & Haverkamp, R. (2006). Beerkan Estimation of Soil Transfer Parameters through Infiltration Experiments-BEST. *Soil Science Society of America Journal*, *70*(2), 521–532. DOI 10.2136/sssaj2005.0026

Loll, P., & Moldrup, P. (2000). *Soil Characterization and Polluted Soil Assessment*. Aalborg University.

Minnesota Pollution Control Agency. (2015). *Design infiltration rates - Minnesota Stormwater Manual*. https://stormwater.pca.state.mn.us/index.php/Determining_soil_infiltration_rates

Mubarak, I., Mailhol, J. C., Angulo-Jaramillo, R., Ruelle, P., Boivin, P., & Khaledian, M. (2009). Temporal variability in soil hydraulic properties under drip irrigation. *Geoderma*, *150*(1–2), 158–165. DOI 10.1016/j.geoderma.2009.01.022

Mueller, L., Behrendt, A., Graham Shepherd, T., Schindler, U., Ball, B. C., Khudyaev, S., Kaiser, T., Dannowski, R., & Eulenstein, F. (2014). Simple field methods for measurement and evaluation of grassland quality. *Environmental Science and Engineering (Subseries: Environmental Science)*, *202979*, 199–222. DOI 10.1007/978-3-319-01017-5_11

Nolz, R., & Kammerer, G. (2017). Evaluating a sensor setup with respect to near-surface soil water monitoring and determination of in-situ water retention functions. *Journal of Hydrology*, *549*, 301–312. DOI 10.1016/j.jhydrol.2017.04.011

Osman, K. T., & Osman, K. T. (2013). Organic Matter of Forest Soils. In *Forest Soils* (pp. 63–76). Springer International Publishing. DOI 10.1007/978-3-319-02541-4_4

Pachepsky, Y. A., & van Genuchten, M. T. (2011). Pedotransfer functions. In *Encyclopedia of Earth Sciences Series: Vol. Part 4* (pp. 556–560). Springer Netherlands. DOI 10.1007/978-90-481-3585-1_109

Perroux, K. M., & White, I. (1988). Designs for Disc Permeameters. *Soil Science Society of America Journal*, *52*(5), 1205–1215. DOI 10.2136/sssaj1988.03615995005200050001x

Philip, J. R. (1957). The theory of infiltration: 4. Sorptivity and algebraic infiltration equations. *Soil Science*, *84*(3), 257–264.

Quirijn, D. J. V. L., & Everton Alves Rodrigues, P. (2018). An alert regarding a common misinterpretation of the van genuchten α parameter. In *Revista Brasileira de Ciencia do Solo* (Vol. 42). Revista Brasileira de Ciencia do Solo. DOI 10.1590/18069657rbcs20170343

Rahmati, M., Weihermüller, L., Vanderborght, J., Pachepsky, Y. A., Mao, L., Sadeghi, S. H., Moosavi, N., Kheirfam, H., Montzka, C., Van Looy, K., Toth, B., Hazbavi, Z., Al Yamani, W., Albalasmeh, A. A., Alghzawi, M. Z., Angulo-Jaramillo, R., Antonino, A. C. D., Arampatzis, G., Armindo, R. A., … Vereecken, H. (2018). Development and analysis of the Soil Water Infiltration Global database. *Earth System Science Data*, *10*(3), 1237–1263. DOI 10.5194/essd-10-1237-2018

Ravi, S., D'Odorico, P., Over, T. M., & Zobeck, T. M. (2004). On the effect of air humidity on soil susceptibility to wind erosion: The case of air-dry soils. *Geophysical Research Letters*, *31*(9). DOI 10.1029/2004GL019485

Reynolds, W. D., & Elrick, D. E. (1986). A Method for Simultaneous In Situ Measurement in the Vadose Zone of Field-Saturated Hydraulic Conductivity, Sorptivity and the Conductivity-Pressure Head Relationship. *Groundwater Monitoring & Remediation*, *6*(1), 84–95. DOI

10.1111/j.1745-6592.1986.tb01229.x

Schaap, M. G., Leij, F. J., & Van Genuchten, M. T. (2001). Rosetta: A computer program for estimating soil hydraulic parameters with hierarchical pedotransfer functions. *Journal of Hydrology*, *251*(3–4), 163–176. DOI 10.1016/S0022-1694(01)00466-8

Schulze-Makuch, D., Carlson, D. A., Cherkauer, D. S., & Malik, P. (1999). Scale Dependency of Hydraulic Conductivity in Heterogeneous Media. *Ground Water*, *37*(6), 904–904.

Šimůnek, J., & van Genuchten, M. T. (1996). Estimating Unsaturated Soil Hydraulic Properties from Tension Disc Infiltrometer Data by Numerical Inversion. *Water Resources Research*, *32*(9), 2683–2696. DOI 10.1029/96WR01525

Šimůnek, Jiří, Angulo-Jaramillo, R., Schaap, M. G., Vandervaere, J. P., & Van Genuchten, M. T. (1998). Using an inverse method to estimate the hydraulic properties of crusted soils from tension-disc infiltrometer data. *Geoderma*, *86*(1–2), 61–81. DOI 10.1016/S0016-7061(98)00035-4

Šimůnek, Jiří, & Van Genuchten, M. T. (1997). Estimating unsaturated soil hydraulic properties from multiple tension disc infiltrometer data. *Soil Science*, *162*(6), 383–398. DOI 10.1097/00010694-199706000-00001

Smettem, K. R. J., Parlange, J. Y., Ross, P. J., & Haverkamp, R. (1994). Three-dimensional analysis of infiltration from the disc infiltrometer: 1. A capillary-based theory. *Water Resources Research*, *30*(11), 2925–2929. DOI 10.1029/94WR01787

Usowicz, B., & Lipiec, J. (2021). Spatial variability of saturated hydraulic conductivity and its links with other soil properties at the regional scale. *Scientific Reports*, *11*(1), 8293. DOI 10.1038/s41598-021-86862-3

van Genuchten, M. T. (1980). A Closed-form Equation for Predicting the Hydraulic Conductivity of Unsaturated Soils. *Soil Science Society of America Journal*, *44*(5), 892–898. DOI 10.2136/sssaj1980.03615995004400050002x

Vanapalli, S. K., Sillers, W. S., & Fredlund, M. D. (1998). The meaning and relevance of residual state to unsaturated soils. *Proceedings of the 51st Canadian Geotechnical Conference*, 1–8.

Watson, K. W., & Luxmoore, R. J. (1986). Estimating Macroporosity in a Forest Watershed by use of a Tension Infiltrometer. *Soil Science Society of America Journal*, *50*(3), 578–582. DOI 10.2136/sssaj1986.03615995005000030007x

Wu, L., Pan, L., Mitchell, J., & Sanden, B. (1999). Measuring Saturated Hydraulic Conductivity using a Generalized Solution for Single-Ring Infiltrometers. *Soil Science Society of America Journal*, *63*(4), 788–792. DOI 10.2136/sssaj1999.634788x

Xu, X., Lewis, C., Liu, W., Albertson, J. D., & Kiely, G. (2012). Analysis of single-ring infiltrometer data for soil hydraulic properties estimation: Comparison of BEST and Wu methods. *Agricultural Water Management*, *107*, 34–41. DOI 10.1016/j.agwat.2012.01.004

Zeitoun, R., Vandergeest, M., Vasava, H. B., Machado, P. V. F., Jordan, S., Parkin, G., Wagner-Riddle, C., & Biswas, A. (2021). In-Situ Estimation of Soil Water Retention Curve in Silt Loam and Loamy Sand Soils at Different Soil Depths. *Sensors*, *21*(2), 447. DOI 10.3390/s21020447

9 Appendices

9.1 Infiltration data

Dobule ring infiltrometer – 90-cm outer ring, 60-cm inner ring diameters

TMV				TMV 2			
Run 1		Run 2		Run 1		Run 2	
Time [min]	Water level [cm]	Time [min]	Water level [cm]	Time [min]	Water level [cm]	Time [min]	Water level [cm]
0	13.1	0	14	0	11.6	0	7.2
2	12.2	10	13.2	4	11.1	10	6.8
4	11.6	20	12.3	8	10.7	20	6.4
6	11.2	30	11.5	12	10.3	50	5
8	10.8	40	11	16	10	80	4
10	10.5	50	10.3	20	9.7	110	3
14	9.8	60	9.6	24	9.4	140	1.9
18	9.1	70	9	28	9.2	170	1
22	8.5	80	8.5	32	9		
26	8	90	8	36	8.8	insertion depth [cm]	
30	7.6			40	8.6	8	
40	6.6	insertion depth [cm]		50	8.2		
50	5.6	8		60	7.8		
60	4.7						
120	2.4						
Gistrup				St. Restrup Forest			
Run 1		Run 2		Run 1		Run 2	
Time [min]	Water level [cm]	Time [min]	Water level [cm]	Time [min]	Water level [cm]	Time [min]	Water level [cm]
0	12.5	0	14	0	23	0	23.5
2	11.6	2	13.5	1	20.5	1	22.6
4	10.8	4	13.2	2	19	2	21.5
6	10.1	6	12.7	3	17.5	3	20.75
8	9.5	8	12.2	4	16.5	4	19.8
10	9	10	11.6	5	15.5	5	19
12	8.4	12	11.1	6	14.5	6	18.2
14	7.8	14	10.4	7	13.5	7	17.2
16	7.1	16	9.9	8	12.5	8	16.3
18	6.4	18	9.4	9	11.5	9	15.5
20	5.7	20	8.8	10	10.75	10	14.8
22	5	22	8.3	11	10	11	13.9
24	4.4	24	7.8	12	9	12	13
26	3.8	26	7.1	13	8.5	13	12.5
28	3	28	6.6	14	7.75	14	11.6
		30	6.1	15	7	15	10.9
		32	5.6	16	6.25	16	10.25
insertion depth [cm]		34	5.1	17	5.5	17	9.5

11		36	4.7	18	4.8	18	8.75
		38	4.2	19	4.2	19	8
		40	3.8	20	3.5	20	7.5
		42	3.4			21	6.75
		44	2.9	insertion depth [cm]		22	6
		46	2.4	10		23	5.5
						24	4.9
						25	4.1
						26	3.75
						27	3
St. Restrup Field 1				St. Restrup Field 2			
Run 1		Run 2		Run 1		Run 2	
Time [min]	Water level [cm]	Time [min]	Water level [cm]	Time [min]	Water level [cm]	Time [min]	Water level [cm]
0	30.5	0	35	0	29.5	1	31.8
1	30	5	34.7	5	26.9	2	31.5
2	29.5	10	34.5	10	25	3	31.2
3	29.2	15	34.4	15	23.2	4	31
4	29	20	34.1	20	21.6	5	30.8
5	28.8	25	34	25	20.1	6	30.5
6	28.6	30	33.9	30	18.8	7	30.3
7	28.4	38	33.6	35	17.4	8	30.1
8	28.3	45	33.5	40	16.5	9	30
9	28.1	60	33	45	15.3	10	29.8
10	28	75	32.6	50	14.3	15	28.8
11	27.9	84	32.4	55	13.2	25	26.9
12	27.8	90	32.1	60	12.1	30	25.9
14	27.6	110	31.7	65	11.2	35	25
16	27.3	163	30	70	10.4	40	24
18	27.1			75	9.6	45	23
20	27	insertion depth [cm]				50	22
25	26.5	4		insertion depth [cm]		55	21.1
30	26			11.6		65	19.8
35	25.8					70	18.9
40	25.5					75	18
45	25.2					80	17
50	25					85	16.2
55	24.8					90	15.5
60	24.6					95	14.9
						115	12
						120	11.3
						125	10.8
						150	7
						155	6.5
						160	5.9

9.2 Gistrup sensor data

METER EC-5 Soil moisture content			
	15cm Sensor 1	**15 cm Sensor 2**	**30cm Sensor**
	m^3/m^3 Water Content	**m^3/m^3 Water Content**	**m^3/m^3 Water Content**
2020-12-13 11.55.00	0.217	0.215	0.242
2020-12-13 12.00.00	**0.218**	0.216	0.242
2020-12-13 12.05.00	**0.251**	0.231	0.243
2020-12-13 12.10.00	**0.431**	0.393	0.244
2020-12-13 12.15.00	**0.455**	0.45	0.251
2020-12-13 12.20.00	0.455	0.454	0.266
2020-12-13 12.25.00	0.455	0.455	0.292
2020-12-13 12.30.00	0.456	0.457	0.321
2020-12-13 12.35.00	0.459	0.46	0.352
2020-12-13 12.40.00	0.46	0.46	0.387
2020-12-13 12.45.00	0.458	0.459	0.402
2020-12-13 12.50.00	0.458	0.459	0.405
2020-12-13 12.55.00	0.457	0.458	0.407
2020-12-13 13.00.00	0.457	0.458	0.408
2020-12-13 13.05.00	0.456	0.457	0.408
2020-12-13 13.10.00	0.456	0.457	0.408
2020-12-13 13.15.00	0.455	0.457	0.408
2020-12-13 13.20.00	0.455	0.456	0.408
2020-12-13 13.25.00	0.454	0.455	0.407
2020-12-13 13.30.00	0.453	0.453	0.405
2020-12-13 13.35.00	0.451	0.452	0.403
2020-12-13 13.40.00	0.45	0.451	0.402
2020-12-13 13.45.00	0.449	0.45	0.401
2020-12-13 13.50.00	0.448	0.45	0.399
2020-12-13 13.55.00	0.447	0.449	0.398
2020-12-13 14.00.00	0.446	0.448	0.396
2020-12-13 14.05.00	0.445	0.448	0.395
2020-12-13 14.10.00	0.444	0.447	0.394
2020-12-13 14.15.00	0.444	0.446	0.393
2020-12-13 14.20.00	0.443	0.441	0.392
2020-12-13 14.25.00	0.442	0.441	0.391
2020-12-13 14.30.00	0.441	0.44	0.39
2020-12-13 14.35.00	0.439	0.439	0.389
2020-12-13 14.40.00	0.438	0.439	0.389
2020-12-13 14.45.00	0.437	0.438	0.388
2020-12-13 14.50.00	0.436	0.438	0.387
2020-12-13 14.55.00	0.435	0.437	0.387

9.3 Soil volumetric water content data

	Volumetric water content [cm^3/cm^3]		
Site	θs	pF 2	pF 2.5
TMV	0.424	0.255	0.201
	0.396	0.230	0.181
	0.460	0.212	0.168
	0.404	0.193	0.155
	0.458	0.232	0.182
	0.414	0.233	0.180
	0.427	0.227	0.175
	0.450	0.219	0.168
TMV 2	0.452	0.283	0.225
	0.464	0.288	0.224
	0.466	0.274	0.222
	0.460	0.260	0.198
	0.433	0.277	0.213
	0.465	0.275	0.220
	0.436	0.267	0.200
	0.454	0.285	0.222
	0.472	0.267	0.205
Gistrup	0.515	0.176	0.144
	0.470	0.163	0.135
	0.463	0.183	0.152
	0.470	0.184	0.157
	0.485	0.176	0.147
	0.494	0.193	0.169
	0.472	0.170	0.135
St. Restrup Forest	0.412	0.283	-
	0.397	0.154	-
St. Restrup Field 1*	0.453	0.131	-
St. Restrup Field 2	0.485	0.178	-
	0.518	0.157	-
	0.497	0.222	-
	0.512	0.202	-
	0.483	0.212	-

*The water content at pF 2 for Field 1 was assumed unrealistic and the mean value from Field 2 was used in the report.

9.4 Saturated hydraulic conductivity calculation

Cumulative infiltration I [L] and infiltration rate [L/T] the direct results from the experiment and are used to estimate Ks once steady state is reached. There are a number of ways of doing this, however for the purposes of this report the hydraulic conductivity is then calculated using Darcy's law:

$$v = -Ks\frac{dH}{dx}$$

Where v is the infiltration rate [cm/min], Ks is the saturated hydraulic conductivity [cm/min] and dH/dx is the hydraulic gradient where H is total pressure head (gravitational and soil-water potential) [cm] and x [cm] is the length of soil through which water infiltrates.

The figure below shows the conceptual model the DRI experiment and how the parameters in Darcy's law are defined.

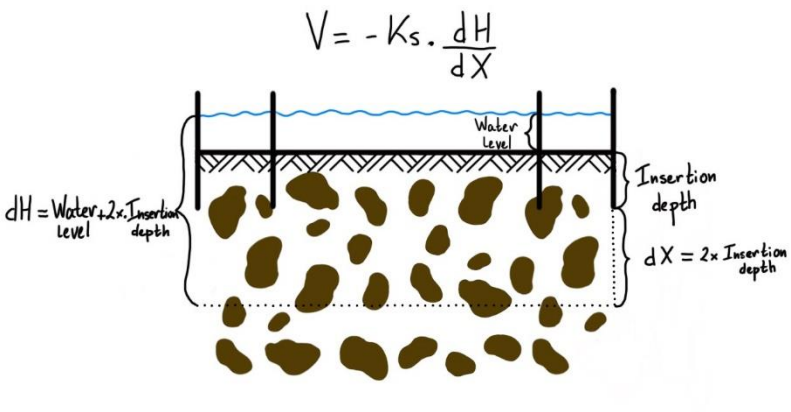

This is in reality a falling head experiment but is treated as a constant head by solving for v in a step-wise manner. The average time between two notations in the falling head experiment is the timestep. For that timestep:

- The Darcy infiltration rate (v) is the change in water level divided by the change in time
- The length of saturated soil (x)'s upper boundary is the soil surface and the lower boundary is assumed to be twice the insertion depth of the outer ring
- The pressure head (H)'s upper boundary is the average water level of the two notations and the lower boundary is assumed to be twice the insertion depth of the outer ring

Given these assumptions the hydraulic conductivity is calculated for each timestep. Example for TMV Run 2:

(14-13,2)/2 — (14-13,2)/(10-0) — (13,6+2*8)/(2*8) — 0,08/1,85

Insertion depth [cm]	8					
water level [cm]	time elapsed [min]	timestep t [min]	Average WL for t [cm]	V [cm/min]	dh/dx	Ksat [cm/min]
14	0	5	13,6	0,08	1,85	0,043
13,2	10	15	12,75	0,09	1,80	0,050
12,3	20	25	11,9	0,08	1,74	0,046
11,5	30	35	11,25	0,05	1,70	0,029
11	40	45	10,65	0,07	1,67	0,042
10,3	50	55	9,95	0,07	1,62	0,043
9,6	60	65	9,3	0,06	1,58	0,038
9	70	75	8,75	0,05	1,55	0,032
8,5	80	85	8,25	0,05	1,52	0,033
8	90		Mean	0,067		0,034
			STD	0,015		0,003

9.5 Danish soils from Hansen library

In the Danish soil library there are no readily available Campbell b and air entry values, which have been used in this project to construct the SWRCs for the comparison soils. The b values were obtained from a log10-log10 plot of water content versus soil-water potential, the slope of which is Campbell b. Air entry was then obtained fitting the Campbell model to the measured water contents using the solver function in MS excel. An example of Ødum 0-40 is given below:

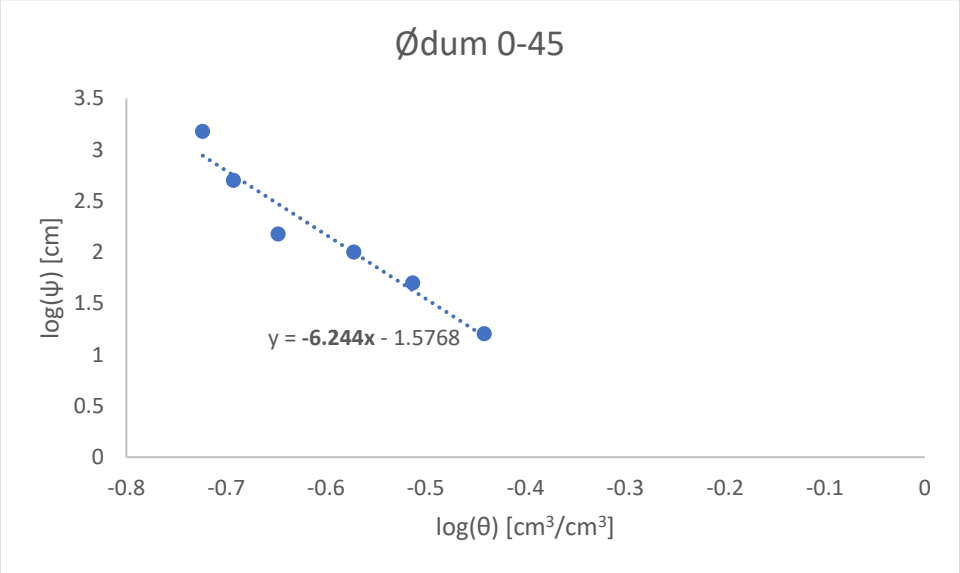

	Ødum 0-40				
Θsat [cm3/cm3]	0.436				
b	6.244				
/ψe/ [cm]	4.68				
	ψ [cm water]	ψ [pF]	Campbell model WC [cm3/cm3]	Measured WC [cm3/cm3]	RMSE
	16	0	0.358	0.362	2E-05
	50	1.70	0.298	0.307	7E-05
	100	2.00	0.267	0.268	1E-06
	150	2.18	0.250	0.225	6E-04
	500	2.70	0.206	0.203	1E-05
	1500	3.18	0.173	0.189	3E-04
					1E-03

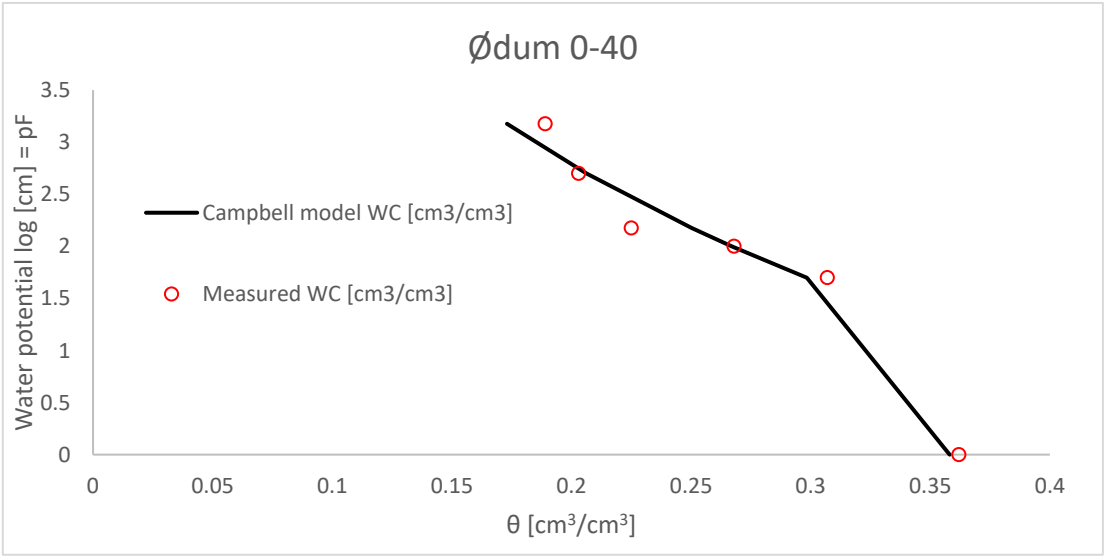

9.6 Applying the two-term Philips equation to infiltration data

The first step is to the generate the new dataset. This is done by combining Run 1 and 2, specifically the accumulated infiltration and time where each Run 2 measurement is added to the last measurement of Run 1. Then the two-term Philip model is fitted using the excel solver function. As previously discussed A is correlated to Ks depending on the elapsed time of the experiment, with A ≈ Ks for long lasting infiltration. As such the solver function was constrained so that the fit could not produce an A value larger than the measured Ks from Run 2. Table Table 16 shows the constrains based on the Ks values from chapters 3 and 4.

Table 16 Constrains for Philip A parameter, based on Ks measurements from Run 2.

	A max [cm/min]
TMV	0.034
TMV 2	0.029
Gistrup	0.183
Forest	0.496
Field 1	0.006
Field 2	0.086

9.6.1 TMV sites

Figure 61a shows a plot of the Darcy velocity versus time is added to help identify where the flow transitions from suction- to mixed- and finally gravity-dominated. Figure 61b shows the results of fitting the Philip model to the combined run datapoints for the TMV sites.

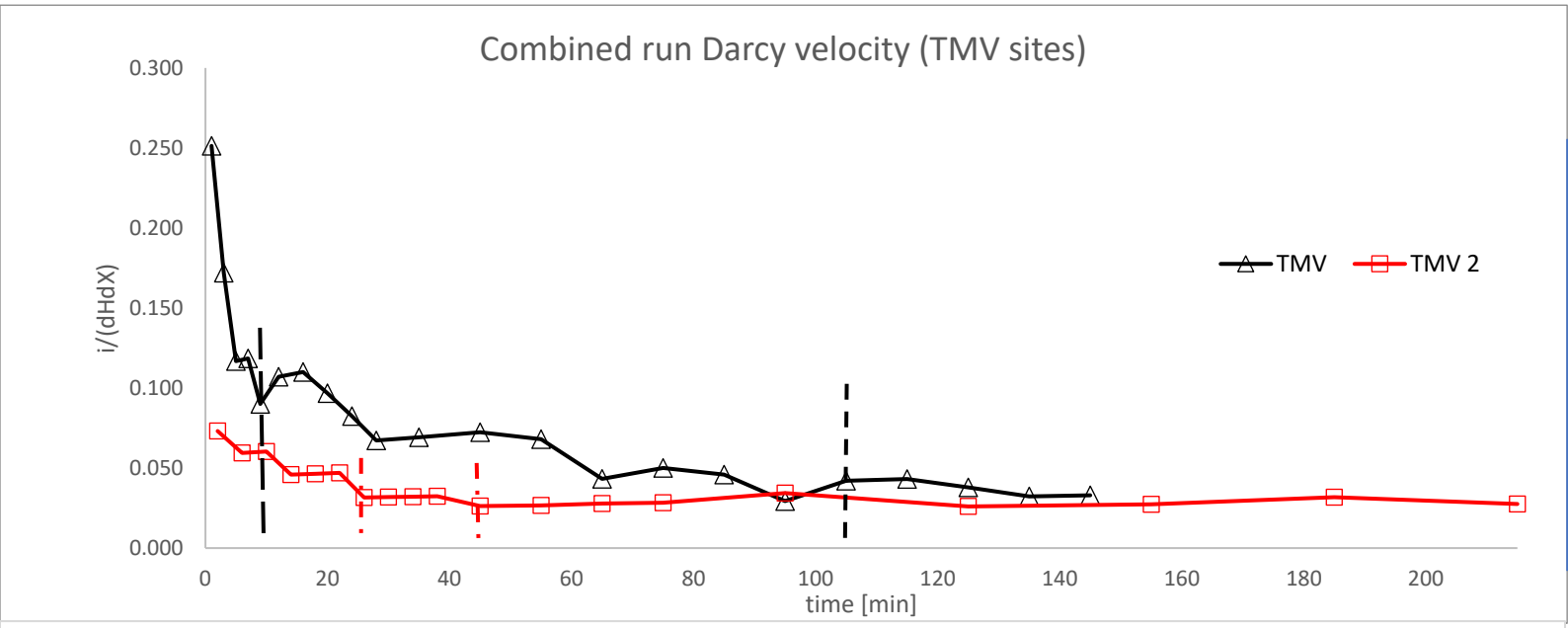

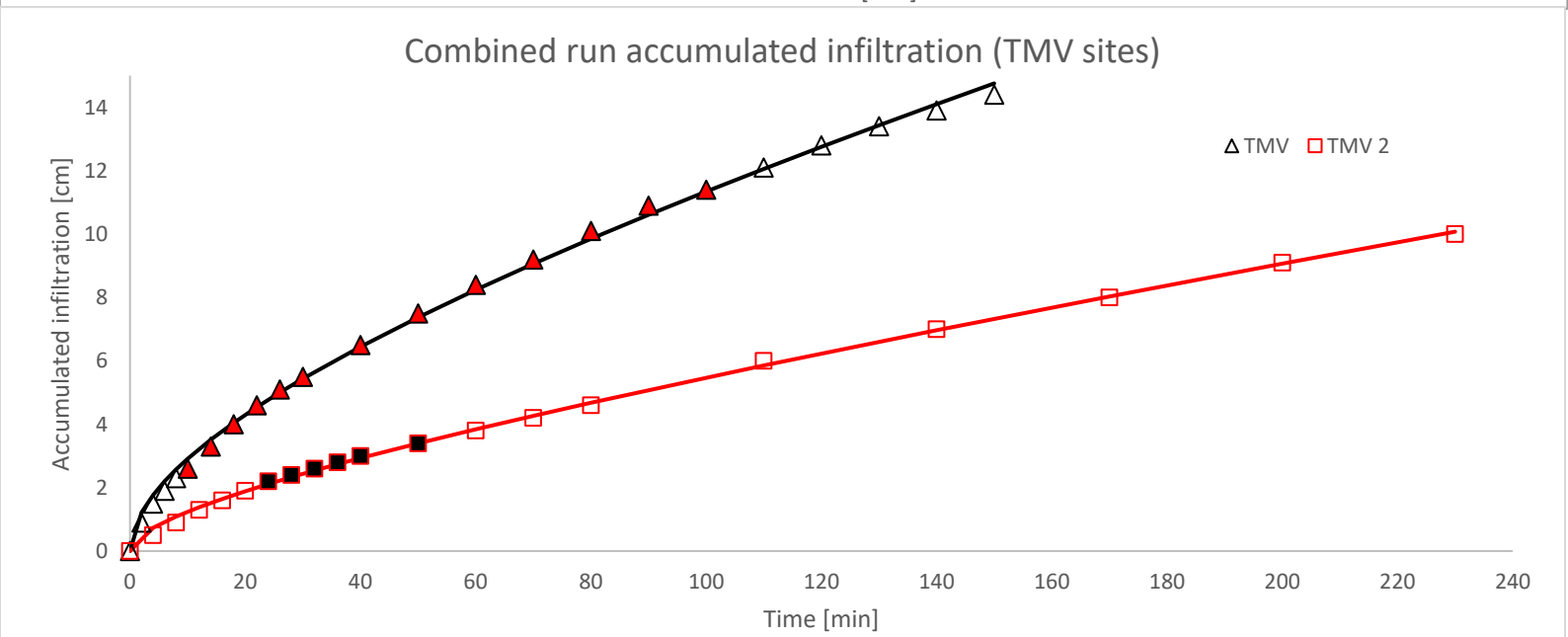

Figure 61 a) Darcy velocity versus time for the combined run of TMV and TMV 2 in black and red, respectively. Dashed lines represent the transition between the three flow regions for their respective sites – suction, mixed and gravity dominated. Division made by eye.
b) Fit of the Philip infiltration model for TMV and TMV 2 in black and red, respectively. Filled symbols represent the mixed flow, as indicated in a). S [cm/√min] = 0.820 ; 0.320 and A [cm/min] = 0.031 ; 0.023 for TMV and TMV 2.

TMV shows a more pronounced suction flow with a wide mixed region whereas this transition is not so clear in the case of TMV 2 especially between mixed and gravity flow. Note that these distinctions were made by eye and their exact placement could be argued. Regarding the fit of the two-term model it can be said that both sites produce a decent result albeit with a slight overestimation of the fit in the suction region.

9.6.2 St. Restrup Fields

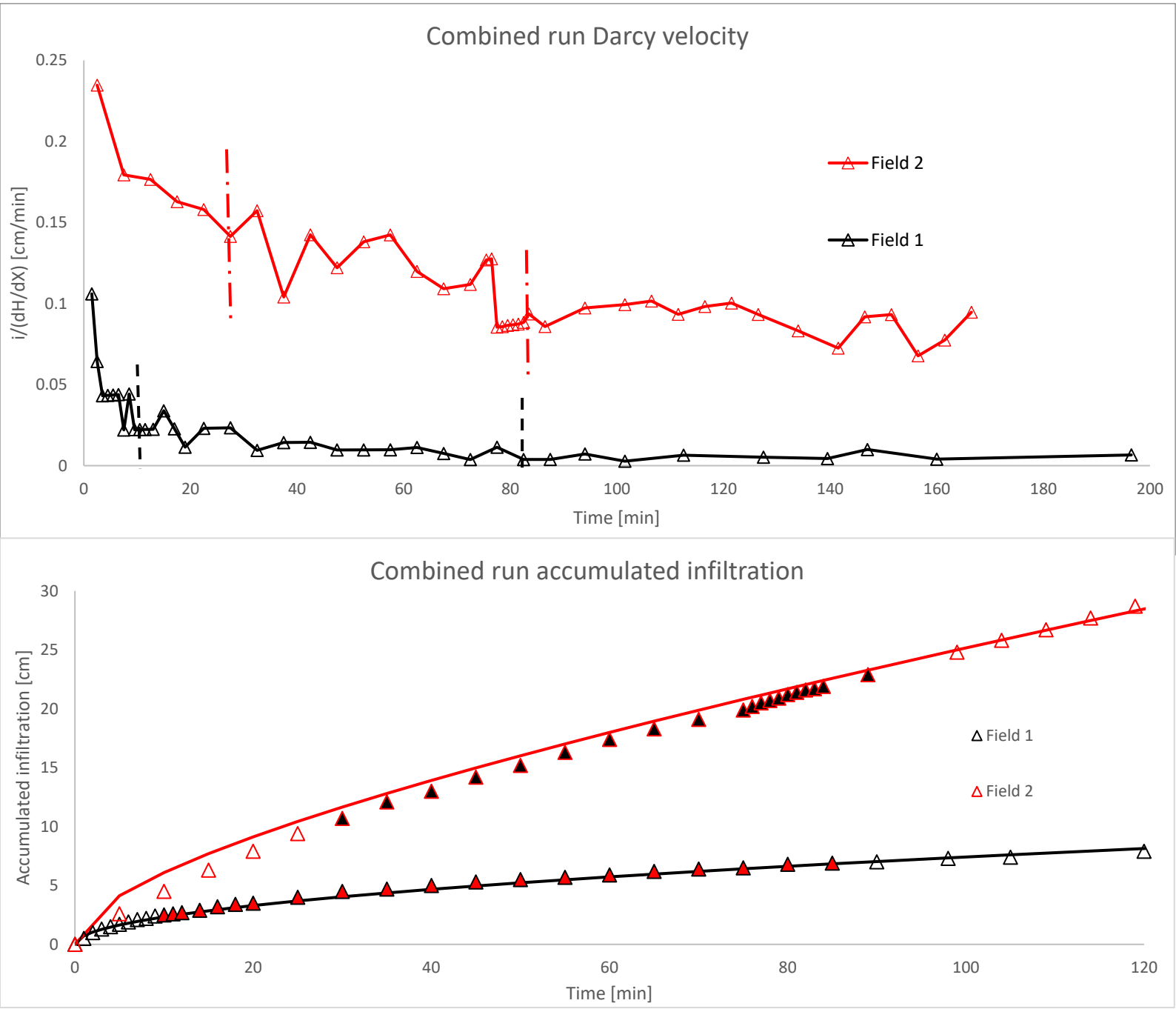

Figure 62 a) Darcy velocity versus time for the combined run of Field 1 and Field 2 in black and red, respectively. Dashed lines represent the transition between the three flow regions for their respective sites – suction, mixed and gravity dominated. Division made by eye.
b) Fit of the Philip infiltration model for Field 1 and Field 2 in black and red, respectively. Filled symbols represent the mixed flow, as indicated in a). S [cm/√min] = 0.732 ; 1.66 and A [cm/min] = 0.001 ; 0.086 for Field 1 and Field 2.

Field 1 has an unsually large number of measurements before transitioning from suction to mixed flow and similarly to TMV 2 the shift from mixed to gravity-dominated flow is not so clearly defined. All three regions in Field 2 are highly suspect and the case where gravity-dominated flow is not achieved at all can be made leaving Field 2 with a very long suction phase transitioning at ~90 minutes to a mixed flow. Regarding the fit Field 2 stands out especially in the beginning where an overestimation of the model is most noticeable. Another interesting note is that the solver chose an A value of 0 for Field 1. A second constraint stating that A cannot be smaller than 0.001 was then used which is the resulting A value for the fit of Field 1.

9.6.3 Gistrup and St. Restrup Forest

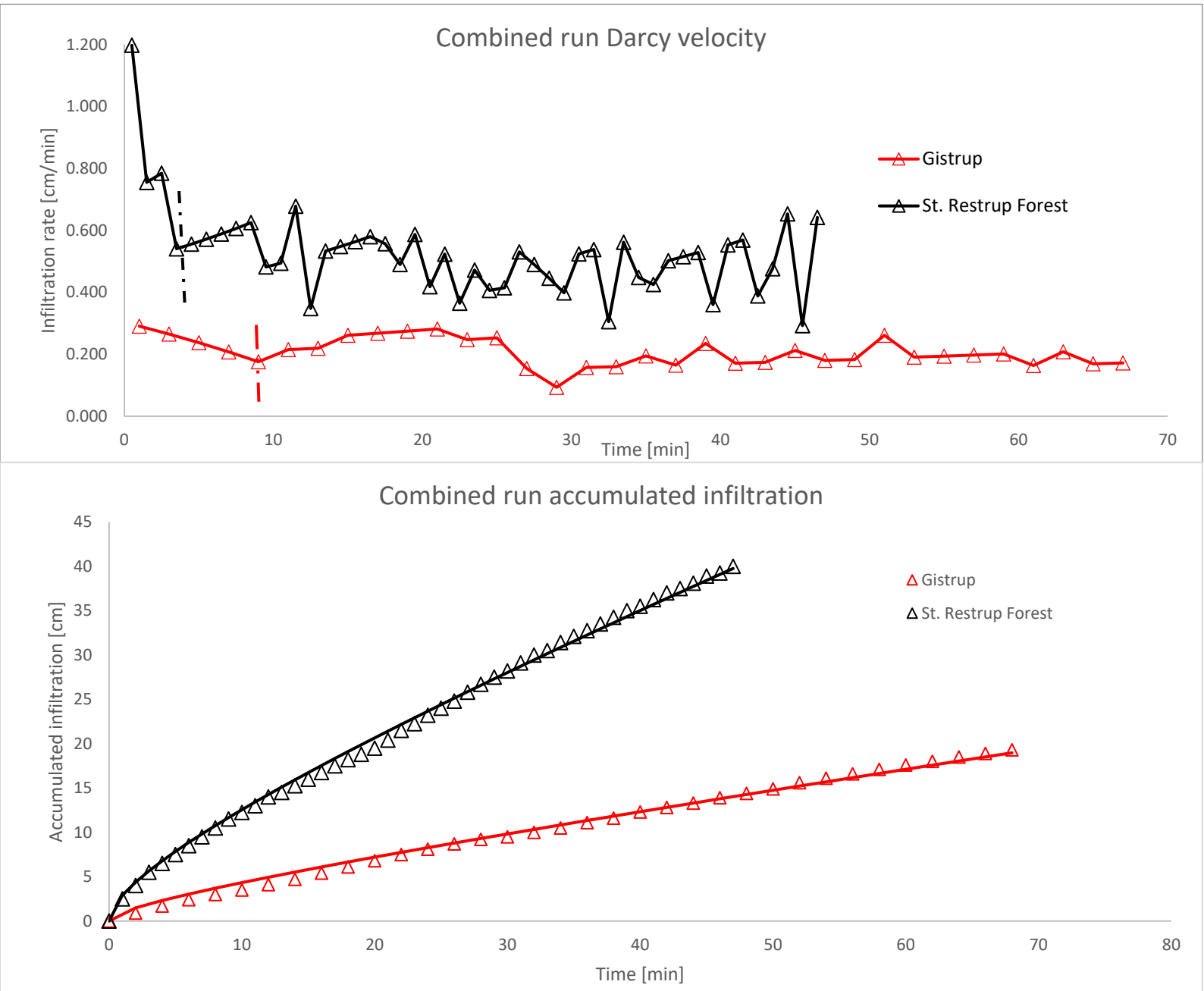

Figure 63 a) Darcy velocity versus time for the combined run of Gistrup and St. Restrup Forest in black and red, respectively. Dashed lines represent the transition between the three flow regions for their respective sites – suction, mixed and gravity dominated. Division made by eye.
b) Fit of the Philip infiltration model for Gistrup and St. Restrup Forest in black and red, respectively. Filled symbols represent the mixed flow, as indicated in a). S [cm/Vmin] = 0.790 ; 2.40 and A [cm/min] = 0.183 ; 0.496 Gistrup and St. Restrup Forest.

Both St. Restrup Forest and Gistrup are good examples of a somewhat easily identifiable suction-dominated short phase followed by what can be described as a very noisy mixed phase in the case of the Forest site and for Gistrup the Darcy velocity shows a slight upward trend. The two-term fit in both cases is slightly off especially in the early and mid-stages.

9.6.4 Resulting changes to the twin curves

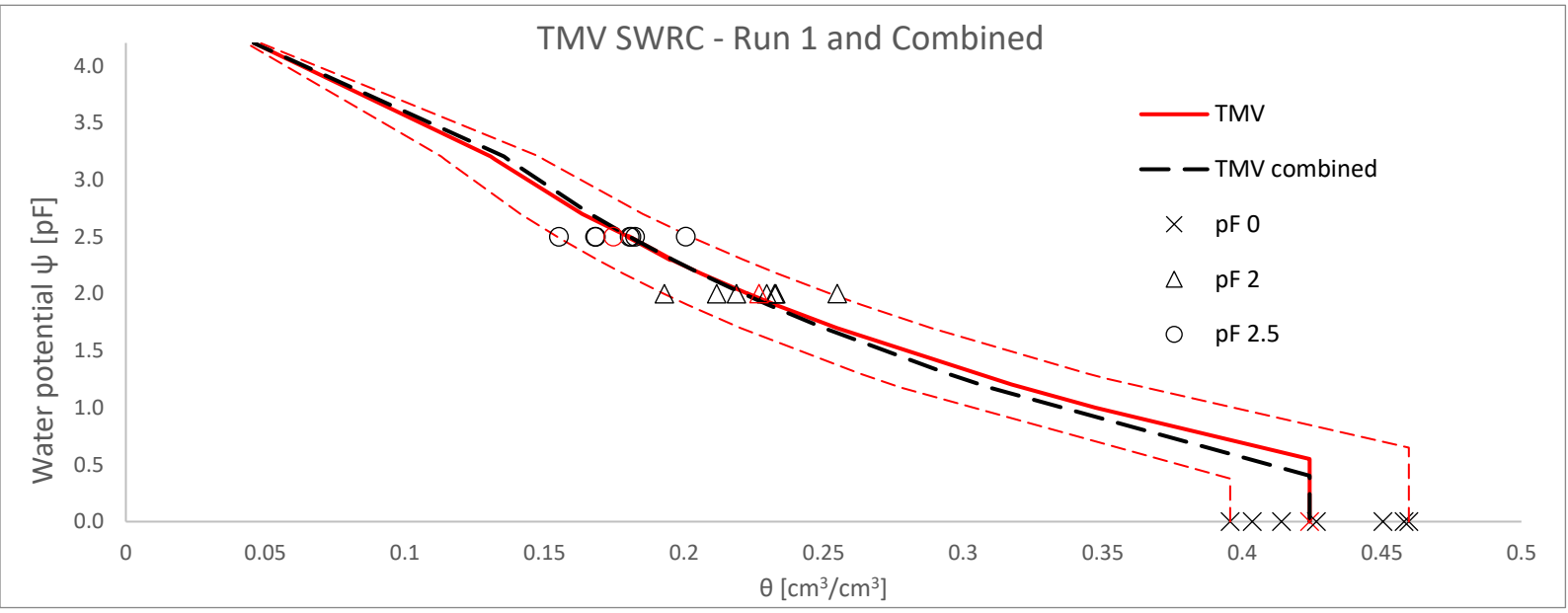

Figure 64 TMV SWRC using b values from Run 1 and the combined run.

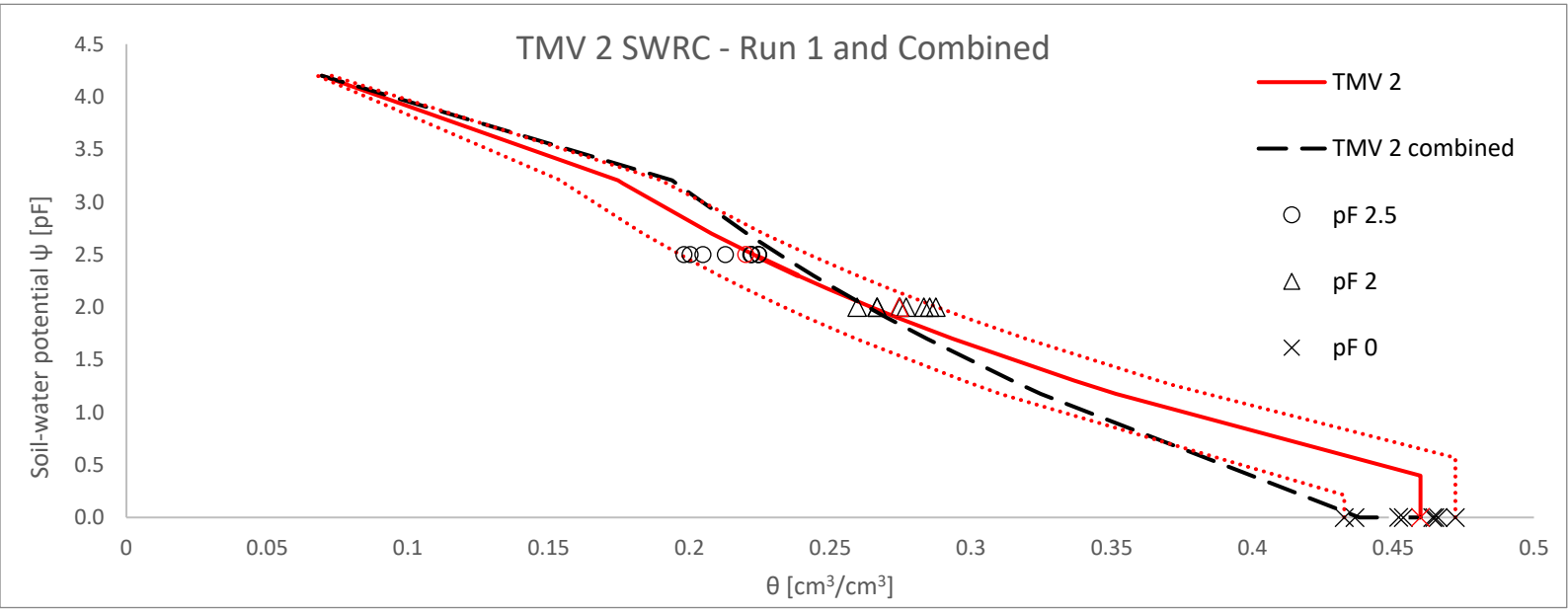

Figure 65 TMV 2 SWRC using b values from Run 1 and the combined run.

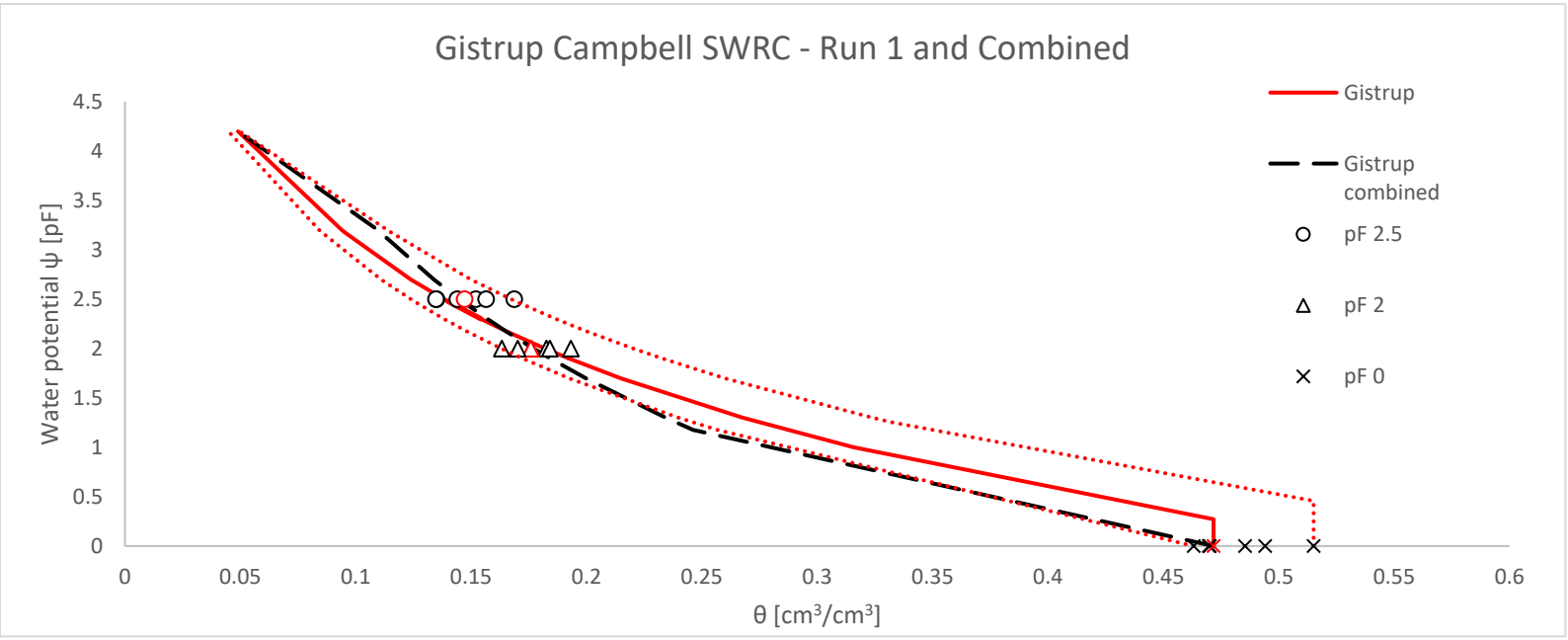

Figure 66 Gistrup SWRC using b value from Run 1 and the combined run.

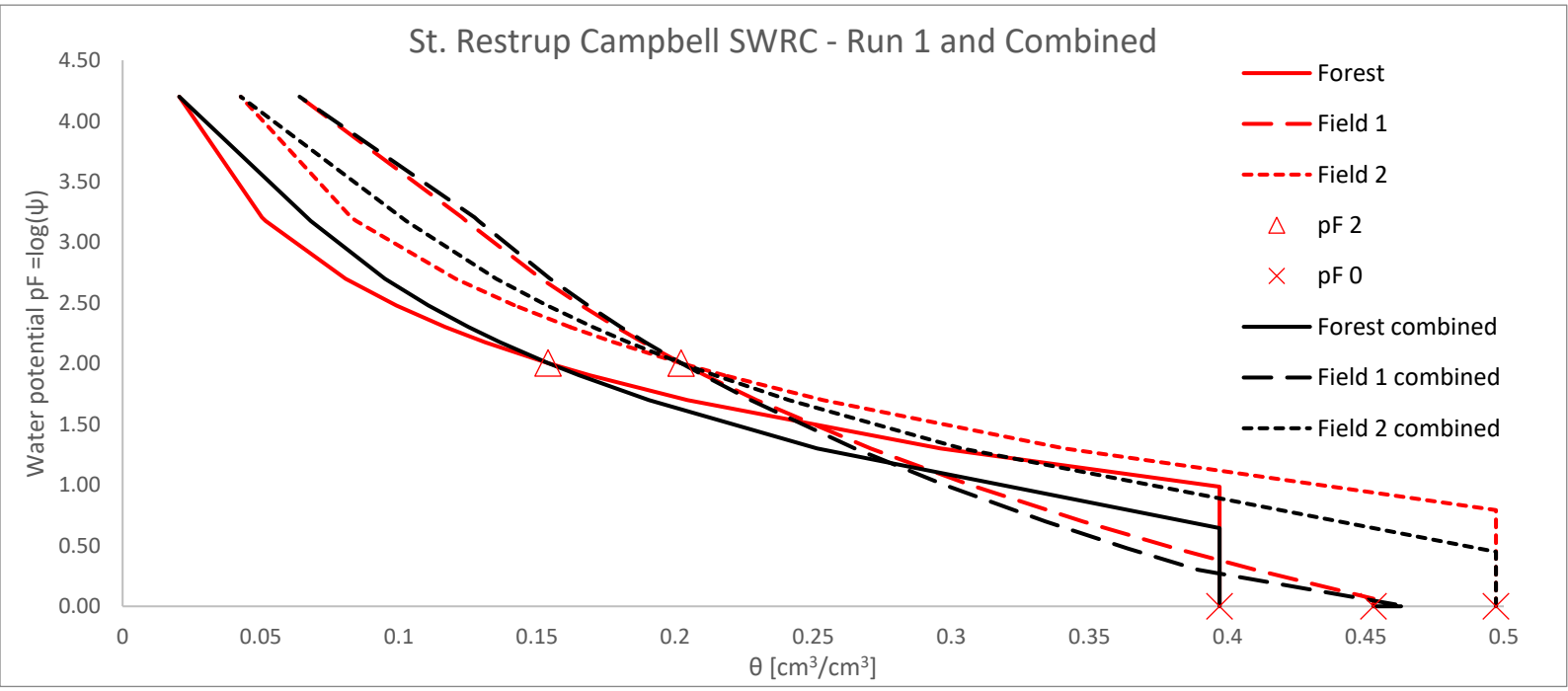

Figure 67 St. Restrup SWRC using b value from Run 1 and the combined runs.

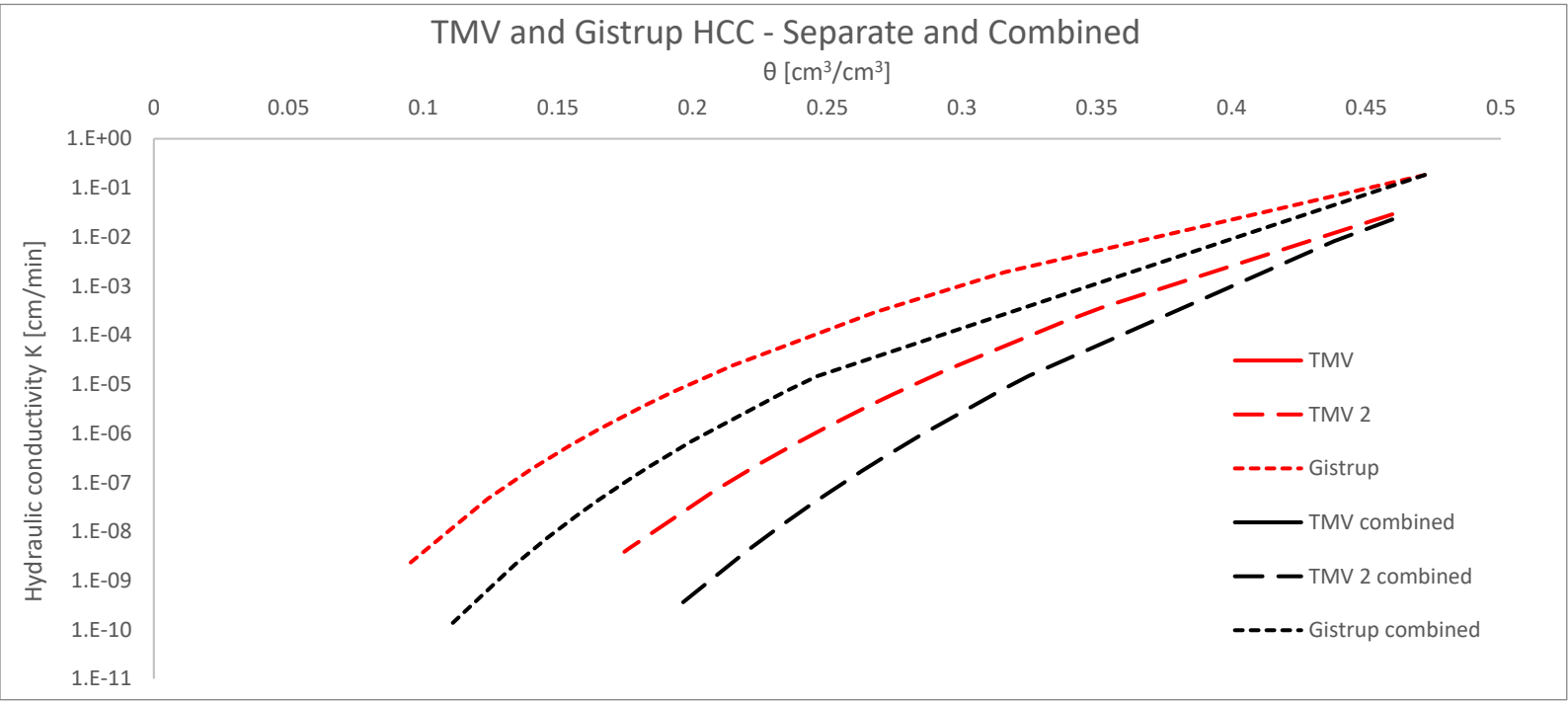

Figure 68 HCCs for TMV and Gistrup sites - default curves in red and Philip fit on combined run in black.

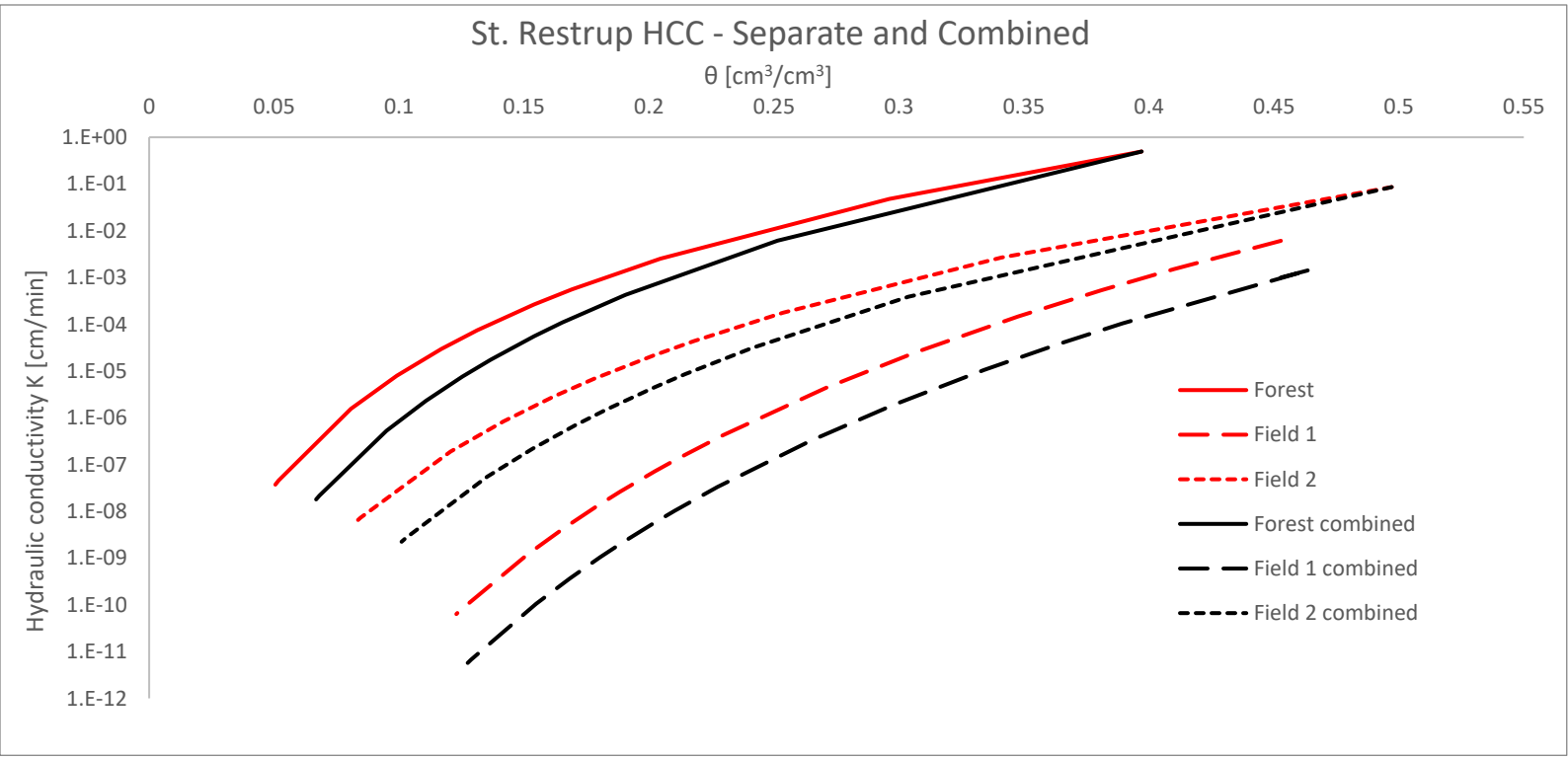

Figure 69 HCCs for St. Restrup - default curves in red and Philip fit on combined run in black.

9.6.5 Summary of parameters and reflection

Table 17 shows the summary of parameter values from the 2-term fit in comparison to the 1-term fit.

Table 17 Summary of parameter values for Philips 1- and 2-term fit to Run 1, 2 and Combined data.

	1 term fit		*2 term fit*		*b*		*ψe [cm]*	
	S [cm/√min]	Ks [cm/min]	S [cm/√min]	A [cm/min]	1-term	2-term	1-term	2-term
TMV	0.972	0.0344	0.821	0.0313	5.19	5.65	3.54	2.53
TMV 2	0.588	0.0289	0.320	0.0227	6.68	9.05	2.50	0.65
Gistrup	1.50	0.183	0.790	0.183	4.18	5.76	1.87	0.355
Forest	4.27	0.496	2.40	0.496	2.48	3.31	9.67	4.41
Field 1	0.852	0.00611	0.732	0.001	5.55	5.98	1.15	0.810
Field 2	2.72	0.0860	1.66	0.0860	3.10	3.98	6.22	2.82

In all cases the 2-term fit resulted in a lower sorptivity value which then increases the Campbell b. As the b increases the slope of the retention curves becomes steeper and in order to fit through the two calibration points at pF 2 and 2.5 the air entry value has to be decreased as seen in Table 17. The result of this is clearly visible in the case of TMV and TMV 2 – for TMV the difference in S and Ks/A is minimal from the 1- and 2-term fits and the resulting SWRC is within the expected margins; for TMV 2 S is nearly halved resulting in a change in b from 6.68 to 9.05 and the resulting air entry is driven from -2.5 [cm] to -0.65 [cm]. This combination of low air entry and steep slope results in a SWRC which likely underestimates water content at the wet end while overestimating it at the dry end, as seen in Figure 65. This tendency is observed in all the other sites as well the only difference being the magnitude of the over- and underestimation. In general it can be concluded that 1) if the fit observed in Figure 61b, Figure 62b and Figure 63b is not satisfactory especially in the beginning of the dataset and 2) the solver function immediately chooses the maximum constraint for A based on the Ks measurements then the resulting change to the parameters and SWRC is large and most likely indicative of an error in either Ks estimations from Run 2 or S estimations from Run 1.